Sources, Modifiable Factors, and Spatiotemporal Variations of $PM_{2.5}$

Submitted in partial fulfillment of the requirements for

the degree of

Doctor of Philosophy

in

Mechanical Engineering

Rebecca R Tanzer Gruener

B.S., Mechanical Engineering, Binghamton University
M.S., Mechanical Engineering, Carnegie Mellon University

Carnegie Mellon University
Pittsburgh, PA

May, 2021

ACKNOWLEDGEMENTS

These past 4.75 years at Carnegie Mellon have been incredibly rewarding. I did not know what to expect when I arrived in Pittsburgh mid-August 2016, but I could not have asked for anything better than what I was met with.

First off, I owe an incredible amount of gratitude towards my advisor, Prof. Albert Presto. The number one thing I tell prospective students considering starting a PhD is to get an idea of who their potential advisor is. If you love your research but can't get along with your advisor, you will have a miserable time. On the other hand if you're even just "ok" about your research but have a great working relationship with your advisor, then you will definitely have a much more pleasant PhD experience. So I cannot thank Albert enough for how we have worked over the past four plus years. His patience and guidance have been invaluable. His encouragement when things were not going so well with my research has always assured me that things will work out (and there were plenty of times where things were "not going well"). On the one hand, he is always ready to help, answer emails with fast turnaround times, schedule last minute meetings, and even physically come into the lab to help troubleshoot when I was most lost. At the same time he has been hands-off in letting me set my own pace of work, my work hours, and direction of where I wanted to go. I have appreciated your flexibility so much and it has really allowed me the opportunity to grow and thrive throughout my time as a PhD student. Thank you for all you have done these past few years. In addition to Albert, I have also gotten a lot of meaningful feedback from my committee members; Dr. R. Subramanian, Prof. Allen Robinson, Prof. Peter Adams, and Prof. Satbir Singh thank you for all of your guidance and help.

Next the mechanical engineering department. The department really became a second home to me here in Pittsburgh. When I first arrived on campus I almost immediately became involved with MEGSO. It has truly enhanced my time as a graduate student here at CMU. Through serving as President and in various other positions on the board I felt like I had the opportunity to not only help other students feel welcomed here at CMU, but it in turn really gave me purpose and made me feel like I belonged here. I am so grateful to all the other students on board over the years as well as other MechEs I've gotten to know over the past few years. I'm not going to name you all at risk of forgetting someone, but I'm really grateful for all the time we've gotten to spend together.

The CAPS lab as a whole has also been an amazing asset throughout my PhD. There were times where I felt less connected to my CAPS lab mates, partially because I sat up in the MechE space in Hamerschlag rather than down in the B-level and partially because my first few years of research focused on field rather than lab work. But despite that I always appreciated our weekly seminars (even when they went virtual) and enjoyed the opportunity to feel that I was part of this amazing research community. As my time in the lab increased over the last two years I too began to feel at home down on the B-level and I'm sad that I will graduate before the weekly coffee hours have the opportunity to start up again in person. However, I'm grateful for the time I've had getting to know many of the CAPS people better over the last portion of my PhD work.

Then of course I cannot conclude my acknowledgments without thanking my friends and family. To my friends, the ones who made the long journey out to visit Pittsburgh over the past few years thank you, and thank you for always being only a phone call away. To my sister who has made the trip more than anyone else I know and still wants to come back, thanks for being the best mix of family and friend. And to my friends that I have made here in Pittsburgh, I literally cannot imagine the past few years without you. You have turned this city where I knew no one on day one to a place that I am so happy to call home.

Thank you to my parents for supporting me throughout this whole process. Thank you for always being there for me and making sure that no matter what I had the best opportunities open to me. Thank you for being the first people to realize I should study engineering, even before we really knew what an engineer was, and even though I didn't want to listen to your suggestions until I came to the conclusion on my own. And thank you for tolerating my crazy timeframes and adventurous spirit. Mom, I know you cried when I told you I got into CMU five years ago because it meant moving farther away, and I'm sorry I loved it here so much that I'm staying, but the ride down the turnpike really isn't so bad.

To my grandparents, Grandma and Bubby, thanks for literally always being my biggest cheerleaders. Throughout the whole PhD process, especially towards the end, I always got a kick out of how invested you two were in how my work was going, when I was going to start writing, what the process was like etc. It often seemed that the two of you were more stressed about my deadlines than I was. And I was always impressed that you both actually read my papers and gave me feedback. I'm so happy that I've gotten to share this experience with you, and that you will get to see me defend my thesis in person.

And to Robbie, my husband. Thank you for being you. As incredible as this PhD process has been, I'd still say a million times the best part about moving to Pittsburgh was getting to meet you. You haven't been a part of my entire PhD experience, but you've been here for most of it. You've experienced a lot of the ups and downs and even agreed to uproot and move to Michigan for my summer internship only weeks after we got married. Thank you for your endless support, listening to me talk about particles and paint, helping with my code, giving good tips on data processing, and making dinner when I'm busy working. I love that I've gotten to share this experience with you, and I can't wait to see where life takes us next. I don't know if I would have imagined when I started this journey that I'd be married and buying a house in Pittsburgh at the end of it, but I could not have pictured a better end to this chapter of life. Looking forward to what life has in store next for us.

And last but not least I must acknowledge my funding sources, without which none of this would have happened: the Allegheny County Health Department, the Steinbrenner Institute, the US EPA's STAR/APM4C program (RD83628601), NSF (CBET1907446). Additionally, this work is part of the Center for Air, Climate and Energy Solution (CACES, www.caces.us). This publication was developed under Assistance Agreement no. RD83587301 awarded by the U.S. Environmental Protection Agency (EPA).

Thank you, enjoy the read!

ABSTRACT

$PM_{2.5}$ as well as various gaseous pollutants are harmful to both human health and the environment. In order to best mitigate the hazardous effects of these pollutants it is important to first understand them. This thesis explores (1) spatial and temporal evolution of emissions as well as (2) emission sources of $PM_{2.5}$. The emission sources evaluated include both field measurements of primary sources (e.g. traffic and industrial) as well as laboratory investigations of less traditional sources of $PM_{2.5}$ (e.g. emissions from volatile chemical products, VCPs). Through the use of state of the art laboratory instrumentation (e.g. PTR-MS and GC-MS) as well as lower-cost sensor networks in the field, a greater understanding of $PM_{2.5}$ emissions, concentrations, and dispersion is obtained.

Air quality monitoring has traditionally been conducted using sparsely distributed, expensive reference monitors. In order to understand variations in $PM_{2.5}$ on a finely resolved spatiotemporal scale a dense network of over 40 low-cost monitors was deployed throughout and around Pittsburgh, Pennsylvania, USA. Monitor locations covered a wide range of site types with varying traffic and restaurant density, varying influences from local sources, and varying socioeconomic (environmental justice, EJ) characteristics. Variability between and within site groupings was observed. Concentrations were higher near the source-influenced sites than the Urban or Suburban Residential sites. Gaseous pollutants (NO_2 and SO_2) were used to differentiate between traffic (higher NO_2 concentrations) and industrial (higher SO_2 concentrations) sources of $PM_{2.5}$. Statistical analysis proved these differences to be significant (COD>0.2). The highest mean $PM_{2.5}$ concentrations were measured downwind (east) of the two industrial facilities while background level $PM_{2.5}$ concentrations were measured at similar

distances upwind (west) of the point sources. We were not able to detect correlation between socioeconomic factors, including the fraction of non-white population and fraction of population living under the poverty line, to increases in $PM_{2.5}$ or NO_2 concentration with our sensor network. This however does not mean that such correlations do not exist either in this city or elsewhere, but rather they may need to be further explored with more sensitive sensor networks. The analysis conducted here highlights differences in $PM_{2.5}$ concentration within site groupings that have similar land use thus demonstrating the utility of a dense sensor network. Our network captures temporospatial pollutant patterns that sparse regulatory networks cannot.

The low-cost sensor network was subsequently used to identify the impact of a decrease in emissions from modifiable factors on pollutant concentrations as a result of the COVID-19 pandemic. COVID-19 related closures offered a novel opportunity to observe and quantify the impact of activity levels of modifiable factors on ambient air pollution in real-time. We use data from a network of low-cost Real-time Affordable Multi-Pollutant (RAMP) sensor packages deployed throughout Pittsburgh, Pennsylvania along with data from EPA regulatory monitors. The RAMP locations were divided into four site groups based on land use. Concentrations of $PM_{2.5}$, CO, and NO_2 following the COVID-related closures at each site group were compared to measurements from "business-as-usual" periods. Overall, $PM_{2.5}$ concentrations decreased across the domain by ~3 $\mu g/m^3$. The morning rush-hour induced CO and NO_2 concentrations at the High Traffic sites were both reduced by ~50%, which is consistent with observed reductions in commuter traffic (~50%). The morning rush-hour $PM_{2.5}$ enhancement from traffic emissions was reduced nearly 100%, from 1.4 $\mu g/m^3$ to ~0 $\mu g/m^3$ across all site groups. There was no significant change in the industrial related intra-day variability of CO and $PM_{2.5}$ at the Industrial sites following the COVID-related closures. If $PM_{2.5}$ National Ambient Air Quality Standards

(NAAQS) are tightened this natural experiment sheds light on to what extent reductions in traffic related emissions are able to aid in meeting more stringent regulations.

This thesis work then turns to laboratory experimentation to quantify emissions from an important source of $PM_{2.5}$. Volatile chemical products (VCPs) have become an increasingly important source of Volatile Organic Compounds (VOCs) and Intermediate-Volatile Organic Compounds (IVOCs) emitted into urban environments. These VOCs play a potentially important role in national Secondary Organic Aerosol (SOA) formation. In this study we conduct headspace and extended emissions tests of paints to quantify the emission factors of I/VOCs over paint's emission timescale. Then SOA yield predictions were calculated. We found that paints are not expected to be a long term emission source of I/VOCs as the majority of all I/VOCs measured reached background levels within two days post paint application. On a national scale paints emit 0.51 kg/person per year of I/VOCs. This means that 291g of I/VOCs are emitted per kg of paint used in the U.S. each year. The SOA mass yield from these emissions were calculated to be 4.7% [+/-2%]. Even though the majority of the I/VOC emissions from the paints were VOCs (59%), the majority of the SOA formed from paint emissions (68%) were from the IVOC portion of the paint emissions. Interestingly the I/VOC paint emissions come predominately from Oil-based paints (making up 87% of the SOA formed from paints) and Semi-Gloss Exterior paints (making up the remaining 13% of SOA formed from paints). Both of these paints are primarily used outdoors where theoretically all of their I/VOC emissions have the opportunity to interact with the ambient environment and form their full potential SOA.

$PM_{2.5}$ is an important pollutant with unwanted negative effects on both human health and the environment. In order to best understand the impacts of $PM_{2.5}$ and to limit those impacts we

need to first understand where it comes from and how concentrations change over time and space. The work in this thesis addresses those two questions.

TABLE OF CONTENTS

TABLE OF TABLES

TABLE OF FIGURES

Chapter 1

Background

1.1 Introduction

$PM_{2.5}$, particulate matter with a diameter of less than 2.5 micrometers, has deleterious effects on human health and the environment (Di et al. 2017; Dockery et al. 1993; Laden et al. 1998). Poor air quality is one of the leading preventable causes of death worldwide (Gakidou et al. 2017). Exposure to elevated concentrations of $PM_{2.5}$ is linked to increased risk of respiratory and cardiovascular disease. Additionally, exposure to other pollutants such as nitrogen dioxide (NO_2) and sulfur dioxide (SO_2) are linked to increased risk of cardiopulmonary mortality, cardiovascular disease, and respiratory disease (Bernstein et al. 2004). In order to quantify the impacts of pollutant exposures on human health as well as their environmental impacts it is important to understand concentrations of various pollutants (e.g. $PM_{2.5}$, and gaseous species), where and what the emission sources are, and how the concentrations change over time and space. In addition to there being merit in understanding concentrations of gaseous species in their own right, SO_2 and NO_2 can also be used to help attribute local enhancements in $PM_{2.5}$ to emissions from coal-burning industries and traffic, respectively (Anttila et al. 2011; Khare and Baruah 2011). To quantify risks associated with exposure to these pollutants, it is necessary to measure and monitor their concentrations in the ambient environment.

Air quality monitoring has traditionally been conducted using sparsely distributed, expensive reference monitors. Traditional networks, like the reference monitoring system set up by the U.S. EPA, are good for capturing long-term temporal trends and inter-city differences

(Chow and Chow 2012), but they are generally too sparse to capture fine-scale, within-city spatial variations (Eeftens et al. 2012). For example in Allegheny County (where the city of Pittsburgh is located) there are currently only four regulatory reference monitors for $PM_{2.5}$ in the entire county (Allegheny County Health Department 2020). The use of only four locations does not accurately represent the air quality throughout the entire county and may in some cases over or underestimate the concentrations of pollutants residents are exposed to.

Fine-tuned monitoring is important to capture intra-city variations in pollutants which can exist down to the sub-kilometer scale (Li et al. 2019). One way to improve spatial coverage of air pollutant monitoring is to deploy large networks of lower-cost sensors (Snyder et al. 2013). Within this work we explore the calibration, deployment and use of a dense network of lower-cost air quality monitors throughout the urban and surrounding areas of Pittsburgh, PA, USA.

Throughout this work we refer to a low-cost sensor network made up of Real-time Affordable Multi-Pollutant (RAMP) sensor packages (Malings et al. 2019; Subramanian et al. 2018; Zimmerman et al. 2018) which include electrochemical gas sensors and $PM_{2.5}$ nephelometers. Each sensor package has up to four different electrochemical sensors for monitoring gasses. These typically include the following sensors: a CO sensor, a NO_2 sensor, a SO_2 or NO sensor, and an O_3 or VOC sensor. Each of the electrochemical sensors have four electrodes. The sensors for each pollutant were calibrated using field collocation with reference monitors where they were exposed to changing pollutant concentrations as well as changing ambient factors (e.g. temperature, relative humidity, etc.). Each sensor was then calibrated based off of the field collocation with either multi-linear regression or machine learning techniques (Malings et al. 2019; Tanzer et al. 2019; Zimmerman et al. 2018). Once calibrated the sensors were deployed in and around the city of Pittsburgh for continuous monitoring.

The sensors were used to monitor changes in pollutant concentrations for years. With this dense network of sensors we were able to see changes in pollutant concentrations over time and space. In chapter two we describe the beginnings of the dense sensor network deployment. We discuss aspects of calibration and initial deployment as well as measurements taken within the first year of sensor network deployment. In chapter two we also utilize the dense sensor network to probe relationships between pollutant concentrations and socio-economic factors (i.e. income and percent minority population). We demonstrate how dense sensor networks can be used to explore aspects of environmental justice that cannot be teased out with sparse regulatory monitors.

The dense sensor network that we have deployed allows us to probe spatially and temporally resolved changes in air quality. We have utilized the low-cost network system to both examine environmental injustice implications as well as understand the impacts of the COVID-19 pandemic on local air quality. In addition to its utility in monitoring status quo pollutant emissions, the low-cost sensor network is also useful in capturing changes in pollutant concentrations as emission sources are modified.

In the beginning of March 2020 the world as we know it changed. The COVID-19 pandemic became present throughout the United States and swiftly state after state began to enforce closures of schools and businesses. People were forced to work from home and minimize travel. These precautions that were put in place to limit transmission of COVID-19 (Sergent et al. 2020) had far reaching effects in many other areas of life. One noticeable result throughout the world was a decrease in commuter traffic, restaurant cooking, and industrial emission sources, all of which contribute greatly to pollutant concentrations in urban environments. This decrease in emission sources led us to wonder if our existing low-cost sensor network would be

able to capture significant decreases in pollutant concentrations as a result of the change in emissions from these modifiable factors.

In chapter three we discuss the impact of the COVID-19 related closures on air quality throughout the city of Pittsburgh and surrounding areas. We analyze data from the twenty-seven RAMP sensors that were still deployed at the start of the pandemic. Through comparisons with historical data from both our sensor network as well as regulatory monitors we assess the impact of reductions in traffic and industry and draw conclusions as to what this means in relation to adoptions of new, lower or no emitting vehicles in the future.

Throughout chapters two and three we discuss ways we sought to understand current $PM_{2.5}$ concentrations. In chapter four we take a turn to further understand sources of $PM_{2.5}$ through laboratory experimentation with less traditional sources of $PM_{2.5}$. There has been a growing consensus that some traditional sources of $PM_{2.5}$ are decreasing in importance compared to other, less traditional sources of $PM_{2.5}$ (Khare and Gentner 2018; McDonald et al. 2018). A large potential source of $PM_{2.5}$ are volatile chemical products (VCPs). Unlike traffic, industry, or restaurant related emissions VCPs contribute to $PM_{2.5}$ concentrations not through primary emissions, but through secondary emissions. Secondary organic aerosol (SOA) can be formed from emissions of volatile organic compounds (VOCs) from VCPs. VOCs are emitted as gases into the atmosphere and react with oxidants (Jimenez et al. 2009; Robinson et al. 2007; Volkamer et al. 2006; Williams et al. 2010; Xu et al. 2015) which result in new particle formation, thus contributing to some portion of the ambient $PM_{2.5}$ concentrations.

In chapter four we discuss laboratory experiments conducted in order to better understand sources of $PM_{2.5}$. These experiments quantified VOC emissions from paints which are an important subclass of VCPS. Both the VOC and less volatile, Intermediate Volatility Organic

Compounds (IVOCs), were measured as paints dried to quantify the I/VOC emissions from paints. The I/VOC emissions from paints were then used along with estimated SOA yields (Cappa and Wilson 2012) to predict SOA mass yield from paints on a national scale.

This work takes a holistic approach to understanding $PM_{2.5}$ concentrations. First we demonstrate the importance of understanding existing $PM_{2.5}$ concentrations on a finely resolved temporal and spatial scale in order to pinpoint point sources and modifiable factors. In chapter two we discuss the deployment of a low-cost sensor network as well as its utility in better understanding potential environmental justice issues. Then in chapter three we continue to utilize the low-cost sensor network to understand changes in pollutant concentrations after a shock to the status-quo emissions system. Finally, we accentuate the importance of laboratory experimentation. In chapter four we quantify the impact of a nontraditional source on secondary $PM_{2.5}$ through emissions measurements from paints. Plainly the objectives of this dissertation are 1) to describe the utilization of a low-cost sensor network to quantify impacts of local (primary) emissions of $PM_{2.5}$ and 2) to quantify the SOA formation potential of a less traditional source of secondary $PM_{2.5}$ (paints). Combined this work sheds increased light on what drives $PM_{2.5}$ concentrations in urban areas.

Chapter 2

Development and Deployment of a Low-Cost Sensor Network

***Contents of this chapter have been published as**: Tanzer R, Malings C, Hauryliuk A, Subramanian R, Presto AA. Demonstration of a Low-Cost Multi-Pollutant Network to Quantify Intra-Urban Spatial Variations in Air Pollutant Source Impacts and to Evaluate Environmental Justice. Int J Environ Res Public Health. 2019 Jul 15;16(14):2523. doi: 10.3390/ijerph16142523. PMID: 31311099; PMCID: PMC6678618.*

2.1 Introduction

Poor air quality has deleterious health effects. Particulate matter with a diameter of less than 2.5 μm ($PM_{2.5}$) dominates the human health burden from environmental exposures. $PM_{2.5}$ is linked to cardiovascular disease and decreased life expectancy (Di et al. 2017; Dockery et al. 1993; Dominici et al. 2006). Other pollutants, including nitrogen dioxide (NO_2), and sulfur dioxide (SO_2) have health effects distinct from $PM_{2.5}$. Exposure to NO_2 and SO_2 contributes to increases in cardiopulmonary mortality, cardiovascular disease, and respiratory disease (Bernstein et al. 2004). SO_2 and NO_2 can be used to help attribute local enhancements in $PM_{2.5}$ to emissions from coal-burning industries and traffic, respectively (Anttila et al. 2011; Khare and Baruah 2011). To quantify risks associated with exposure to these pollutants, it is necessary to measure and monitor their concentrations in the ambient environment.

Air quality monitoring has traditionally been conducted using sparsely distributed, expensive reference monitors. Traditional networks are good for capturing long-term temporal trends and inter-city differences (Chow and Chow 2012), but they are generally too sparse to capture fine-scale within-city spatial variations (Eeftens et al. 2012). Though there can be pollutant spatial variations at the sub-km scale (Li et al. 2019), within this study, we define “fine-

scale" as variations between different neighborhoods (~1 km^2) throughout a large urban area. One way to improve spatial coverage of air pollutant monitoring is to deploy large networks of lower-cost sensors (Snyder et al. 2013).

High spatial density networks of lower-cost monitors can be used to inform small-scale spatial variations in air pollution by providing real-time, on-the-ground measurements of air pollutants. However, previous studies using lower-cost sensors have usually focused on calibration or on calibration plus the deployment of a few nodes (Cross et al. 2017; Esposito et al. 2016; Hagan et al. 2018; Moltchanov et al. 2015). Many fewer papers demonstrate results from a large network of low-cost sensors (Caubel et al. 2018; Mead et al. 2013). In this study, we present results from a one-year deployment of a network of lower-cost monitors in Pittsburgh, PA, USA, focusing on 42 sensors in the network.

Widespread deployment of low-cost sensor networks also enables the investigation of environmental justice within a city. Environmental justice (EJ) is the fair treatment and meaningful involvement of all people regardless of race, color, national origin, or income with respect to the development, implementation and enforcement of environmental laws, regulations and policies (EPA 2014). The state of Pennsylvania defines a census tract with greater than or equal to 20% of the population living below the poverty line and/or greater than or equal to 30% of the population belonging to a minority group as an "EJ area" (Environmental Justice Work Group 2001). According to this definition, EJ areas are not necessarily areas that are currently experiencing environmental injustice. Rather, they are areas that have a high risk of experiencing environmental injustice as indicated by their socio-economic status.

In this study, we utilize our dense network of air quality monitors to investigate whether the EJ areas in Pittsburgh do in fact have lower air quality in comparison to non-EJ areas. This

definition of environmental injustice fits most closely with disparate exposure inequality. Disparate exposure inequality occurs when people belonging to a specific social group are more exposed to one or more environmental pollutants than they would be if the group was randomly distributed among the rest of the population (Downey 2011).

Clark et al. used land-use regression (LUR) models to show that in the U.S. non-white (minority) populations often live in areas with higher air pollution (Clark, Millet, and Marshall 2014, 2017). They used a national LUR for NO_2 to show that non-white populations are exposed to about 31% (3 ppb) higher mean concentrations of NO_2, than white populations, primarily due to traffic emissions (Clark et al. 2017). However, the exposure inequality trends identified by Clark et al. may not be identical in every city, as emission sources, land use, and population distributions might be idiosyncratic.

In this study, we use the RAMP (Real-time Affordable Multi-Pollutant sensor package) (Malings, Tanzer, Hauryliuk, Kumar, et al. 2019; Subramanian et al. 2018; Zimmerman et al. 2018), a lower-cost monitor consisting of electrochemical gas sensors and $PM_{2.5}$ nephelometers, to investigate spatial patterns in air pollution and exposure inequality in Pittsburgh. Sensor sites were distributed in such a way as to assess the variability in pollutant concentrations near known point sources and across urban and suburban/background locations. Using the low-cost sensors, we show that it is possible to detect enhancements of criteria pollutants that can be attributed to local sources like industry and traffic.

We also use the RAMP data to investigate exposure inequality in EJ and non-EJ areas as defined by the state of Pennsylvania. Previous work assessing air quality in EJ areas has typically used either national models that may not account for specific intra-urban pollutant variations (Clark et al. 2014, 2017) or used short-term (e.g., 1–3 week) intra-city measurements (Krudysz et

al. 2009). The expansiveness of our dense, low-cost sensor network, which was deployed for over a calendar year, captures pollutant measurements over various socio-economic areas within a city, allowing us to compare measurements taken in different EJ and non-EJ communities over a significant amount of time. The measurements lead us to conclude that socio-economic (EJ) factors do not necessarily determine $PM_{2.5}$ exposures in different parts of Pittsburgh.

2.2 Materials and Methods

2.2.1 Measurement Locations

This paper focuses on data from forty-two RAMPs that were deployed throughout the greater Pittsburgh area in western Pennsylvania over April 2017–May 2018. Figure 2.1 shows the locations of RAMP sites throughout Pittsburgh and surrounding Allegheny County. RAMP sites cover a range of areas with varying land use and proximity to nearby emissions sources such as traffic, food cooking, and industry. The RAMP sites range from suburban residential sites with low traffic and low restaurant density, to downtown sites with high traffic and high restaurant density, to industrially influenced sites. RAMP sites also encompassed both EJ and non-EJ communities. While all of the RAMPs were nominally deployed for a year, the sites experienced various amounts of downtime due to sensor failures, power loses, and occasional returning of RAMPs to the Carnegie Mellon University campus for calibration (Malings, Tanzer, Hauryliuk, Kumar, et al. 2019). Figure 2.8 in the Supplementary Information shows data coverage by season for each site.

1) Figure 2.1 Map of sampling domain

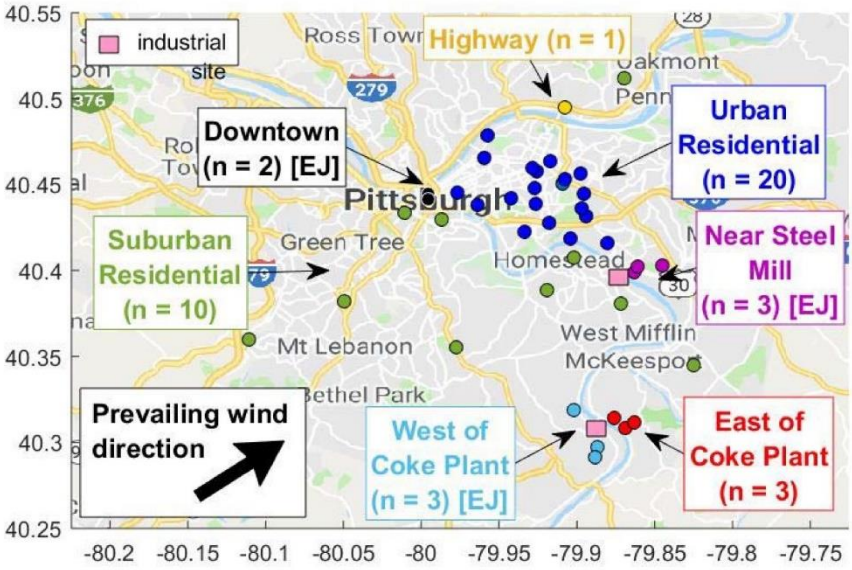

Dots indicate locations of 42 Real-time Affordable Multi-Pollutant sensor package (RAMP) monitors that were deployed throughout Pittsburgh. The sites were categorized into 2 Downtown sites, 20 Urban Residential sites, 10 Suburban Residential sites, 1 Near Highway site, 3 Near Steel Mill sites, 3 sites West of a Coke Plant, and 3 sites East of a Coke Plant based on traffic density, restaurant density, and proximity to industrial point sources (shown as pink squares). The prevailing wind direction is also shown; a wind rose is displayed in the Supplementary Information.

The 42 sites were classified into seven categories: Downtown (N = 2 sites), Urban Residential (N = 20), Suburban Residential (N = 10), Highway (N = 1), Near Steel Mill (N = 3), West of Coke Plant (N = 3), and East of Coke Plant (N = 3). In Figure 2.1, similar RAMP locations, representative of particular micro-environments, are indicated with different colors. Sites were classified based on known land use. For Downtown, Urban and Suburban Residential, and Highway sites, the vehicle density within a 100-m radius and restaurant density within a 500-m radius of the site were used for classification. Values of vehicle and restaurant density were normalized by dividing the densities at each site by the maximum value across the entire sampling network for each variable. Downtown sites are located in the central business district

and were in the top 30% of vehicle and restaurant densities. Urban Residential sites were located within the city limits and had moderate traffic density (below the 60th percentile) along with low restaurant density (within the first quartile). Suburban residential sites were those sites that were located outside of the city limits and experienced low vehicle and restaurant densities (within the first quartile). As the names suggest, the Urban and Suburban Residential sites were located in residential and mixed-use neighborhoods, typically at private residences or public schools. The Highway site was located 10 m from the edge of a limited-access highway.

Sites classified as Near Steel Mill, West of Coke Plant, and East of Coke Plant were defined by proximity to industrial point sources. The Near Steel Mill and East of Coke Plant sites were all within 1500 m of a steel mill and metallurgical Coke plant, respectively. These sites were east, and therefore generally downwind of, the respective point sources. West of Coke Plant sites were within 2000 m of the Coke plant in the generally upwind direction of the Coke plant.

The sites are listed in Table 2.8 in the Supplementary Information. Each site is assigned a numerical identifier that is used in subsequent figures. The site groupings are as follows: Downtown (Site 1–2), Urban Residential (3–22), Highway (23), Suburban Residential (24–33), Near Steel Mill (34–36), West of Coke Plant (37–39), and East of Coke Plant (40–42). The three sites Near the Steel Mill, three West of the Coke Plant, and the two Downtown sites are all classified as EJ communities by the state of Pennsylvania. To identify locations as EJ or not, census data was obtained. The latitude and longitude for each RAMP location were extracted and input into the EPA environmental justice screening tool, EJSCREEN. EJSCREEN was created by the U.S. EPA as a preliminary step in evaluating environmental justice issues (Zhao et al. 2018). The tool works in such a way that given a latitude and longitude it can output different socio-economic factors for the census block group in question. The census block group where

each RAMP was located was identified and the percent of the population living below the poverty line and the percent of the population belonging to a minority group was extracted for each identified census block group.

2.2.2 Measurement Devices and Calibration

The Real-time Affordable Multi-Pollutant (RAMP) sensor package was used for this study. RAMPs were developed in a partnership between Carnegie Mellon University and SenSevere Limited Liability Company. Details about the RAMP monitoring package, including communication and data storage, are provided in Zimmerman et al. (Zimmerman et al. 2018). The RAMP data are recorded at a resolution of one data point approximately every 15 s, but for this study the data have been down-averaged to hourly mean concentrations. The RAMPs can measure up to four gaseous pollutants using electrochemical sensors from AlphaSense Ltd. The gaseous pollutants considered in this study are nitrogen dioxide (NO_2, NO_2-B43F) and sulfur dioxide (SO_2, SO_2-B4). NO_2 and SO_2 measurements were used as tracers for different $PM_{2.5}$ sources (traffic and industrial point sources respectively). The RAMPs also included electrochemical sensors for measuring total oxidants (Ox, Ox-B431) and carbon monoxide (CO, CO-B41), as well as a nondispersive infrared (NDIR) CO_2 sensor (SST CO_2S-A) which also provided temperature and relative humidity data. Measurements from these additional three gaseous pollutant sensors are not used directly in this study.

Electrochemical gas sensors are commonly used in low-cost monitors because of their low cost to manufacture, selectivity, and simplicity (Kumar et al. 2015; Stetter 2008). These sensors consist of four electrodes. A redox reaction occurs between the working and counter electrodes when the sensor is exposed to the target pollutant. The reaction generates a potential difference which then can be correlated with concentrations of the pollutant. An auxiliary

electrode in this four-electrode unit accounts for temperature and relative humidity effects. However, numerous studies have shown that assuming a linear relationship between sensor signal and concentration is insufficient to account for impacts of temperature, humidity, and sensitivity to species other than the target pollutant (Cross et al. 2017; Hagan et al. 2018; Malings, Tanzer, Hauryliuk, Kumar, et al. 2019; Snyder et al. 2013; Spinelle et al. 2015; Zimmerman et al. 2018).

In this work, we follow the calibration method of Zimmerman et al. for NO_2 (Zimmerman et al. 2018). This method uses (1) ambient collocation of RAMPs with EPA-grade reference monitors and (2) supervised machine learning algorithms to convert electrochemical sensor response to pollutant concentrations. Zimmerman et al. showed that a random forest machine learning algorithm provided the best performance for determining NO_2 concentrations from RAMPs. The random forest calibrations yield precision and bias of ~25% for NO_2. It has recently been shown that similar performance can be achieved using generalized calibration models rather than developing a unique calibration model for each RAMP (Malings et al. 2019). Therefore, general calibration models were used for all of the RAMP NO_2 data in this study.

To calibrate the SO_2 sensors, we collocated sixteen RAMPs with a reference grade SO_2 monitor (Model 100A, Teledyne-API, San Diego, CA, USA) for three months at site 41. This site is <1 km east of the Coke plant and is often impacted by SO_2 emissions from the plant. From the collocation a multi-linear regression calibration model was developed and applied to the SO_2 sensors (Subramanian et al. 2018). Details of the SO_2 sensor collocation and calibration can be found in the Supplementary Information.

Each RAMP includes an optical $PM_{2.5}$ monitor. Thirty-nine of the RAMPs used a Met-One Neighborhood PM Monitor (NPM) (Met One Instruments, Grants Pass, OR, USA) and the remaining 3 RAMPs used PurpleAir PA-II monitors. Table 2.1 in the Supplementary Information lists which sensor was placed at each site. These low-cost particulate matter sensors employ light scattering optical techniques instead of the traditional EPA regulatory PM monitoring techniques which include tapered element oscillating microbalances (TEOMs) and beta attenuation monitors (BAMs). Light scattering (also called nephelometry) is used in lower-cost sensors because they are cheap to manufacture, have low power requirements to operate, and have fast response times (Kelly et al. 2017; Rai et al. 2017; Wang et al. 2015). Light scattering devices typically are made up of an infrared emitting diode (IRED), a phototransistor, and focusing lens. When the particles pass through the sensor, they scatter light. The intensity of the scattered light is measured by a phototransistor and correlated with PM mass. Drawbacks to the light scattering technique include sensitivity to changes in temperature, relative humidity, particle composition, and size distribution (Jayaratne et al. 2018; Koehler and Peters 2015; Zheng et al. 2018).

To account for these effects, primarily the humidity artifact, we correct the as-reported $PM_{2.5}$ mass concentrations to "BAM-equivalent" $PM_{2.5}$ mass concentration. A detailed explanation of the correction method used here can be found in Malings et al. (Malings et al. 2019). Briefly, we first correct for aerosol hygroscopic growth using temperature and relative humidity measured by each RAMP and the average particle composition measured in Pittsburgh. We then adjust the hygroscopic growth-corrected concentration to "BAM-equivalent" (values that can be directly compared to U.S. EPA standards) to account for aerosol size distribution

effects by using a linear regression obtained by collocating the RAMPs with regulatory BAM monitors at sites 5 and 41.

This study considers data collected over a period of one year at each sampling site. However, the same RAMP was not deployed at each site for the entire study period. RAMPs are routinely brought back to our central reference site at the Carnegie Mellon University campus either for maintenance or for periodic calibration checks. As noted by Malings et al., the calibrations for gases measured by the RAMPs are robust for approximately 6–12 months, so the data used here are within the bounds for normal operation of these low-cost sensors (Malings et al. 2019). In a separate paper, Malings et al. demonstrated that the $PM_{2.5}$ measurements are robust for yearlong deployments (Malings, Tanzer, Hauryliuk, Saha, et al. 2019).

2.3 Results and Discussion

2.3.1 Intraurban $PM_{2.5}$ Variability and the Impact of Point Sources

Although $PM_{2.5}$ is largely regional (Robinson et al. 2007), local point sources can be responsible for generating local spikes in $PM_{2.5}$ mass. An example of pollution spikes due to local sources is shown in Figure 2.2, which compares 12 hours of $PM_{2.5}$ measurements at all 42 sites. $PM_{2.5}$ concentrations are elevated relative to other sites at the three East of Coke Plant sites (40–42) starting at 2:00 a.m. on January 14th, 2018. $PM_{2.5}$ concentrations at these sites increase from ~10 $\mu g/m^3$ to as much as 100 $\mu g/m^3$ over the course of several hours.

2) Figure 2.2 Example of high $PM_{2.5}$ event associated with local emissions

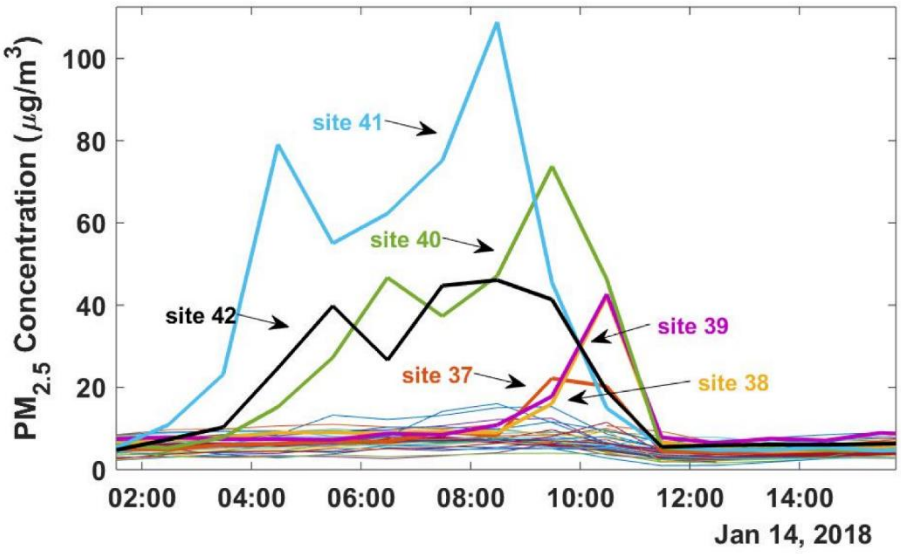

This figure is exemplary of periods of time throughout the study period when sites surrounding the Coke plant (indicated by thick lines) experienced elevated $PM_{2.5}$ concentrations due to plant emissions while all other sites (thin lines) maintained background $PM_{2.5}$ concentrations.

Prior to 8:00 a.m. the winds were blowing from the southwesterly direction; however, at 8:00 a.m. the winds shifted and began to blow from the northeasterly direction. This is accompanied by a drop in $PM_{2.5}$ at sites 40–42 and a concurrent increase in $PM_{2.5}$ at the West of Coke Plant sites (37–39), which were then downwind of the emissions source. The spikes measured at sites 37–42 were not observed at any other sites in the network, suggesting that this was a local enhancement due to emissions from the Coke plant.

Repeated instances of these types of spikes increase the long-term average concentrations at sites 40–42 which are predominately downwind of the Coke plant. Similarly, the Near Steel Mill sites, which are predominately downwind (east) of the steel mill (sites 34–36) also have higher long-term average $PM_{2.5}$ concentrations than the sites that are upwind (west) of the steel mill in the suburban residential area (sites 27, 28, and 31). Figure 2.3 compares the

$PM_{2.5}$ measurements across the sampling network. The annual average concentration at each site ranges from 7.5 to 25.8 µg/m^3, with the majority of sites having an average concentration less than the U.S. EPA annual standard of 12 µg/m^3.

3) Figure 2.3 Average $PM_{2.5}$ concentrations across RAMP network

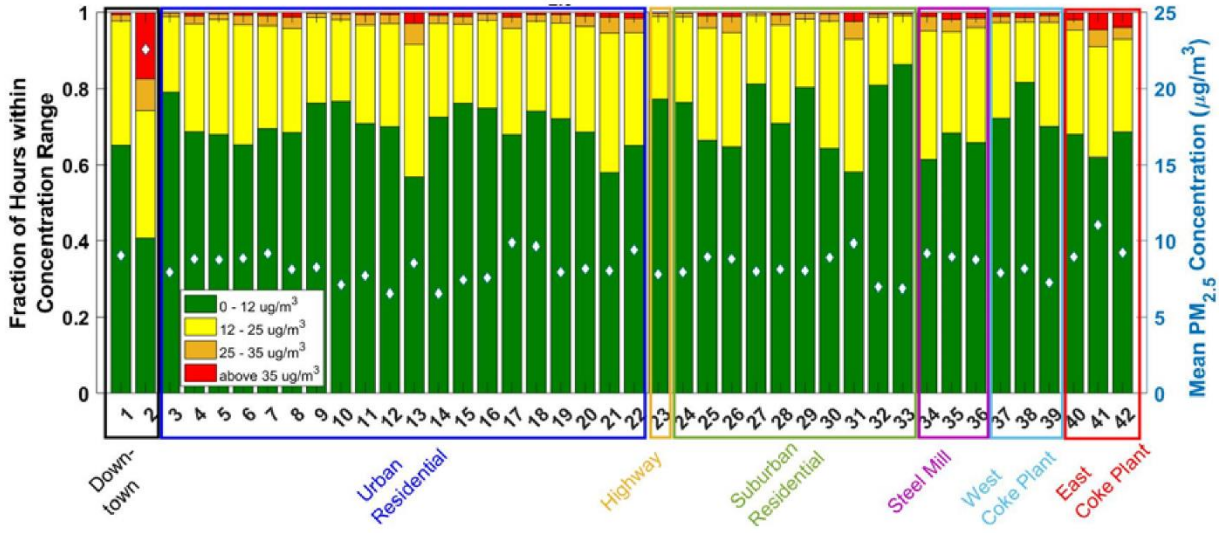

The bars show the fraction of hourly averaged $PM_{2.5}$ measurements within each of four concentration ranges based on EPA and WHO regulatory cutoffs. Mean $PM_{2.5}$ concentration is indicated within each bar as a white diamond.

The bar plot of each location in Figure 2.2 is subdivided into four categories: measurements where the hourly averaged $PM_{2.5}$ concentration was (1) less than 12 µg/m^3 (2) 12–25 µg/m^3 (3) 25–35 µg/m^3 and (4) greater than or equal to 35 µg/m^3. These cutoffs were chosen based on EPA and World Health Organization (WHO) daily and annual average $PM_{2.5}$ standards. The 25 µg/m^3 level is the WHO 24-h exposure standard; if concentrations are above this threshold for more than 24 h, that would be hazardous according to the WHO. With the exception of site 2, which is described in more detail below, all sites had $PM_{2.5}$ lower than 12 µg/m^3 for over 57% of hours, and concentrations were less than 25 µg/m^3 for over 91% of all hourly data.

Sites that had relatively higher percentages of hours with measured $PM_{2.5}$ above 25 $\mu g/m^3$ were further investigated. Sites with elevated annual average $PM_{2.5}$ are generally impacted by local enhancements, and therefore experience concentrations exceeding 25 $\mu g/m^3$ more often than sites that are far from either point sources or areas of high traffic density. Site 2 has the highest percent of hours above 25 $\mu g/m^3$ (25.9%). This anomalously high occurrence of elevated $PM_{2.5}$ concentrations can be attributed to the fact that site 2 is located downtown in a street canyon approximately ten meters away from the exhaust of a restaurant with a wood-fired pizza oven. These cooking emissions drive the elevated $PM_{2.5}$ concentrations for site 2.

The three East of Coke Plant sites (40–42) also experienced elevated frequencies of hourly $PM_{2.5}$ concentrations exceeding 25 $\mu g/m^3$. They are located within 1500 m of the coke plant, in the predominantly downwind direction. These sites experienced $PM_{2.5}$ concentrations over 25 $\mu g/m^3$ for 4.8%, 8.2%, and 6.9% of the sampling period. In contrast, across all other sites (excluding site 2), concentrations above 25 $\mu g/m^3$ occur only 3.2 ± 1.7% of the time. Sites 41 and 42 were more than two standard deviations higher than this average, while site 40 was on the upper end of that range.

Two of the sites East of the Coke Plant (41 and 42) experience higher $PM_{2.5}$ concentrations than the third site. The presence of these differences points to the utility of dense lower-cost networks of air quality monitors, as a single, expensive regulatory monitor would be incapable of capturing this level of fine-scale spatial variability.

Large differences in $PM_{2.5}$ concentration exist between different site groupings. The difference in $PM_{2.5}$ concentrations upwind and downwind of the Coke plant illustrate sharp $PM_{2.5}$ gradients that can result from industrial point sources. The three West of Coke Plant sites (37–39), which are similarly close (1–2 km) to the Coke plant as the East of Coke Plant sites,

have $PM_{2.5}$ greater than 25 μg/m^3 only 2.7%, 2.6%, and 2.7% of the time, respectively. This is similar to the Urban and Suburban Residential sites.

We can also use Figure 2.3 to assess how the frequency of elevated $PM_{2.5}$ concentration varies in EJ versus non-EJ communities. Sites 37–39 are classified as EJ communities, whereas sites 40–42 are non-EJ communities. However, sites 40–42 experience a higher frequency of hours with elevated $PM_{2.5}$ concentrations than sites 37–39. The low-cost sensor network in this region is able to detect influences from point sources on a finely resolved spatial scale in a way that illuminates differences in EJ and non-EJ communities.

Figure 2.3 shows all of the data collected during our study period at each site. Additional plots separating the data by season are shown in Figure 2.9 in the Supplementary Information. $PM_{2.5}$ concentrations vary seasonally, with lower concentrations in the spring than in the other three seasons; mean $PM_{2.5}$ concentration in the fall, winter, spring and summer were 11.2, 10.5, 8.7, and 13.9 μg/m^3 respectively. Across the network, $PM_{2.5}$ concentrations exceeded 25 μg/m^3 for only 1.5% of hours in the spring, versus 5.25%, 4.35%, and 5.00% in the summer, fall, and winter, respectively. The spatial pattern of high $PM_{2.5}$ concentrations, however, remains consistent from season to season, largely driven by local emissions. The restaurant impacted site 2 always has the highest $PM_{2.5}$ concentration, and sites 40–42 East of the Coke Plant have more frequent instances of $PM_{2.5}$ greater than 25 μg/m^3 than West of Coke Plant or Residential sites.

The coefficient of divergence (COD) is a metric that can be used to determine the significance of $PM_{2.5}$ concentration differences between sites. The COD is computed using Equation (1) for each pair of sites.

$$\mathrm{COD} = \sqrt{\frac{1}{N}\sum_{i=1}^{N}\left(\frac{x_{iA} - x_{iB}}{x_{iA} + x_{iB}}\right)^2} \quad (1)$$

N is the number of paired observations, x_{iA} is the measurement at time period i for site A, and x_{iB} is the measurement at the time period i for site B, where each time period i is one hourly averaged $PM_{2.5}$ measurement. A threshold of 0.2 is typically used to identify pairs of sites that are significantly different (COD > 0.2) from sites that are similar (COD < 0.2) (Krudysz et al. 2009; Stetter 2008).

During our evaluation of these low-cost sensors by collocation with a reference monitor, the majority of the sensor pairs showed a COD below 0.2. Figure 2.10 in the Supplementary Information shows the results of analysis conducted on 48 RAMPs that were collocated at site 7. While 6 pairs of RAMPs at the collocation had CODs over 0.2, the remaining 1122 pairs of RAMPs showed a COD less than 0.2. Hence, we expect that when the sensors are deployed, CODs greater than 0.2 signify actual differences in $PM_{2.5}$ concentration and are not due to sensor noise.

Figure 2.4 shows the COD for hourly averaged $PM_{2.5}$ concentrations between each pair of sites. The COD suggests that there is significant spatial heterogeneity across the RAMP network on an hour-to-hour basis. More than half of the pairwise COD values are greater than 0.2. The analyses of Figure 2.2 and Figure 2.3 above focused on the most extreme differences (e.g., site 2 versus all other sites). However, the COD matrix in Figure 2.4 shows that there are also subtle, but meaningful, differences between many more sites, even those within a site class.

4) Figure 2.4 Coefficients of Divergence

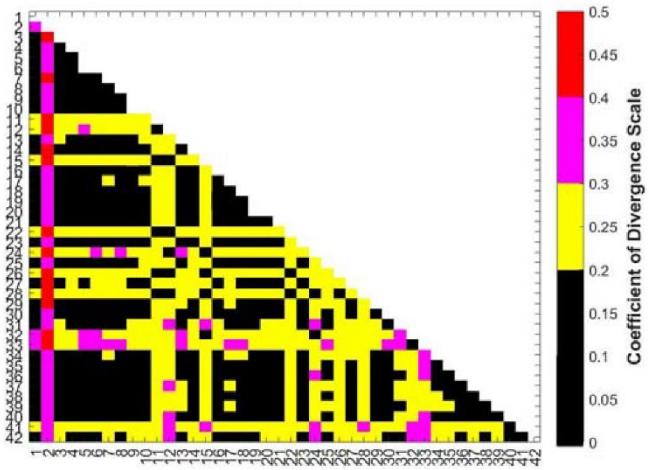

Pairwise hourly coefficients of divergence (COD) for $PM_{2.5}$. As the COD for the majority of pairs is greater than 0.2 there exists heterogeneity on an hourly basis between the sites.

Although we are not able to quantify all of the sources of variability that drive CODs to be greater than 0.2 between site pairs, one source of variability is emissions from local point sources. The CODs between the East of Coke Plant sites and sites not impacted by point sources are for the most part greater than 0.2. As shown in Figure 2.2, emissions plumes can impact different sets of sites at different times, depending on meteorological conditions. Plumes can also advect downwind, and there are examples in our dataset of plumes starting near the Coke plant that eventually impact some, but not all, of the Urban Residential sites. This time lag (in addition to dilution) while plumes travel from one area to another can cause differences in $PM_{2.5}$ concentrations measured on an hourly basis between sites and thus lead to significant differences in hourly averaged $PM_{2.5}$.

2.3.2 Multi-Pollutant Patterns

The gaseous pollutants measured by the RAMPs offer insight into the sources driving the inter-site differences in $PM_{2.5}$ concentrations. In this section, we use NO_2 as an indicator for

traffic emissions and SO_2 as a marker for industrial emissions to aid in describing the $PM_{2.5}$ trends at various site types.

Figure 2.5a shows the average diurnal pattern of $PM_{2.5}$ for each site group. The diurnal patterns at each of the seven study areas (Downtown, Urban Residential, Highway, Near Steel Mill, Suburban Residential, West of Coke Plant, and East of Coke Plant) were determined by averaging the measurements taken at each respective hour of the day for all of the locations within each study area. For the Downtown $PM_{2.5}$ diurnal we ignored site 2, and therefore only site 1 was used. As described above, site 2 is heavily impacted by emissions from a nearby restaurant and therefore may not be representative of the broader downtown area. For the rest of the site groups all sites within the group were included in calculating the diurnals.

5) Figure 2.5 Diurnal patterns of $PM_{2.5}$ and NO_2

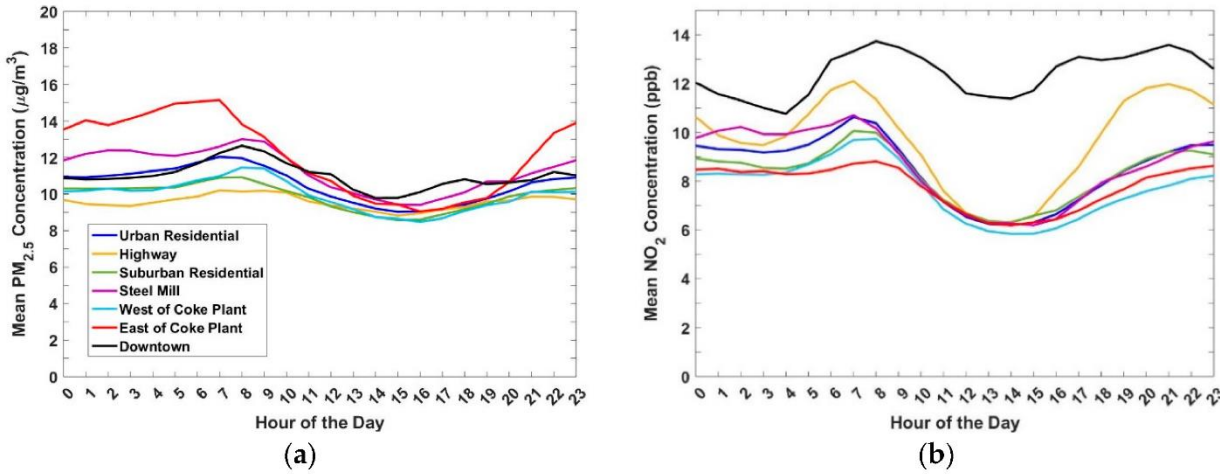

***(a)** Hourly averaged diurnal patterns of $PM_{2.5}$ within each site group. Downtown site 2, which is impacted by emissions from a nearby restaurant, is not included. (**b**) Mean diurnal patterns of NO_2 for each of the site groups. All sites were used because the restaurant near site 2 is not a major NO_2 source.*

Some common trends are observed across the sampling domain. $PM_{2.5}$ concentrations increase in the morning at most sites (~7–9 a.m.). This general trend is mirrored by NO_2 (Figure

2.5b), which also exhibits a domain-wide increase during the morning rush hour. The concurrent morning peaks in $PM_{2.5}$ and NO_2 are indicative of rush hour traffic emissions, combined with low atmospheric mixing height. $PM_{2.5}$ concentrations reach a minimum around 3–4 p.m. as the atmosphere becomes more well mixed. There is no early evening $PM_{2.5}$ enhancement during the evening rush hour at most of the sites.

Figure 2.5 shows that multi-pollutant concentration patterns, and therefore exposure, change throughout the day. In the evening through early morning the East of Coke Plant and Near Steel Mill sites have the highest mean $PM_{2.5}$ concentrations. People who live in these areas are presumably at home during these times, and therefore likely to be exposed to elevated $PM_{2.5}$ relative to other areas in our study domain. However, during the day, Downtown has the highest $PM_{2.5}$ concentrations. This means that someone who lives in one of the areas East of the Coke Plant or Near the Steel Mill but works Downtown could have higher exposures than someone who both lives and works in one of the industrially influenced areas. This has important implications for public health; it may not be enough to incorporate one's residence in exposure assessment, since workday exposures in downtown or other commercial areas may be significantly different than in residential neighborhoods.

There are differences in the diurnal trends and in the absolute concentrations between site groups. For example, all of the sites except for Downtown exhibit a sharp drop in $PM_{2.5}$ concentrations after the morning rush hour. This is driven by a decrease in the traffic source and an increase in atmospheric mixing height. In Downtown; however, $PM_{2.5}$ concentrations decrease more gradually throughout the workday. This can be attributed to elevated traffic emissions throughout the day relative to other areas, along with contributions from street canyon effects and restaurant cooking (Gu, Hugh Z Li, et al. 2018). The measured NO_2 concentrations

suggest that traffic is a driver for the excess $PM_{2.5}$ in downtown. NO_2 in Downtown remains high during the day compared to other site groups and is the only site group (with the exception of the Highway site) that shows an afternoon rush hour peak in NO_2.

The East of Coke Plant sites and Near Steel Mill sites experience some of the highest $PM_{2.5}$ concentrations at all times of the day. The enhancements in mean $PM_{2.5}$ concentration at the East of Coke Plant sites and Near Steel Mill sites are larger in the late evening through early morning than the enhancements observed at any of the other sites. The individual contributions of micrometeorology and higher industrial emissions at night cannot be separated with this dataset and should be investigated in future work. In contrast to the elevated $PM_{2.5}$, NO_2 concentrations at these sites during the day are similar to the Urban and Suburban Residential sites; hence, unlike Downtown, traffic is likely not a significant contributor to the higher PM levels in the area. On the other hand, SO_2 concentrations at the Near Steel Mill and East of Coke Plant sites are frequently elevated above background levels. This suggests that industrial emissions play an important role.

SO_2 measurements were used as a tracer for industrial emissions. Figure 2.6 shows the number of hours for which SO_2 concentrations exceeded 50 ppb (99.8th percentile of SO_2 measurements) at the nine sites near the steel mill and Coke plant. Instances of high SO_2 were most frequent at the East of Coke Plant and Near Steel Mill sites (which are usually downwind), suggesting that emissions from these sources contribute to the occasions of high $PM_{2.5}$ shown in Figure 2.3.

6) Figure 2.6 High SO_2 frequency

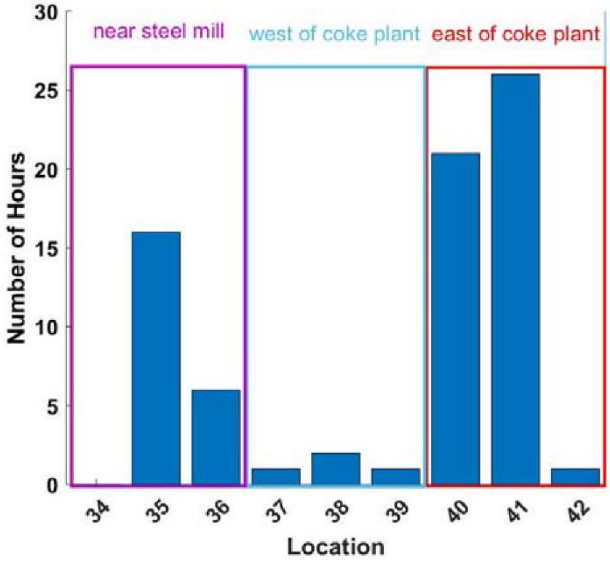

Frequency of high SO_2 concentrations. Bars show the number of hours with SO_2 greater than 50 ppb from November 2017 through May 2018 at the nine sites located near the coke plant and steel mill. Sites downwind of the coke plant have the most frequent occurrences of high SO_2.

We investigated correlations between background-corrected $PM_{2.5}$ concentration and SO_2 concentration to test whether these pollutants have a common source. The background-corrected $PM_{2.5}$ concentration was obtained by subtracting the $PM_{2.5}$ measured at Urban Residential site 5 from the measured $PM_{2.5}$ concentration at the source influenced sites. Background-corrected $PM_{2.5}$ concentration and SO_2 concentrations were normalized for each site and scatter plots for each site are shown in the Supplementary Information (Figure 2.11). The mean R^2 value for correlation between $PM_{2.5}$ and SO_2 for the nine source impacted sites is 0.32 (ranging from 0.16–0.56), compared to near zero correlation at the background sites (R^2 at site 5 = 0.03). In particular, variations in SO_2 explain about 40% of the variation in $PM_{2.5}$ at sites 41

and 42 (East of the Coke Plant sites), which is significantly higher than any of the other source impacted sites. As observed earlier, these two sites also saw significantly higher $PM_{2.5}$ than the Urban and Suburban Residential sites. This suggests that the elevated $PM_{2.5}$ concentrations at sites East of the Coke plant are more heavily influenced by emissions from the Coke plant when compared to the other source impacted sites in the area, and even among sites east (downwind) of the Coke plant, there can be differences that are revealed by a high-density sensor network. The West of Coke Plant sites have lower SO_2 than the East of Coke Plant sites, echoing the results for $PM_{2.5}$ because these sites are often upwind of the source. Furthermore, a regulatory SO_2 reference monitor located at site 5 (Urban Residential) recorded zero hours of SO_2 concentration above 50 ppb during the study period. The overall story is that the industrial emissions drive the elevated $PM_{2.5}$ concentrations in the areas downwind of the Coke and steel plants, not traffic.

Figure 2.6 also shows that there is heterogeneity within the site classes. One of the Near Steel Mill sites (site 34) never experienced SO_2 greater than 50 ppb during the study period. Likewise, site 42 had fewer instances of high SO_2 than sites 40 and 41. Although there are broad similarities in sites with similar land use and nearby sources, there is variability even within site classes. The COD for SO_2 for all site pairs between the nine sites near industrial facilities was greater than 0.2. A plot of the pairwise COD for SO_2 at these nine sites is found in the SI, Figure 2.12. The heterogeneity between SO_2 concentrations within site groupings further demonstrates the utility of a high-density multi-pollutant network.

2.3.3 Exposure Inequality and Environmental Justice

Figure 2.7 examines exposure inequality and environmental justice of $PM_{2.5}$ and NO_2 as a function of two socio-economic variables: percent of the population living below the poverty line

and percent of the population belonging to a minority group. Although there are numerous socio-economic factors available for assessing environmental justice, this study only analyzes these two factors as they are the indicators for environmental justice regions in the state of Pennsylvania. The mean $PM_{2.5}$ concentration for all of the non-EJ sites is 10.3 µg/m^3 (standard deviation = 1.5 µg/m^3) and the mean $PM_{2.5}$ concentration for all of the EJ sites is 10.6 µg/m^3 (standard deviation = 1.0 µg/m^3), which suggests no significant difference in $PM_{2.5}$ concentrations based on EJ status of the census block group.

7) Figure 2.7 Environmental justice analysis

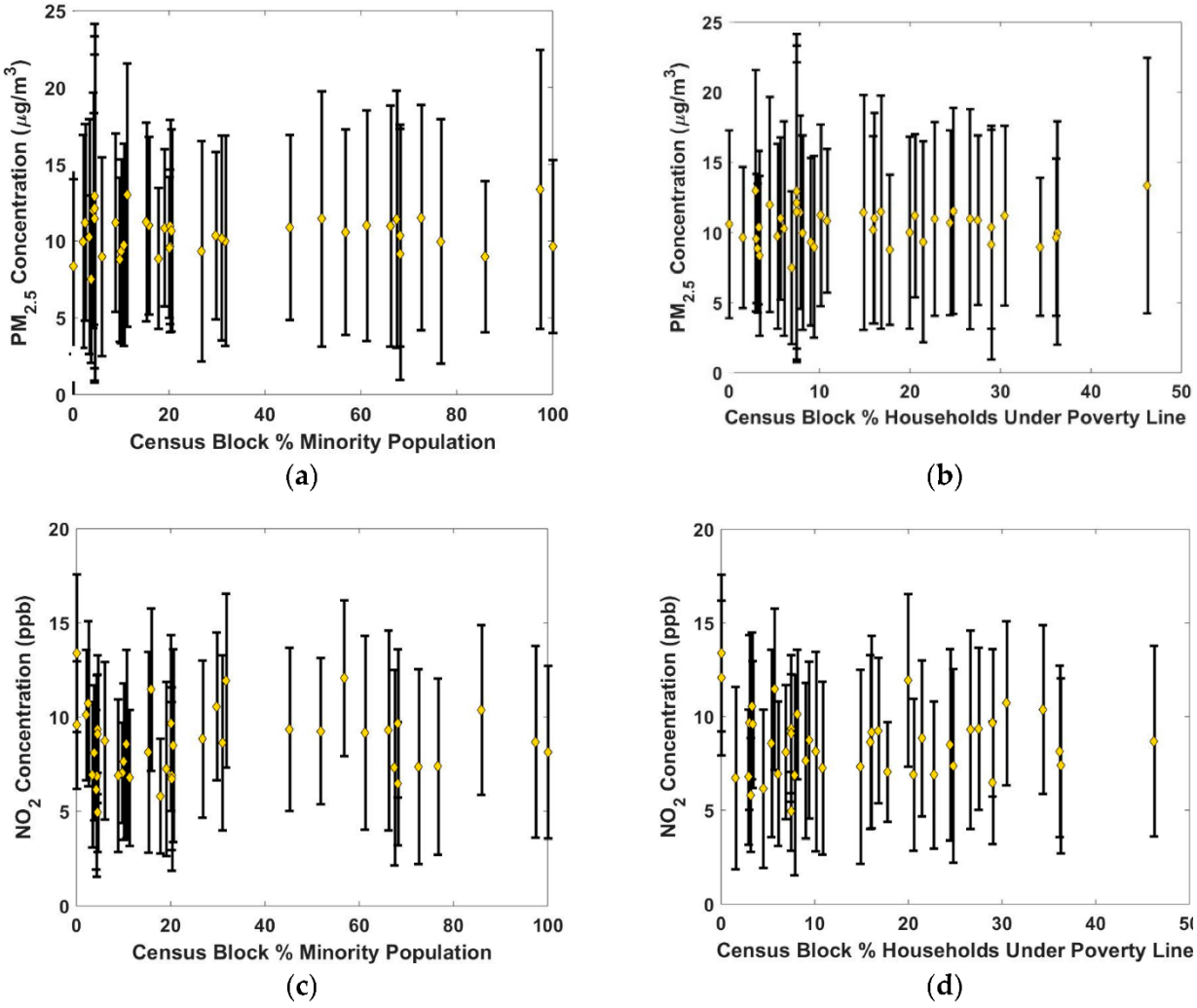

*Environmental justice analysis showing mean (yellow diamond) and standard deviation (whiskers) at each site. Site 2 was not included in the $PM_{2.5}$ analysis due to the impact of the local restaurant emissions at that site. (**a**,**b**) show the lack of correlation between $PM_{2.5}$ concentrations and percent of the population who (**a**) belong to a minority group or (**b**) are living below the poverty line. (**c**,**d**) similarly show the lack of correlation between NO_2 concentrations and the same two socio-economic variables.*

Spearman's rho, a non-parametric measure of rank correlation, can be used to test the relationship between two variables. A Spearman's rho with an absolute value of less than 0.20 is indicative of very weak correlation between the variables, only above 0.60 is the correlation considered strong. The Spearman's rho between mean $PM_{2.5}$ concentration at a site and percent of the population living below the poverty line in the census block group is 0.05. The Spearman correlation between mean $PM_{2.5}$ and percent of the population belonging to a minority group is similarly low (0.01). This means that the relationship between mean $PM_{2.5}$ concentration and socioeconomic (EJ) variables cannot be described by a monotonic function; $PM_{2.5}$ concentration does not increase with increasing EJ indicators.

The Spearman's rho between the mean NO_2 concentrations at the RAMP sites and the socio-economic variables is similarly low; 0.01 and 0.06 when comparing mean NO_2 at a site to percent of the population living under the poverty line and percent minority group, respectively. The mean NO_2 for EJ sites was 8.85 ppb (standard deviation = 1.58 ppb) while the mean NO_2 concentration for non-EJ sites was 8.32 ppb (standard deviation = 2.00 ppb). In other words, NO_2 concentrations are not systematically higher in EJ communities than non-EJ communities within our study domain.

In contrast to our findings, Clark et al. showed strong correlation between EJ communities and elevated NO_2 concentrations and reported that on a national scale the population weighted mean NO_2 concentrations for non-whites were 5 ppb higher than for whites

in 2000 and 2.9 ppb higher in 2010 (Clark et al. 2017). There are several possible explanations for the disagreement of our results with those of Clark et al. One potential explanation is methodological. Clark et al. used a national land use regression model estimate of NO_2 whereas we use a dense network of sensors within the county. We have 42 monitors running in the relatively small study domain, while Clark et al. used a model that was trained on the national EPA monitoring system that only includes two monitors in our domain. Additionally, Clark et al. reported on average trends throughout the nation. There is no requirement that each individual city follow these trends; due to different socio-economic factors, Pittsburgh may not follow the national average trend. For example, several of the Urban Residential sites are located in neighborhoods that are a mix of middle to upper income families and college students. The student population increases the percent of non-white population while decreasing the average income of the areas. There may also be nuanced differences with the ways that minority populations were defined in each study that may have impacts on the results. For example, in our study we simply defined percent minority population as the non-white portion of the population. If we were to break the non-white portion of the population into different subgroups there may be different patterns that arise in our results. Furthermore, many of the EJ areas, as defined by race and income, are typically upwind of industrial facilities and thus less impacted by these emissions.

2.4 Conclusions

A dense network of over 40 lower-cost monitors was deployed within the city of Pittsburgh and surrounding areas in Allegheny County. The dense sensor network was able to detect significant differences in $PM_{2.5}$ concentration between groups of sites within the study domain, and also between sites within a site group with similar characteristics. NO_2 was used as

a tracer for traffic emissions and SO_2 was used as a tracer for industrial emissions. Downtown and near Highway sites experienced elevated $PM_{2.5}$ and NO_2 concentrations that were dominated by traffic emissions. Sites downwind of industrial sources such as the Near Steel Mill sites and East of Coke Plant sites experienced elevated $PM_{2.5}$ concentrations influenced by industrial point sources, indicated by higher SO_2 levels. No relationship was found linking two socio-economic variables to elevated $PM_{2.5}$ or NO_2 concentrations within our sampling network.

Our analysis demonstrates the value of a dense sensor network. Our network is able to capture temporospatial pollutant patterns that cannot be resolved by the sparse network of regulatory monitors. We grouped our sensors into seven categories and observed significant variations both within and between categories. Even if the regulatory monitoring network had one site in each of our seven land-use-based categories (and it does not), it would not be able to capture all of the spatial variations that we present here. Coupling measurements of $PM_{2.5}$ and gases allows us to attribute the observed temporospatial pollutant patterns to specific source classes, which demonstrates the benefit of multipollutant sensor networks.

The approach we use here could easily be replicated in other cities. While the mix of sources may be different—for example, the coke plant is somewhat unique to our sampling domain—networks of multi-pollutant sensors should be capable of capturing pollutant patterns and attributing them to traffic versus other sources.

2.5 Supplemental Information

2.5.1 SO_2 Calibration

In this study we collocated sixteen RAMPs with a reference grade SO_2 monitor (Teledyne T100A) for three months at site 41. This site is less than 1 km east of the coke plant. SO_2 is a known byproduct of coke production. Hourly averaged SO_2 concentrations ranged from

~0 to greater than 100 ppb during the collocation period at site 41, which provided sufficient dynamic range for training calibration models.

Following Zimmerman et al. and Malings et al., we developed both multi-linear regression (MLR) and machine learning based neural network (NN) calibrations for SO_2. The inputs for the MLR model are net SO_2 signal, temperature, and relative humidity measured by the RAMP. The inputs for the NN model were net signal for five gaseous pollutant sensors (SO_2, CO, NO_2, O_3, and CO_2), temperature, and relative humidity.

At the calibration site both the MLR and NN models performed well, with R^2 of 0.60 and 0.75, respectively, for calibration testing. However, when the models were applied to a RAMP at a second collocation site with a reference monitor (site 35) the performance of the NN model drastically dropped (R^2 = 0.11). The MLR model on the other hand maintained acceptable performance (R^2 = 0.54). This decrease in performance by the more complex NN calibration model may be attributed to an overtraining of the model on the source mixture at site 41. This in turn led to less transferability of the NN-based calibration. Therefore, the MLR calibration model was used here.

8) Figure 2.8 Seasonal data coverage

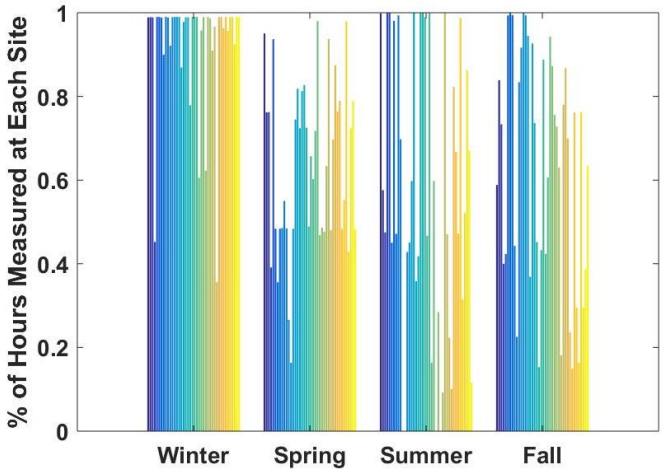

42 vertical bars are shown for each RAMP in each season. The heights of the bars indicate the percent of hours measured in each season at each of the 42 RAMP sites. These 42 sites were sub selected down from an original list of 77 RAMPs to include only sites that were collecting data for at least half of a year (4380 hours) during the study period. Good seasonal coverage was obtained using this dataset. The median coverage per season per RAMP was 69% of the season covered.

1) Table 2.1 RAMP locations

Identifier	Area	Type of PM monitor
1	Downtown	MetOne
2	Downtown	MetOne
3	Urban Residential	MetOne
4	Urban Residential	MetOne
5	Urban Residential	MetOne
6	Urban Residential	MetOne
7	Urban Residential	MetOne
8	Urban Residential	MetOne
9	Urban Residential	MetOne
10	Urban Residential	MetOne
11	Urban Residential	MetOne
12	Urban Residential	MetOne
13	Urban Residential	MetOne
14	Urban Residential	MetOne
15	Urban Residential	MetOne
16	Urban Residential	MetOne
17	Urban Residential	MetOne
18	Urban Residential	MetOne
19	Urban Residential	MetOne
20	Urban Residential	MetOne
21	Urban Residential	MetOne
22	Urban Residential	MetOne
23	Highway	MetOne
24	Suburban Residential	MetOne
25	Suburban Residential	MetOne
26	Suburban Residential	Purple Air
27	Suburban Residential	MetOne
28	Suburban Residential	Purple Air
29	Suburban Residential	MetOne
30	Suburban Residential	MetOne
31	Suburban Residential	MetOne

32	Suburban Residential	MetOne
33	Suburban Residential	Purple Air
34	Steel Mill	MetOne
35	Steel Mill	MetOne
36	Steel Mill	MetOne
37	West of Coke Plant	MetOne
38	West of Coke Plant	MetOne
39	West of Coke Plant	MetOne
40	East of Coke Plant	MetOne
41	East of Coke Plant	MetOne
42	East of Coke Plant	MetOne

Each site was assigned to an area grouping and a number from 1 to 42. The last column indicates whether the RAMP's $PM_{2.5}$ monitoring device was a MetOne nephelometer or a PurpleAir laser sensor.

9) Figure 2.9 Seasonal $PM_{2.5}$ concentrations

(a)

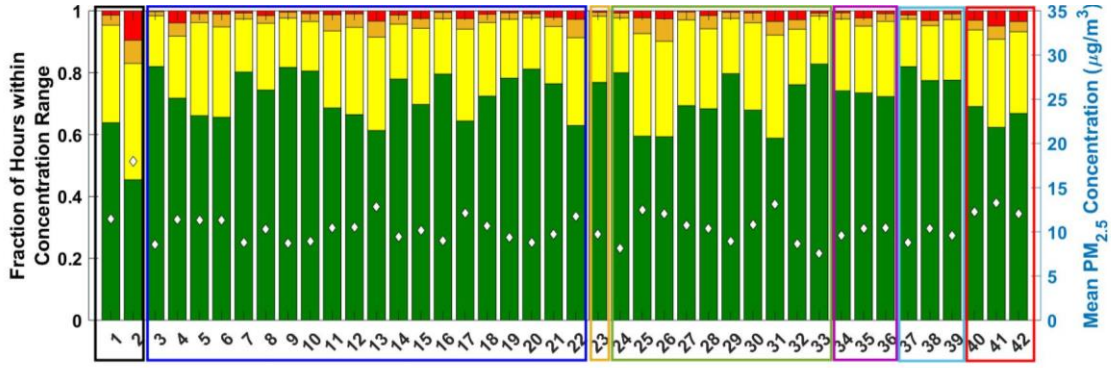

(b)

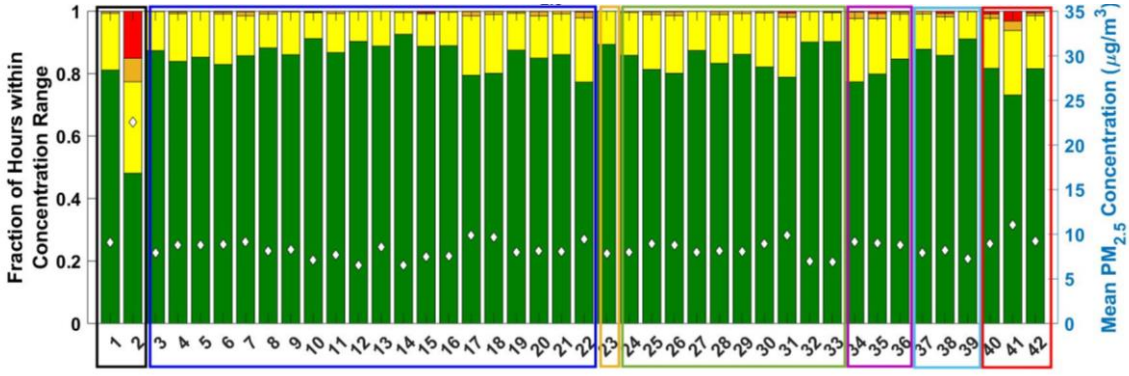

(c)

(d)

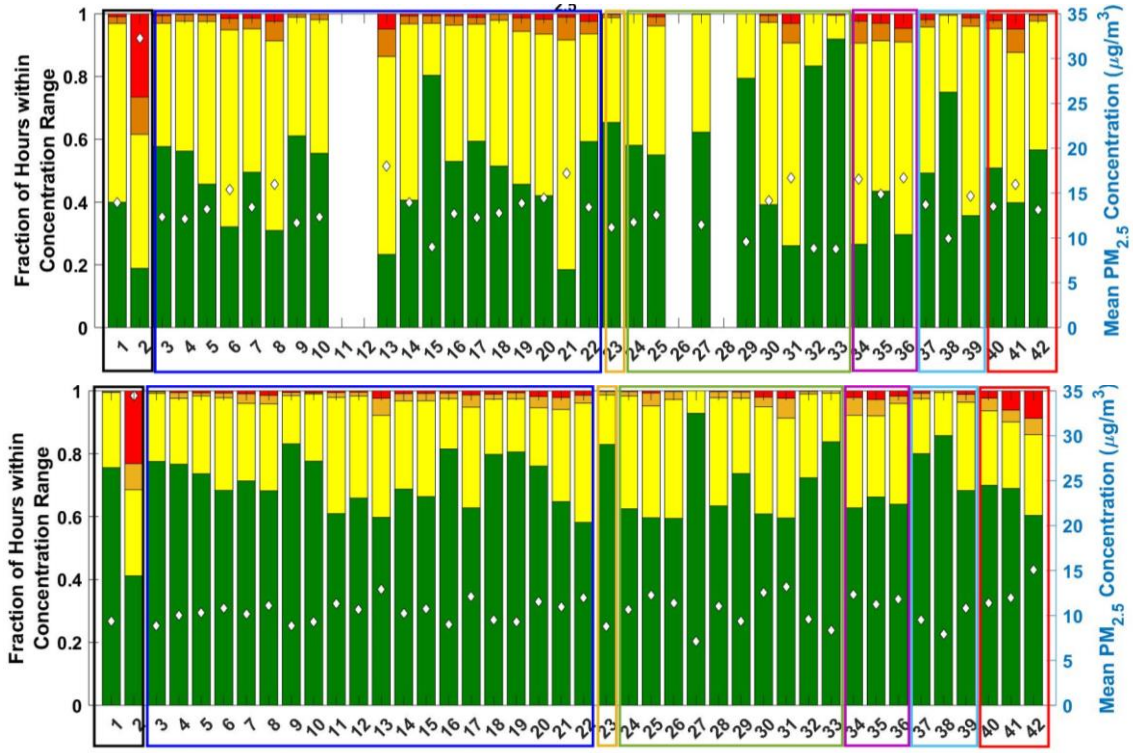

Green bars are fraction of hours with $PM_{2.5}$ concentration less than 12 μg/m^3, yellow bars [12-25) μg/m^3, orange bars [25-35) μg/m^3, and red bars are fraction of hours greater than or equal to 35 μg/m^3. The data from Figure 3 in the text was subdivided by season to differentiate the seasonal differences in $PM_{2.5}$ at each site for (a) winter, (b) spring, (c) summer, and (d) fall.

10) Figure 2.10 Co-located RAMP variability

48 RAMPs were collocated at site 7. The hourly averaged COD for each pair of sensors at this collocation was calculated and all but 6 pairs had insignificant differences in measurement from the other

sensors. From this we conclude that the differences in COD that are shown in Figure 4 can be attributed to actual differences in measured $PM_{2.5}$ and not sensor noise.

11) Figure 2.11 Relationship between excess $PM_{2.5}$ and SO_2

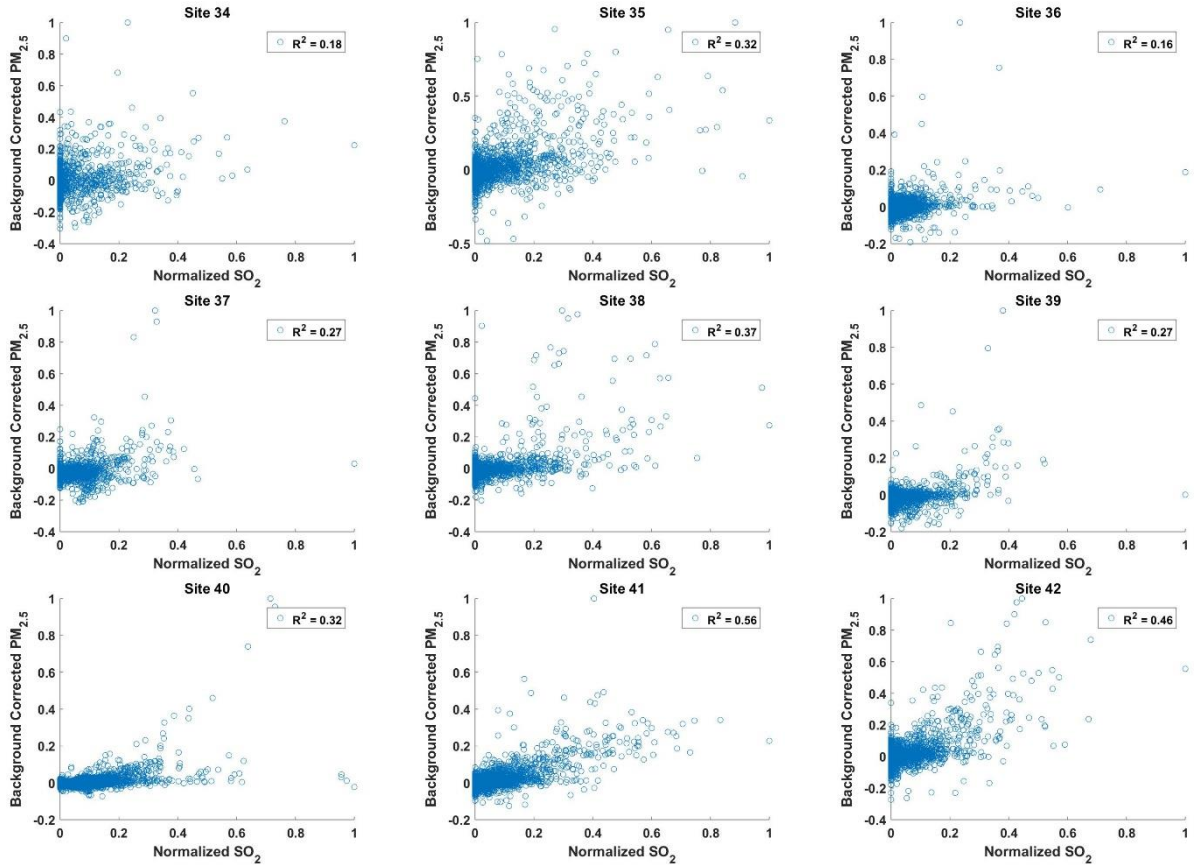

The background corrected $PM_{2.5}$ concentration was calculated for each site by subtracting the $PM_{2.5}$ concentration measured at an Urban Residential site (site 5) from the source influenced sites. The hourly averaged background corrected $PM_{2.5}$ concentrations were then normalized and correlated to the normalized SO_2 measurements at each of the sites near industrial facilities. Two sites downwind of the coke plant (sites 41 and 42) show the strongest correlation between $PM_{2.5}$ and SO_2 indicating that the elevated $PM_{2.5}$ concentrations at those locations are heavily influenced by SO_2 carrying industrial emissions.

12) Figure 2.12 SO_2 variability

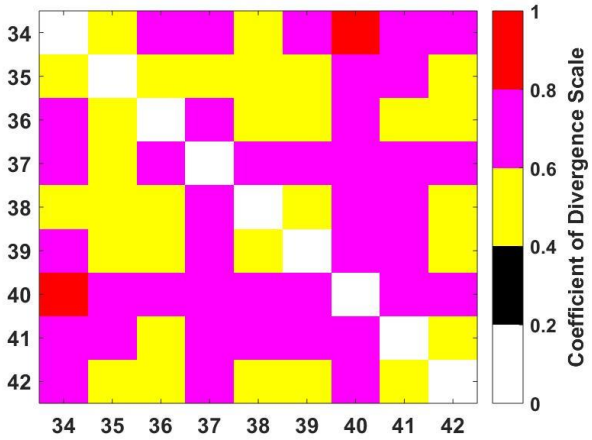

The COD plot for SO_2 concentrations at the nine sites near the industrial facilities (Near Steel Mill, East of Coke Plan, and West of Coke Plant) demonstrates that there are significant differences (COD>0.2) in SO_2 concentration between sites influenced by these point sources.

13) Figure 2.13 Wind measurements

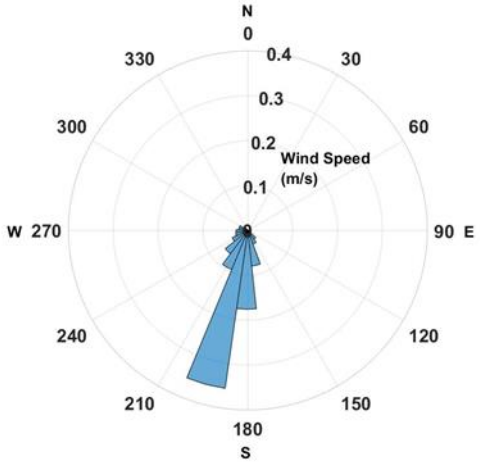

Wind measurements were taken using an RM Young 81000 Sonic Anemometer from January 2018 through December 2018. An exemplary one-month subset of this data is displayed in the wind rose showing one-minute averaged measurements of wind direction and speed. The prevailing wind direction throughout the study domain was from southwest to northeast.

Chapter 3

Utilization of a Low-Cost Sensor Network

***Contents of this chapter have been published as**: Tanzer-Gruener, R., Li, J., Eilenberg, S.R., Robinson, A.L., Presto, A.A., 2020. Impacts of modifiable factors on ambient air pollution: a case study of COVID-19 shutdowns. Environ. Sci. Technol. Lett. 7 (8), 554–559. https://doi.org/10.1021/acs. estlett.0c00365.*

3.1 Introduction

Sources of urban ambient air pollution are generally associated with human activities such as traffic, cooking, and electricity generation. These sources are modifiable factors; emissions can be modulated either by changing activity levels or the source intensity. Air pollution regulation in the U.S. has traditionally relied on reducing emission factors rather than curbing activity. Although previous studies have assessed impacts of event-related step changes in emission sources on air quality, (Friedman et al. 2001; Heinrich et al. 2002; Ransom and Pope III 1995; Rich et al. 2015) social distancing measures implemented in response to COVID-19 offer a natural experiment to observe and quantify the impacts of modifiable factors, specifically large shocks to activity, on ambient air pollution in real-time with an unprecedented scope, speed, and duration.

In March 2020, 48 U.S. states implemented precautions to limit transmission of COVID-19. (Sergent et al. 2020) In many cases, these measures represented a step-change in activity and accompanying pollutant emissions. This study focuses on data collected in Pittsburgh, Allegheny County, PA, which is representative of the rapid changes in activity associated with social distancing measures. A timeline of the closures affecting Pennsylvania and the upwind state of Ohio can be found in Table 3.2 in the Supplemental Information (SI) and show that activity was

"business as usual" through March 13 (Bosco 2020; Kiser 2020; Parsons 2020; Williams 2020; Wolf 2020a) and rapidly transitioned to lower activity, with the majority of schools and non-essential businesses closed or operating in reduced capacity by March 16.

The closing of schools and businesses has a clear impact on activity levels and therefore air pollutant emissions. In this paper, we use data from both a distributed network of low-cost air pollutant sensors and the Environmental Protection Agency (EPA) regulatory network to examine how changes in activity impacted ambient air pollution. We compare concentrations of fine particulate matter ($PM_{2.5}$; for which Allegheny County has been at least partially in nonattainment since 1997 (Pennsylvania Department of Environemental Protection, 2016)), CO, and NO_2 from the post-COVID shutdown period (March 14-April 30, 2020) to business as usual periods in 2019 and 2020.

3.2 Materials and Methods

CO and $PM_{2.5}$ were measured using a distributed network of low-cost sensors. The Real-time Affordable Multi-Pollutant (RAMP) sensor package has been deployed throughout the city of Pittsburgh and surrounding suburbs since 2016. (Zimmerman et al. 2018) The RAMPs use electrochemical sensors (AlphaSense LLC) to measure CO. $PM_{2.5}$ is measured via light scattering using either MetOne Neighborhood Monitors or PurpleAir PA-IIs. Previous work details the calibration (Malings et al. 2019) and deployment (Subramanian et al. 2018; Tanzer et al. 2019; Zimmerman et al. 2020) of these sensor packages.

In March 2020 there were 27 active RAMP sites in the Pittsburgh region (locations shown in Figure 3.3). The RAMP sites were grouped into 4 categories based on land-use: High Traffic (n = 3), Urban Residential (n = 11), Suburban Residential (n = 8), and Industrial (n = 4).

Site groupings were determined according to the same methodology as was used in previous work (Tanzer et al. 2019) and are described in detail in the SI.

One concern with low-cost pollutant sensors is measurement uncertainty. (Castell et al. 2017; Cross et al. 2017; Eilenberg et al. 2020; Hagan et al. 2018; Snyder et al. 2013) We have previously shown that mean absolute error relative to a reference measurement in hourly averaged CO measurements is $\pm$49ppb. (Zimmerman et al. 2018) Uncertainty in $PM_{2.5}$ is a strong function of averaging time; 1-hr data has a relatively large uncertainty (~4µg/m^3) that falls to <1µg/m^3 after sufficient averaging time. (Eilenberg et al. 2020; Malings et al. 2019) In this paper grouping sites increases effective averaging time, reducing uncertainty to 0.6µg/m^3. (Eilenberg et al. 2020)

To supplement the RAMP data, EPA Air Quality System (AQS) data collected by the Allegheny County Health Department (ACHD) from two NO_2 sites was also analyzed (one High Traffic site, one Suburban Residential; shown in Figure 3.3).

To quantify traffic reduction we compared traffic camera data on Interstate 376, a main commuter highway, in March 2020 (post-closures) to historical vehicle counts (pre-closures) during the same time of day (8am: morning rush-hour). We estimate that rush-hour commuter vehicle traffic decreased by 48%. This estimate is consistent with Google mobility data which estimates that in Allegheny County workplace related mobility decreased by 45%. (Google LLC 2020)

3.3 Results and Discussion

3.3.1 Concentration reductions due to activity changes

Figure 3.1 and Table 3.3 compare CO and $PM_{2.5}$ concentrations for pre- and post-COVID periods. Overall, concentrations during the pre-COVID period in 2020 (March 1-13) are similar

to the same period in 2019. March 2019 concentrations are shown as box plots and cumulative distribution functions (CDFs) in Figure 3.1. The data in Figure 3.1 suggest that the main emission sources and atmospheric conditions were similar between 2019 and 2020 before social distancing.

CO and $PM_{2.5}$ concentrations are lower during the post-COVID period (March 14-April 30, 2020) compared to the "business as usual" periods in both 2019 and 2020. For example, across the entire RAMP network, mean $PM_{2.5}$ concentrations were 29% (~3µg/m^3) lower following the COVID-related closures (6.7µg/m^3) compared to March 2019 (9.5µg/m^3).

We treat CO as a marker of fresh combustion emissions from vehicular traffic and industrial activity. At the High Traffic and Urban Residential sites, traffic is the dominant source of CO. The CO timeseries at these site groups is punctuated by occasional traffic-related spikes; these spikes decreased by 19% (High Traffic) and 23% (Urban Residential) post-closures. The reduced frequency of high CO spikes is also evident in the CDFs. Median CO is identical for High Traffic and Urban Residential for pre- and post-COVID, but the mean and 90th percentile concentration at High Traffic sites are 19% and 38% lower, respectively, because of a lower frequency of high concentration events.

The impact of traffic on the High Traffic and Urban Residential sites is also evident in the diurnal patterns in Figure 2. Pre-COVID there is a clear increase in CO concentrations between an overnight stable period (2-3am) and the morning rush hour (7-8am). During the post-COVID period, both the absolute peak CO and the intra-day difference attributable to traffic are smaller.

NO_2, which is also a marker for traffic emissions, shows a similar pattern as CO (Figure 3.5). Concentrations are lower and less variable, and the morning rush-hour enhancement is smaller in the post-COVID period when compared to March 2019.

The Industrial sites also have frequent spikes in CO (Figure 3.1), though these are dominated by industrial emissions. These industrially driven CO spikes persist in the post-COVID period. The CDFs in Figure 3.1 are indistinguishable for pre- and post-COVID, suggesting that the industrial sites continued emitting post-COVID closures.

14) Figure 3.1 Hourly averaged $PM_{2.5}$ and CO

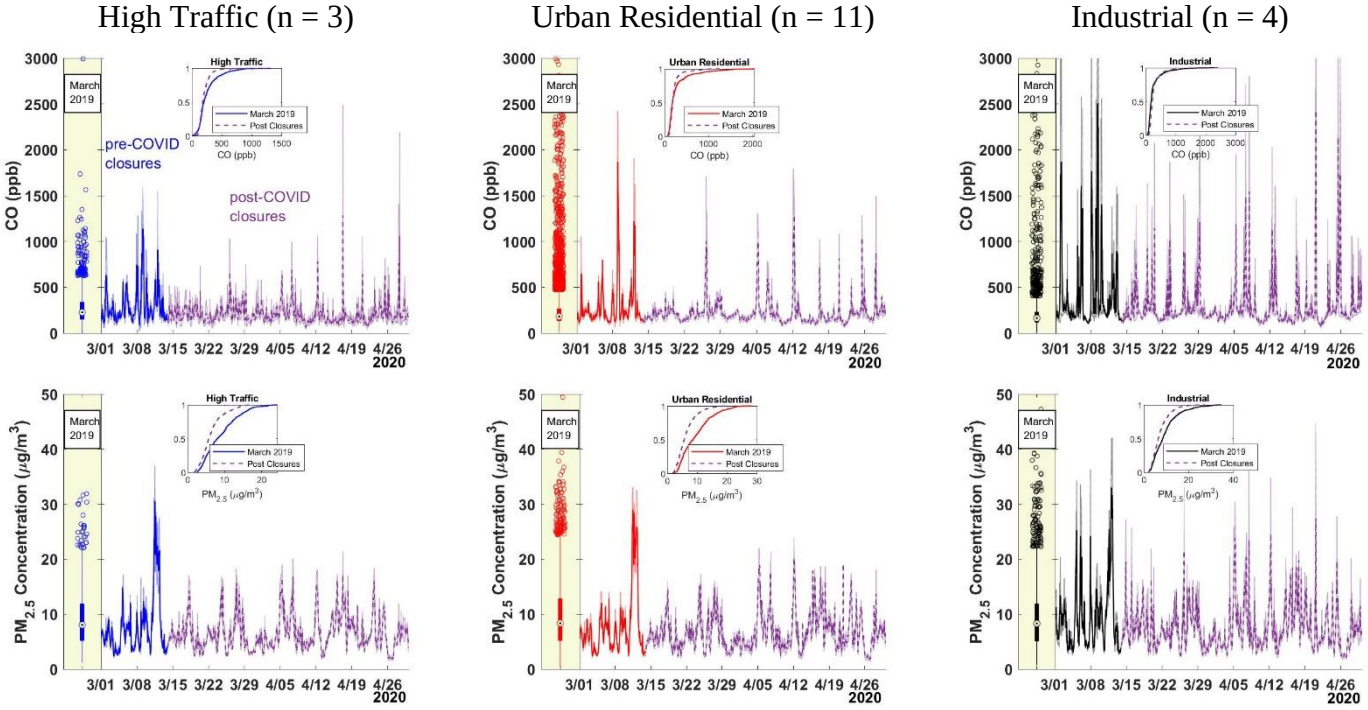

Hourly average concentrations of $PM_{2.5}$ and CO for three of the site groupings during March-April 2020. Suburban Residential sites are shown in Figure S2 in the SI. The solid (pre-COVID closures) and dashed (post-COVID) lines are the mean concentrations for all the sites in each group. The shaded area around each line represent the 25th and 75th percentiles of the data from the site groups. The boxplots show the corresponding March 2019 data for all sites in each site group. The center of the boxes (indicated by a dot) is the median. The boxes show the interquartile range. The whiskers represent 2.7 standard deviations and the outliers are shown as circles. The insets in each panel show the cumulative distribution function (CDF) for the data from March 2019 compared to the data from March and April 2020 after the COVID-related closure.

Figures 3.1 and 3.2 show similar trends for $PM_{2.5}$ as CO. Concentrations during the pre-COVID period in 2020 are similar to March 2019. Concentrations in the post-COVID period are lower and less variable. For example, Figure 3.2 shows that for the High Traffic sites the $PM_{2.5}$

increase associated with the morning rush hour fell from 1.4 µg/m^3 in 2019 to zero in the post-COVID period.

Figure 3.2 shows that the majority of the $PM_{2.5}$ enhancement at the industrially influenced sites occurs at night, consistent with previous studies. (Tanzer et al. 2019) This is because of a combination of emissions and boundary layer height. During overnight hours, the boundary layer is low. Many sources, such as traffic, have less activity overnight, whereas the steel mill and coke plant impacting the industrial sites operate 24 hours. Thus, there are local enhancements of $PM_{2.5}$ overnight at the Industrial sites. (Presto et al. 2016; Weitkamp et al. 2005) Although $PM_{2.5}$ concentrations decreased at the Industrial sites in the post-COVID compared to pre-COVID periods (24% reduction), these sites still had higher concentrations than all other site groups suggesting industrial activity continued during the shutdown.

15) Figure 3.2 $PM_{2.5}$ and CO diurnal patterns

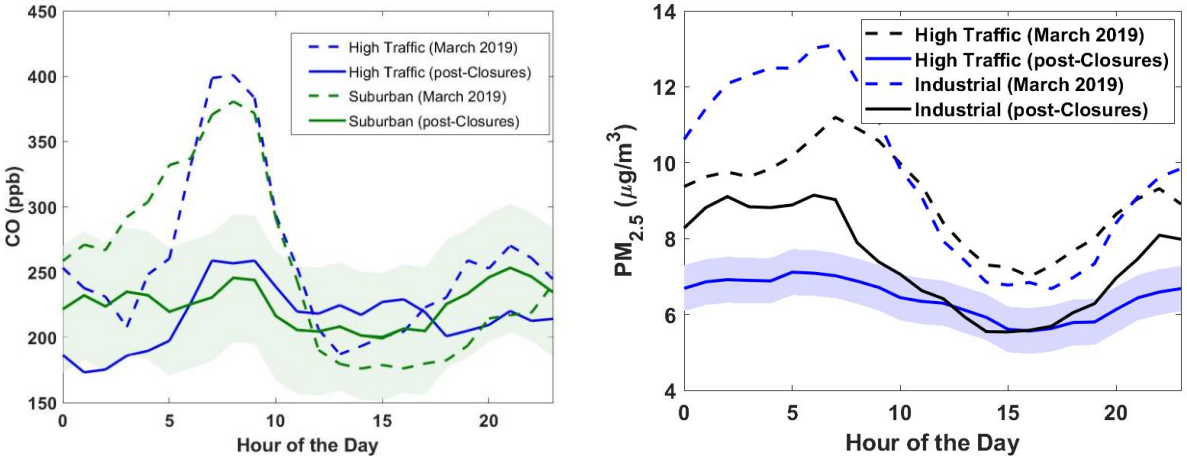

Average diurnal patterns for selected site groups for CO (left) and $PM_{2.5}$ (right). Dashed lines show the pre-closure diurnal patterns from March 2019 and the solid lines show the 2020 post-COVID period. The shaded areas around the lines for the Suburban post-closure (left) and High Traffic post-closure (right) diurnal indicate the instrument uncertainty for each instrument (0.6 µg/m^3 and 49 ppb for $PM_{2.5}$ and CO, respectively). Intra-day variability in CO and $PM_{2.5}$ concentrations decreased drastically following the COVID-related closures.

There are several potential challenges when attributing the observed changes in pollutant concentrations (Figures 3.1 and 3.2) to activity changes for specific sources. (Boogaard et al.

2017) One challenge is decoupling changes attributable to sources from changes in meteorology. We benchmarked the pre- and post-COVID periods to historical weather data from NOAA and sounding data (Oolman 2020) (Figure 3.6 and Table 3.4 in the SI.) (Current Results 2020; National Centers for Environmental Information 2020)

A second challenge is how to define the base case (i.e., the period without impacts of COVID). Our analysis above compares the post-COVID period in 2020 to both pre-COVID 2020 (March 1-13) and March 2019. Figures 3.8 and 3.9 show that annual average $PM_{2.5}$ concentrations in Pittsburgh have been nearly constant since 2012, and that $PM_{2.5}$ concentrations measured at 27 of 30 RAMPs operating in 2018 and 2019 did not have statistically significant differences between years. Thus, our overall conclusions should not be strongly impacted by the choice of base case.

One additional challenge with attributing $PM_{2.5}$ reductions to changes in human activity is that the majority of $PM_{2.5}$ mass is secondary. (Jimenez et al. 2009; Robinson et al. 2007) In the following section, we compare intra-day variations in enhancements associated with local emissions, to minimize influences of outside factors (i.e. upwind emissions, boundary layer height, and weather) that may confound comparisons between the pre- and post-COVID periods.

3.3.2 Changes in source-related intra-day enhancement of pollutant concentrations

We defined two intra-day enhancements which focus on traffic and industrial-related emissions (Table 3.1). We define the traffic-related enhancement as the difference between the morning rush-hour peak (mean 7-8am) and the overnight stable period with a minimum in traffic volume (mean 2-3am) for $PM_{2.5}$, CO, and NO_2 for pre-COVID (n = 31 days) and post-COVID (n=48 days). The differences are averaged across all sites in each group. The industrial enhancement is defined as the difference between the overnight mean (2-4 am) for each of the

Industrial group sites and the mean of the five Suburban Residential sites with the lowest concentrations. As with the traffic enhancement, the industrial enhancement is calculated daily for each of the Industrial sites and then averaged for the site group.

2) Table 3.1 Traffic and industrial enhancements

	Site Group	Pre-COVID Traffic Related Intra-day Enhancement	Post-COVID Traffic Related Intra-day Enhancement		Pre-COVID Industrial Related Intra-day Enhancement	Post-COVID Industrial Related Intra-day Enhancement
$PM_{2.5}$ ($\mu g/m^3$)	*High Traffic*	**1.4**	0.0		n/a	n/a
	Urban Residential	**1.4**	0.2		n/a	n/a
	Suburban	**1.2**	-0.2		n/a	n/a
	Industrial	0.4	-0.5		**2.8**	**1.7**
CO (ppb)	*High Traffic*	**180**	**89**		n/a	n/a
	Urban Residential	**86**	41		n/a	n/a
	Suburban	**96**	25		n/a	n/a
	Industrial	**104**	-25		**82**	**110**
NO_2 (ppb)	*High Traffic*	**8.2**	**4.1**			
	Suburban	**2.8**	**0.4**			

Intra-day source specific concentration changes associated with traffic and industrial emissions at each site group. The traffic enhancements for $PM_{2.5}$ and CO were calculated for all four site groups. NO_2 data was only available for two ACHD sites. Industrial enhancements were only computed for the Industrial sites. Enhancements larger than the instrumental uncertainties are shown in bold font.

For all site groups, the pre-COVID traffic enhancements of NO_2 and CO scale with traffic intensity. CO enhancements are largest at the High Traffic sites (180 ppb), approximately double the enhancement at the other site groups (86-104ppb $\pm$49ppb). The correlation between land-use (i.e., traffic volume) and traffic-related CO enhancements, along with the fact that CO is non-reactive, (Möllmann-Coers et al. 2002) supports the use of CO as a tracer for traffic

emissions in these locations. NO_2 traffic enhancement at the High Traffic ACHD site was 8.2 ppb (±0.05ppb) compared to 2.8 (± 0.2) ppb at the Suburban site.

The traffic enhancements fell after COVID closures. Enhancements of CO and NO_2 fell at High Traffic sites by 50%; this is consistent with the observed 48% reduction in commuter traffic. Morning CO enhancements fell to nearly zero in Suburban areas (96 to 25 [±49] ppb), suggesting a larger fractional reduction in traffic volumes in those areas, consistent with people working and schooling from home. The traffic CO enhancement became negative in Industrial areas, meaning that concentrations at 7-8am were lower than 2-3am, possibly from dilution as the boundary layer grows coupled with reduced emissions.

$PM_{2.5}$ enhancements during the morning rush-hour in the pre-COVID period were more uniform across site groups. For High Traffic, Urban Residential, and Suburban Residential groups, the morning rush-hour $PM_{2.5}$ enhancement was 1.2-1.4μg/m^3, suggesting that traffic impacts on $PM_{2.5}$ are broadly distributed. There is a regional increase in morning $PM_{2.5}$, consistent with the more regional nature of $PM_{2.5}$. (Jimenez et al. 2009; Li et al. 2016; Robinson et al. 2007; Tang et al. 2004) In the post-COVID period the $PM_{2.5}$ morning traffic enhancements for all site groups are within instrument uncertainty of zero. Enhancements decreased by 0.4-1.4μg/m^3, demonstrating the regional impact of traffic on $PM_{2.5}$.

The overnight industrial $PM_{2.5}$ enhancement at Industrial sites was 2.8μg/m^3 in the pre-COVID period and 1.7 μg/m^3 post-COVID. Thus, during both pre- and post-COVID, there is a $PM_{2.5}$ enhancement at Industrial sites that is larger than the measurement uncertainty (0.6μg/m^3). The corresponding CO industrial enhancement (82 ppb pre-COVID, 110 ppb post-COVID) was also larger than instrument uncertainty in both periods. Thus, while operations at the industrial sources may have changed between pre- and post-COVID, our measurements indicate that these

sources remained in operation in the post-COVID period. This observation is consistent with the fact that processes related to steel manufacturing were included on the list of essential businesses in Pennsylvania. (Wolf 2020b)

The intra-day differences shown in Table 3.1 are defined based on diurnal changes in measured pollutant concentrations. The results shown here may be sensitive to the specific times used to define these intra-day variations. However, the sensitivity analysis in Figure 3.7 shows that the pattern across site groups do not change when different sets of hours are used to calculate the enhancements.

3.4 Implications

Our data show a clear decrease in air pollution especially during the morning rush hour traffic driven in large part by reductions in vehicle traffic. While the COVID-related shutdowns are unprecedented and do not likely represent the new status quo, they can offer insights into air pollution under future emissions scenarios. Figure 3.2 and Table 3.1 suggest that a 50% reduction in vehicle emissions (e.g., via tighter emissions standards or widescale adoption of electric vehicles) could essentially eliminate the morning rush hour peak in $PM_{2.5}$, CO, and NO_2. This could reduce acute exposures, especially in high traffic or near-road environments.

In addition to traffic activity reductions, we also estimated reductions in restaurant activity and electricity consumption as described in the SI. However, determining the impacts of reductions in restaurant emissions and electricity generation on measured pollutant concentrations are more difficult. Neighborhoods with high restaurant impacts experience an additional ~1μg/m^3 of $PM_{2.5}$ compared to areas with low restaurant activity. (Gu, Hugh Z. Li, et al. 2018) Our estimated change in restaurant activity using Google mobility data and observations of restaurant hours (~60%) would drop this impact to ~0.4μg/m^3. However, the

RAMP network does not have sufficient sites in high- and low-restaurant areas to examine this impact in greater detail. Impacts of changes in electricity demand are also difficult to determine directly from our data, as much of the $PM_{2.5}$ from power plants is in the form of secondary sulfate. (Morris et al. 2013) Upwind changes in power plant emissions would therefore be convolved with changes in other upwind emissions and weather patterns. Reductions in electricity generation and restaurant emissions may contribute to the lower overnight background concentrations observed in the post-COVID period.

The most recent policy assessment review for the $PM_{2.5}$ National Ambient Air Quality Standards (NAAQS) recommended a revision to the annual $PM_{2.5}$ NAAQS to as low as 9μg/m^3. Such a reduction is estimated to reduce the $PM_{2.5}$ related mortality rate by 21-27%. (US EPA 2019) The Pittsburgh domain considered here has an annual average $PM_{2.5}$ concentration of 9.5μg/m^3. While evaluating the full impact of vehicle traffic on $PM_{2.5}$ requires a more thorough assessment of impacts on primary and secondary $PM_{2.5}$, we can use the observed changes in the morning rush hour peak to make a first-order estimate for the impacts of major changes to vehicle emissions on the annual average $PM_{2.5}$. Table 3.1 shows that the morning rush hour peak enhancement fell from 1.4 μg/m^3 to ~0 μg/m^3. This translates to a reduction of 0.12 μg/m^3 in the daily average $PM_{2.5}$ concentration, which would account for a third of the necessary reduction to reach a hypothetical 9 μg/m^3 standard. Thus, reductions beyond morning rush-hour traffic emissions may be needed to reach 9 μg/m^3 in urban areas.

3.5 Supplemental Information

3) Table 3.2 COVID closure timeline

Date	State	Event
6-Mar-20	PA	First two confirmed COVID-19 cases in the state.

9-Mar-20	OH	Governor DeWine declares a state of emergency.
12-Mar-20	OH	Announcement that all K-12 schools are to be closed starting Monday, March 16th.
12-Mar-20	OH	Ban on gatherings of more than 100 people.
13-Mar-20	PA	Announcement that all K-12 schools are to be closed starting Monday, March 16th.
15-Mar-20	OH	All bars and restaurants are to be closed starting at 9pm.
19-Mar-20	PA	Statewide shutdown of all non-life sustaining businesses starting March 21st.
22-Mar-20	OH	Statewide stay-at-home order announced.

Timeline of COVID-19 related closures in the state of Pennsylvania where this study takes place and the upwind state of Ohio where regional emissions measured in Pittsburgh historically originate from.

3.5.1 Site Groupings

The 27 RAMP sites were broken down into 4 categories: High Traffic (n = 3), Urban Residential (n = 11), Suburban Residential (n = 8), and Industrial (n = 4). This breakdown only equals 26 sites, the 27th site was not included in any site group because it did not properly fit into any category as it was a much more background, rural location. It was however used to aid in background correction calculations, so we include this RAMP in our network count. Briefly, the High Traffic sites are located either in downtown Pittsburgh or along major highways, Residential sites are classified either as Urban (within the City of Pittsburgh boundaries) or Suburban (outside of the city's boundaries), and Industrial sites are downwind of either a large metallurgical coke plant (n = 2) or an integrated steel mill (n = 2).

The classifications of the four site groups were based off of the vehicle density within a 100-meter radius and restaurant density within a 500-meter radius of the site. Values of vehicle and restaurant density were normalized by dividing the densities at each site by the maximum

value across the entire sampling network for each variable. High Traffic sites included both two downtown and one near highway site. The downtown sites are located in the central business district and were in the top 30% of vehicle and restaurant densities while the highway site was located within 10 meters from the edge of a limited-access highway.

Urban Residential sites were located within the city limits and had moderate traffic density (below the 60th percentile) along with low restaurant density (within the first quartile). Suburban Residential sites were those sites that were located outside of the city limits and experienced low vehicle and restaurant densities (within the first quartile). As the names suggest, the Urban and Suburban Residential sites were located in residential and mixed-use neighborhoods, typically at private residences or public schools. Sites classified as Industrial were defined by proximity to industrial point sources. Two of the sites were within 1500 meters of a steel mill and the remaining two were within 1500 meters of a metallurgical coke plant. These sites were east, and therefore generally downwind of, the respective point sources

16) Figure 3.3 Map of RAMP sites

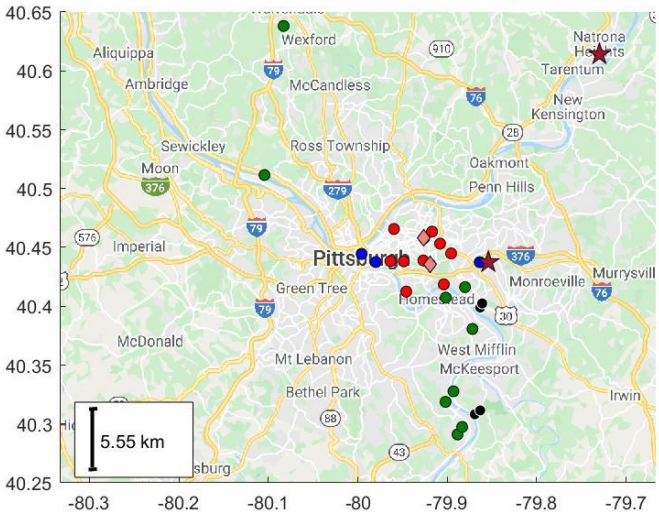

The map (generated using a Google API and MATLAB) shows the locations of air quality monitoring sites within the city of Pittsburgh and the surrounding areas where the air quality monitoring sites used in this study are located. The circles and two diamonds indicate locations

of CO and $PM_{2.5}$ monitoring by RAMP monitors. The blue dots are the locations of the High Traffic sites (n = 3), the red dots and red diamonds are the Urban Residential sites (n = 11), the green dots are the background and Suburban Residential sites (n = 9), and the black dots are the Industrial sites (n = 4). The five Suburban Residential sites with the lowest $PM_{2.5}$ concentrations were used to calculate background concentrations at the Industrial sites. For the Urban Residential sites two locations are indicated by diamonds instead of circles because those two sites were operational throughout March 2020, but they were not running in March 2019. Therefore, no data was available for those locations to determine changes in concentration for site specific calculations. The two maroon stars indicate the two Allegheny County Health Department (ACHD) sites where NO_2 data was collected.

17) Figure 3.4 CO and $PM_{2.5}$ at suburban sites

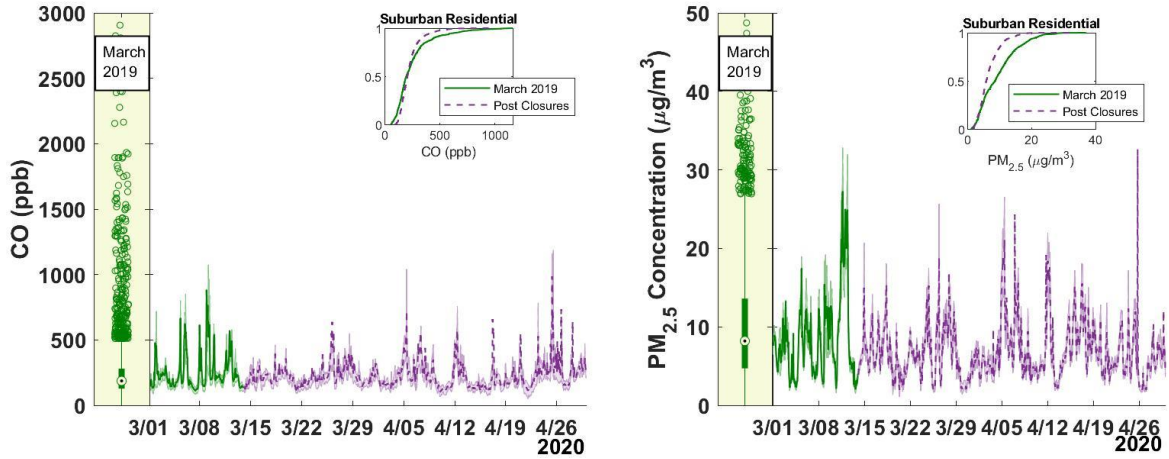

Shown are timeseries of the March 2020 CO and $PM_{2.5}$ data for the Suburban Residential sites not included in the main text. As in Figure 1 in the main text, the dashed purple lines in each of the timeseries indicate the concentrations corresponding to the time period after the COVID-19 related closures began. The solid and dashed lines in the timeseries plots are the mean concentrations for all the sites in the Suburban Residential grouping, while the shaded area around each line represent the 25^{th} and 75^{th} percentiles of the data from the site group at that time. The boxplots show the corresponding March 2019 data for all sites in the Suburban group. The center of the box is the median, the top and bottom of the box represents the 25^{th} and 75^{th} percentiles of the data for the entire month in the site group. The whiskers of the boxes represent 2.7 standard deviations and the outliers represent the remaining data. The insets in each panel show the cumulative distribution function (CDF) for the data from March 2019 compared to the data from March and April 2020 after the COVID-related closure. The shift in the two CDF's show the clear shift in the distribution of both CO and $PM_{2.5}$ concentrations at the Suburban sites, the period of time following the closures are more likely to have lower concentrations of CO and $PM_{2.5}$ compared to the period of time before the closures.

4) Table 3.3 Statistics for average CO and $PM_{2.5}$ concentrations

	CO	$PM_{2.5}$

	Mean	25th	75th	90th	Mean	25th	75th	90th
March 2019	263	147	279	537	9.5	5.1	12.4	17.4
March 2020 pre-closures	312	176	349	631	8.2	4.5	9.6	14.6
March/April 2020 post closures	**233**	162	**258**	**365**	**6.7**	**4.4**	**8.5**	**11.4**

Descriptive statistics for the average CO and $PM_{2.5}$ concentrations over the entire RAMP domain and time frame. Numbers that appear in bold and underlined indicate measurements from March 2020 post-closures that are significantly different from either the March 2019 and/or March 2020 pre-closure datasets. All metrics for both CO and $PM_{2.5}$ measurements are different beyond the uncertainty of the measurements between the "business as usual" data to the post-closure data aside from the 25th percentile of the CO data.

3.5.2 Significance Testing

A Mann-Whitney U Test was conducted to compare the March 2020 post-COVID closure data to the March 2020 pre-COVID closure data and the March 2019 data. The Mann-Whitney U Test was performed because the data is continuous, non-parametric, and unpaired. Based on the results of the test the March 2020 post-COVID closures CO and $PM_{2.5}$ measurements were both significantly lower than the March 2020 pre-COVID closure period and the March 2019 period.

18) Figure 3.5 Diurnal NO_2

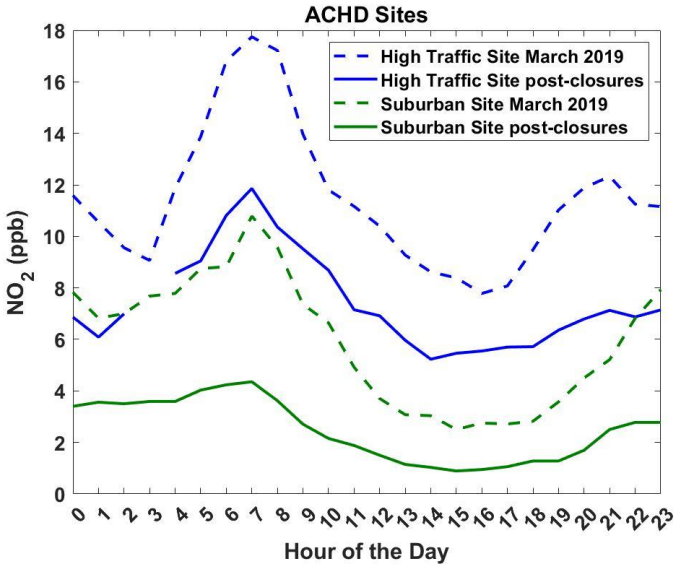

The diurnal patterns for the NO_2 measurements from the Allegheny County Health Department's two monitoring sites are shown. One site was near a highway and the other was in a background suburban area. The variation before the closures at the High Traffic site mirrors that of the CO concentrations at the RAMP High Traffic sites and there is a clear reduction in NO_2 concentrations post-closures similar to the CO concentrations. The Suburban site's NO_2 measurements similarly mimic the CO diurnal patterns observed at the RAMP Suburban Residential sites. Although the NO_2 concentrations at the Suburban site start out lower than the measurements at the High Traffic site, they still experience a significant reduction in their absolute values and daily variation following the COVID-related closures.

19) Figure 3.6 Boundary layer height

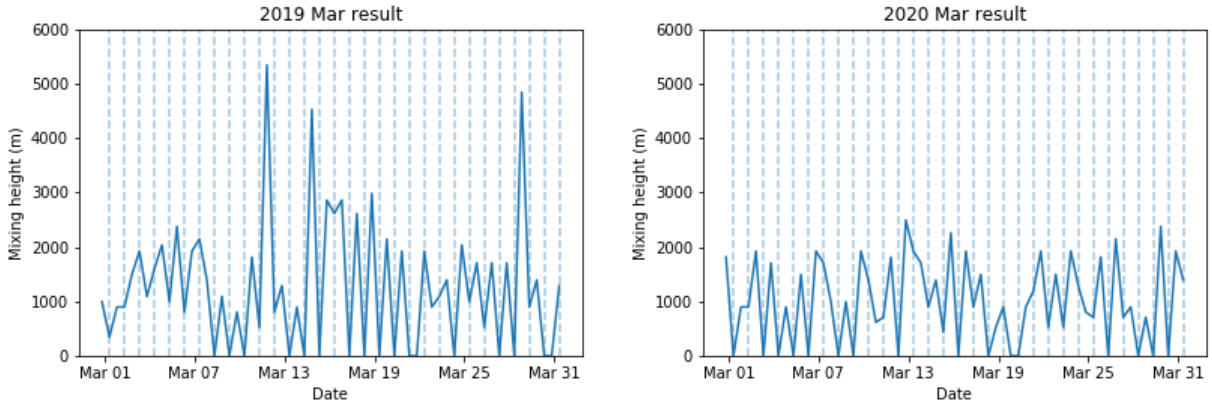

Shown are the boundary layer heights for the different time periods (March 2019 and March 2020) derived from the University of Wyoming's sounding data. The boundary layer height for the month of March 2019 was similar to March 2020 post-closures, with inversions 50(±5)% of the time. An inversion is defined here as a day with a 0 m mixing height. However, there are a higher frequency of strong temperature inversions during the first two weeks of March 2020 (61.5% of the days).

5) Table 3.4 Meteorology

	Average March and April Values in Pittsburgh, PA (1981-2010)	March 2017	March 2020	March 14, 2020 – April 30, 2020 (post-COVID closures)
Rainfall	6.13 inches	4.91 inches	5.64 inches	9.91 inches
Normalized Rainfall per day	0.10 in/day	0.16 in/day	0.18 in/day	0.21 in/day

Temperature Low	30°F	31°F	36.6°F	39°F
Temperature High	62°F	49°F	54.6°F	57°F

The thirty-year average high and low temperatures as well as rainfall for March and April (1981-2020) are shown in the table alongside the rainfall and temperature bounds in March and April after the COVID-related closures (March 14th, 2020 through April 30th, 2020). The temperature bounds for our study period are not significantly different from the thirty-year temperature bounds, so we do not expect the temperature to affect the concentrations of pollutants post-COVID closures. There was however more rainfall in the post-COVID closure period than the average expected rainfall for March-April. The rainfall received in March 2020 (0.18 inches/day) most closely matches the rainfall from March 2017 (0.16 inches/day) in recent years. We compared the mean $PM_{2.5}$ concentration from four Allegheny County Health Department sites (Lawrenceville, Parkway East, Lincoln, and Liberty) in 2017 to the concentrations at the sites in March 2020 post-closures. Based on this comparison we found there was still a significant decrease in $PM_{2.5}$ concentration after the closures when compared to March 2017 (0.80µg/m^3 reduction across all sites and a reduction of 2.48µg/m^3 at the High Traffic, Parkway East site).

20) Figure 3.7 Sensitivity analysis

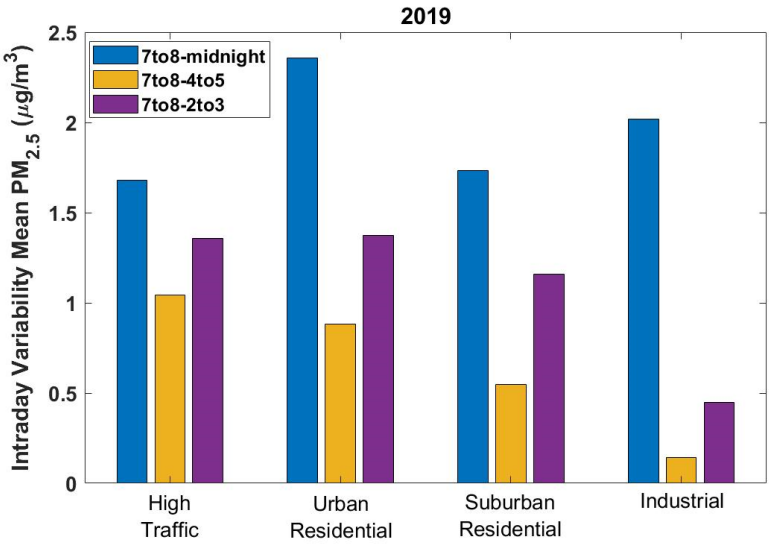

A sensitivity analysis was performed by selecting varying times as the background pre-morning rush-hour concentration. We show that although the determination of the morning rush-hour enhancement is dependent on the hour of the night used as the background the pattern of enhancement by site group remains the same. Ultimately hours 2-3 am were selected as the background time because they made the most physical sense for isolating the morning rush-hour traffic enhancement. Traffic data from the Pennsylvania Department of

Transportation show that the lowest number of cars are on the road between 2-3 am.

3.5.3 Determination of Restaurant Activity and Electricity Consumption Reduction

Reductions in restaurant activity were estimated using a combination of information from Google mobility data and observations of local restaurants' hours' reductions. The estimate of restaurant activity reduction was approximately 60%.

For electricity we calculated the decrease in the metered hourly electricity load supplied by Duquesne Light Company (DLC). This data was made publicly available by PJM Interconnection LLC, a competitive wholesale electricity market. DLC is the energy services holding company which provides electricity for ~600,000 customers (homes and businesses) in Allegheny and neighboring Beaver Counties. The mean metered hourly load for March 2019, March 2020 pre-closures, and March 2020 post-closures was 1467.9, 1406.9, and 1319.9MW, respectively. The mean decrease in electricity use post-closures was 8%.

3.5.4 Year-to-Year Differences in $PM_{2.5}$ And Impacts on Reference Year Selection

The impacts of COVID-19 related shutdowns identified in this analysis could be influenced by the selection of 2019 as the base case. We believe that this is a minor source of uncertainty.

Long-term average pollutant concentrations have been relatively stable in Pittsburgh since ~2012. Figure S6 shows the annual average $PM_{2.5}$ at all of the EPA AQS monitoring sites in Allegheny County from 2003-2018. While there is a slow overall decline in $PM_{2.5}$, year-to-year changes in recent years have been small.

21) Figure 3.8 Average annual $PM_{2.5}$

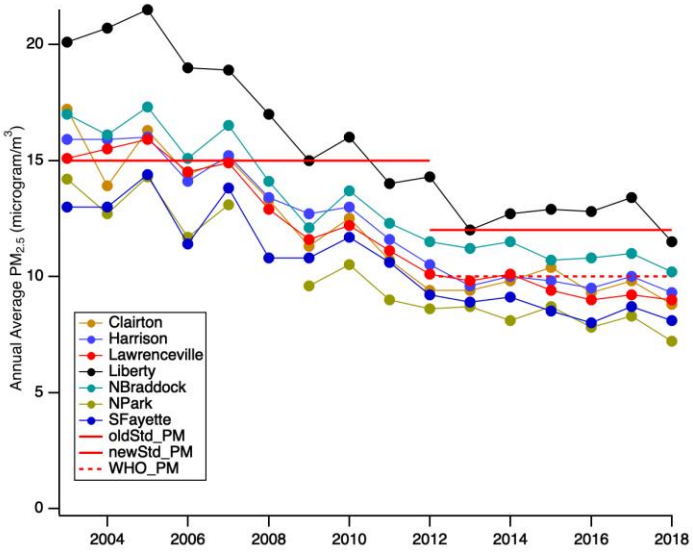

Annual average $PM_{2.5}$ measured across Allegheny County, PA from 2003-2018. Horizontal red lines show the EPA $PM_{2.5}$ NAAQS (15 µg/m^3 before 2012 and 12 µg/m^3 since) and the World Health Organization suggested limit of 10 µg/m^3. Concentrations have been stable since ~2012. We also compared $PM_{2.5}$ concentrations measured by RAMPs in 2018 and 2019. Two examples are shown in Figure 3.9. In each case 2018 and 2019 measurements are nearly identical. Across 30 RAMPs that have data for 2018 and 2019, only three had statistically significant differences between 2018 and 2019.

22) Figure 3.9 ECDF of $PM_{2.5}$

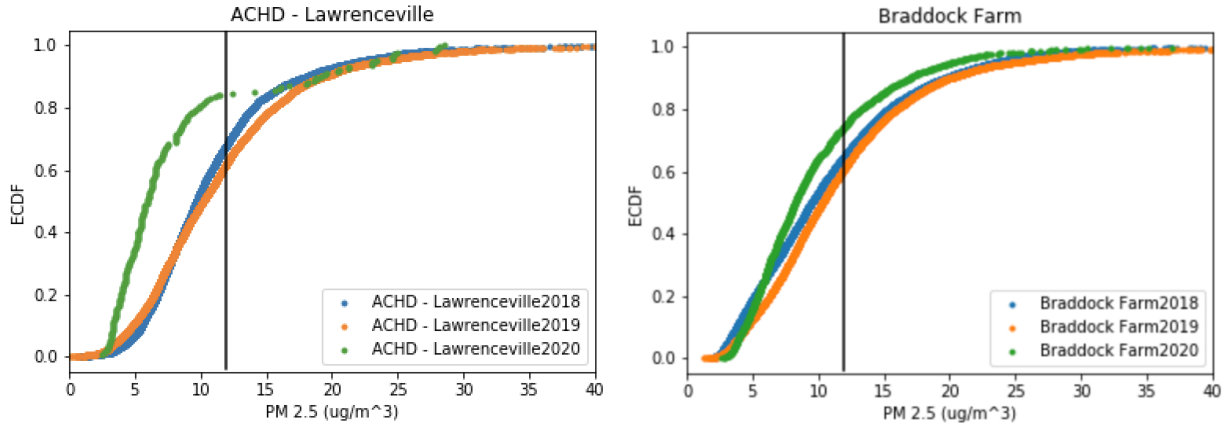

Empirical CDFs (ECDF) of hourly $PM_{2.5}$ measured at two RAMP locations. The left panel shows an Urban Residential location, and the right panel shows an Industrial location. 2020 data (green) have a different CDF in part because the dataset only covers January and February, whereas 2018 and 2019 data cover the entire year. Figures 3.8 and 3.9 suggest that the overall conclusions of our analysis would be the same whether we used 2018, 2019, or an average of the two as the base case. Lastly, we rely primarily on intra-day differences as a metric. Short-term average pollutant concentrations (e.g., a one- or two-week average) can be impacted by meteorological factors such as boundary layer height or precipitation frequency. For example, a simple comparison of the mean $PM_{2.5}$ concentration during the morning rush hour before and after the closures may be influenced by more frequent inversions or rain. Comparisons of intra-day differences should be less impacted by meteorology than daily or weekly average concentrations. The morning rush hour peak in CO, NO_2, and $PM_{2.5}$ is driven largely by fresh emissions; thus, the difference between the morning peak and overnight trough is an approximate indicator of total emissions in the airshed. Additionally, even if there are more inversions in one time period than another, the rush hour emissions are emitted into (or on top of) the already elevated $PM_{2.5}$ concentration. Thus, the intra-day differences should be less impacted by meteorology than the average concentrations.

6) Table 3.5 County measurements of $PM_{2.5}$ and CO

ACHD Sites	March/April 2019	March 2020 pre-closures	March/April 2020 post-closures
$PM_{2.5}$	12.2	11.9	8.0
CO	302	321	249

Shown are the mean $PM_{2.5}$ and CO measurements over the March/April 2019, March 2020 pre-COVID related closure period, and the March/April COVID-related closure period from Allegheny County Health Department regulatory monitoring sites. $PM_{2.5}$ measurements are from four different sites that would fit into the site groupings from this paper. The four sites are as follows: 1 Urban Residential, 2 Industrial, and 1 High Traffic. For CO there were only three measurement sites with data in our time range. These three CO sites are classified as follows: 1 Urban Residential and 2 High Traffic. The reductions in $PM_{2.5}$ post closures are 32% and 39% from March 2020 pre-closures and March/April 2019, respectively. The reductions in CO post closures are 22% and 23% from March 2020 pre-closures and March/April 2019, respectively. These reductions of overall mean concentrations across the domain are consistent with the reductions measured by the low-cost RAMP sensor network.

Chapter 4

Watching Paint Dry: I/VOC Emissions from Architectural Coatings and their Impact on SOA Formation

Contents of this chapter are being prepared for publication as*: Tanzer-Gruener R, Dugan LD., Bier ME., Robinson AL., Presto AA. Watching Paint Dry: I/VOC Emissions from Architectural Coatings and their Impact on SOA Formation. In prep for journal TBD*

4.1 Introduction

$PM_{2.5}$, particulate matter with a diameter of less than 2.5 micrometers, has deleterious effects on human health and the environment (Di et al. 2017; Dockery et al. 1993; Laden et al. 1998). Exposure to elevated concentrations of $PM_{2.5}$ is linked to increased risk of respiratory and cardiovascular disease, making poor air quality one of the leading preventable causes of death worldwide (Gakidou et al. 2017). $PM_{2.5}$ is not uniform in shape, size, or composition and varies in different regions throughout the world.

A significant portion of $PM_{2.5}$ mass (20-90%) is organic aerosol (OA) (Zhang et al. 2007). OA can be further classified as either primary (POA) or secondary (SOA). SOA forms through reactions in the atmosphere and makes up a significant portion of ambient OA even in urban areas (Jimenez et al. 2009; Robinson et al. 2007; Volkamer et al. 2006; Williams et al. 2010; Xu et al. 2015). SOA can be formed when pollutants which are emitted as vapors such as volatile organic compounds (VOCs) react with oxidants and the subsequent products condense into the particle phase. Here we define VOCs as organic compounds with saturation concentrations (C*) greater than 3.2×10^6 $\mu g/m^3$. Less volatile organic vapors, known as Intermediate Volatile Organic Compounds (IVOCs, $3.2 \times 10^6 \geq C^* \geq 3.2 \times 10^2$) also play an

important role in SOA formation (Chan et al. 2009; Miracolo et al. 2010; Presto et al. 2010) with approximately 45% of SOA formation coming from primary IVOCs (Zhao et al. 2014).

Historically, mobile sources have been a large source of anthropogenic SOA precursors (McDonald et al. 2013; Pollack et al. 2013). However, as vehicles have become cleaner due to regulations and new technologies the importance of SOA formation from non-combustion volatile chemical products (VCPs) has increased (Bishop and Stedman 2008; Khare and Gentner 2018; McDonald et al. 2018). According to McDonald et al., VCPs make up about a quarter of VOC emissions in the U.S.; that is about twice as much as diesel and gasoline exhaust emissions combined (McDonald et al. 2018). Despite the prevalence of VCPs as VOC emitters, most chemical transport models that predict SOA formation from anthropogenic sources continue to focus on combustion sources (Hodzic et al. 2010; Jathar et al. 2017; Murphy et al. 2017) despite the fact that VCPs are thought to have significant SOA yields (Shah et al. 2020). In order to correct this imbalance, it is imperative to quantify the magnitude and composition of SOA-forming emissions from VCPs.

One difficulty in understanding emissions from VCPs is that these products cover a wide range of forms and functions including cleaning supplies, personal care products, paints and coatings, and other products. Of these products some are more atmospherically relevant than others due to their timescales and modes of emission. Paints and coatings, which made up 13% of the U.S. organic solvent consumption for 2012 (McDonald et al. 2018), are thought to play a significant role in contributing to VOC emissions, with estimated emissions at > 50tons per day (Khare and Gentner 2018). Furthermore according to Seltzer et al., VOC emissions to the atmosphere across the VCP sector are largest for paints and coatings, making up 33% of the VCP

emissions and amounting to approximately 3.1kg of VOC emissions per person per year in the United States (Seltzer et al. 2020).

Although paint emissions have been quantified for years (Guo et al. 1999; Kiil 2006; Silva et al. 2003; Stockwell et al. 2020; Zhao et al. 2016) there has been little effort towards understanding VOC and IVOC (henceforth I/VOC) emissions with respect to their effect on SOA formation. For example there have been studies that quantified potential emissions of hazardous VOCs (Chang 1999; Clausen et al. 1991; Zhao et al. 2016), as well as emissions of individual VOCs from paints (Gandolfo et al. 2018; Gkatzelis et al. 2021; Lin and Corsi 2007), studies which quantified the VOC emissions of paints with respect to indoor air quality (Fortmann et al. 1998), and even some work which quantified the outdoor ozone reactivity of paint emissions (Goliff et al. 2012). However, little experimental work has quantified I/VOC emissions from paints and their impact on SOA formation. This work experimentally quantifies the I/VOC emissions factors over the drying period of paints spanning a wide range of architectural coatings in order to understand the contribution of architectural coatings to national VOC concentrations and SOA formation potential.

4.2 Instrumentation and Methods

4.2.1 Materials

The paint sector is very large. Under the US Census Bureau's classification of "architectural coatings" (category#: 3255101) the mass of paints utilized per year, scaled to the 2021 population, is 3.1 Tg (US Census Bureau 2012). There is a lot of potential variability across this large sector stemming from differences in solvent (water versus oil), manufacturer, gloss level (high versus low), indoor vs outdoor, etc. One of the major differentiators between paints are whether they are oil (alkyd) or water (acrylic/latex) based. Fifty years ago the overwhelming

majority of paints were oil-based because of their great resistance to wear and ease of application. However, oil-based paints contain much higher levels of VOCs and are more detrimental to the environment as a result over the past few decades the prevalence of water-based paints have increased due to their lower VOC content, ease of cleanup, and faster drying times. In general water-based paints have <250g/L of VOCs while oil-based paints are required to have <380g/L of VOCs. There do exist "low-VOC" paints which are required to have <5g/L of VOCs. It is important to note however that these requirements are tied to the VOCs in the solvent portion of the paints and does not account for additional solvents that are used in the pigments and binders.

Our approach was to sample across as much of this phase space as possible. The census inventory includes paints that fall under 23 classifications which can be grouped into six overarching paint categories: Oil, Flat, Semi-gloss Interior, Semi-gloss Exterior, High Gloss, and Satin. We tested paints from each of those categories. Additionally, we chose paints from companies that hold major share in the US paint market and selected types that covered a broad range of uses (indoor vs. outdoor, gloss levels, and solvent vs. water-based paints).

In total six paints were selected. Five were latex (water-based) paints of varying gloss levels. Four were for indoor use (Flat, Satin, Semi-Gloss Interior [SemiInt], and High Gloss) and one was for outdoor use (Semi-Gloss Exterior [SemiExt]). Lastly we selected one oil-based paint. A full description of the paints selected can be found in Table 4.2 in the SI.

We conducted two types of experiments for each of the paints (1) a headspace sample and (2) an extended emission experiment. Each of these experiment types are described in detail below. During extended emissions testing, each paint sample was applied to an approximately 58

cm^2 piece of drywall. Drywall was selected as the painting material as it is a commonly painted surface material throughout the United States.

4.2.2 Procedures

We conducted experiments to quantify the composition and emissions of paints. Headspace experiments were used to obtain a fingerprint of paint vapors. In these experiments we sampled directly (~5 cm) above open paint cans that were placed in a fume hood. Figure 4.7 in the SI shows a schematic of the headspace experimental setup.

Extended emission experiments used a 1.2 L aluminum flux chamber (shown in Figure 4.7 of the SI). At the start of each extended emission experiment a piece of pre-cut drywall was weighed. Following weighing the drywall was painted, re-weighed (to determine the weight of the paint applied), and immediately placed into the chamber. As shown in Table 4.3, most experiments used ~0.7 – 2 g of paint. The chamber was then sealed and sampling began. VOC-filtered air was pulled through the flux chamber at a flowrate of 0.37 slpm. This gave a residence time of 3.2 minutes.

We used multiple methods to quantify the composition of paint I/VOCs in both the headspace and extended emissions experiments. VOCs and more volatile IVOCs (e.g., naphthalene) were measured with a quadrupole PTR-MS (Proton Transfer Reaction Mass Spectrometer) (Lindinger, Hansel, and Jordan 1998). Paints are made up of a wide range of oxygenated compounds and the PTR-MS is well suited to measure oxygenated VOCs (OVOCs) (De Gouw et al. 2003; De Gouw and Warneke 2007). Furthermore OVOCs are of interest with regard to SOA formation as recent work has suggested (Charan, Buenconsejo, and Seinfeld 2020; Janechek et al. 2019; Li and Cocker 2018; Wu and Johnston 2017). The PTR-MS was

operated in scan mode from *m/z* 21 to 155 and sampled continuously for the entirety of the extended emissions tests (typically 48 hours).

IVOCs were primarily quantified using Tenax sorbent tubes followed by thermal desorption GC-MS (gas chromatography-mass spectrometry) analysis. Tenax TA was selected as the sorbent material because it performs well while sampling in high moisture environments and is known to be effective at measuring I/VOCs (Helmig and Vierling 1995; Maier and Fieber 1988; Rothweiler, Wäger, and Schlatter 1991). A full description of the GC-MS system as well as tube cleaning and analysis procedures can be found in the SI. Tenax tube sampling times were selected based off of preliminary PTR-MS data and were collected over one-hour intervals. The goal was to sample with Tenax tubes during hours 0-1, 1-2 approximately hour 4-5, approximately hour 8-9, 24 hours after paint application, and 48 hours after paint application. Table 4.3 in the SI shows the exact sampling times for each experiment.

4.2.3 Analysis and Compound Identification

23) Figure 4.1 Volatility binning and compound class grouping

a)

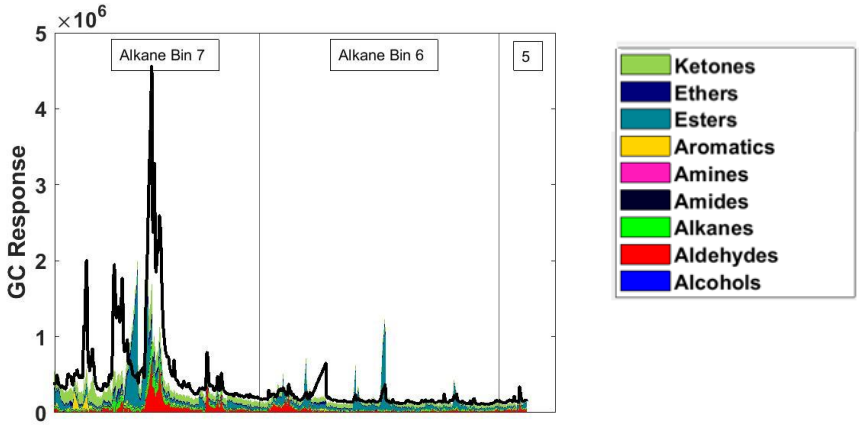

b)

c)

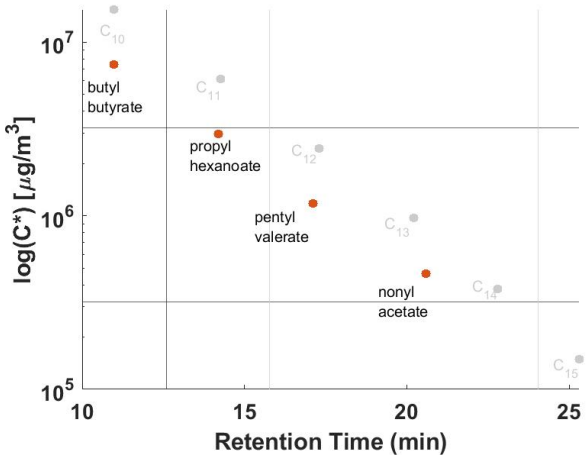

(a) The total ion chromatograph of a Satin headspace sample is shown by the thick black line. Signal decomposed into compound class contributions using marker ions is shown with the colored shading. Vertical lines show logarithmically spaced C bins determined from alkane volatility (e.g., Alkane Bin 7 corresponds to the C* = 10^7 μg/m^3 bin). The relationship between retention time and volatility is shown for a series of alkanes (b) and esters (c). Panel (c) also shows the alkanes as light points to highlight the offset in ester volatility relative to alkanes. Since esters have a different relationship between volatility and retention time than alkanes, a different set of C* bin boundaries are used, as shown in (c).*

Our goal is to quantify I/VOC emissions by both volatility (C*) and composition. There are several challenges to this. First, the mixture of IVOCs captured on the Tenax sorbent tubes cannot be fully separated with one-dimensional gas chromatography. Instead, most of the GC

signal appears as an unresolved complex mixture (UCM). An example chromatograph is shown in Figure 4.1a. There are very few well-defined peaks, and instead most of the mass elutes as a broad UCM hump.

Previous work (Zhao et al. 2013) has used GC-MS analysis to quantify UCM emissions from combustion systems. We draw on and expand those methods here. Our GC-MS uses a DB-5 column, so retention time is related to volatility. Previous work has used the retention time-volatility relationship to map the UCM to the volatility basis set for combustion emissions (Ma et al. 2016; Presto et al. 2012; Xu et al. 2020). An example of this binning is shown in Figure 4.1b for a series of n-alkanes. There is a nearly linear relationship between log(C*) and alkane retention time. This relationship can in turn be used to lump the UCM into logarithmically spaced C* bins, which are shown as vertical lines in Figure 4.1a and b.

Combustion emissions are dominated by aliphatic and aromatic hydrocarbons. Since variations in hydrocarbon volatility are mostly a function of carbon number (rather than molecular structure) (Pankow and Asher 2008), in previous work a single relationship between retention time and volatility has been sufficient. However, paint emissions contain other, often more polar, compound classes (e.g., ketones, aldehydes, alcohols, and esters) that may have different relationships between C* and retention time.

An example of differing C*-retention time relationship is shown for a series of esters in Figure 4.1c . While retention time and C* show a log-linear relationship for the esters, the esters are offset relative to the alkanes. This means that we cannot use the C* bins defined by alkane retention times for the esters; hence Figure 4.1c shows different boundaries for the C* bins for esters. Thus, in order to bin the UCM mass emitted from the paints, we need to separately quantify volatility for each compound class of interest. We therefore calibrated the C*-retention

time relationship for nine classes of compounds (alcohols, aldehydes, alkanes, amides, amines, aromatics, esters, ethers, and ketones) and defined separate retention time windows for each C* bin. Full details are presented in the Table 4.4 in the SI.

Mapping the UCM volatility requires apportioning the GC signal into the nine compound classes shown in Figure 1a. This was done using marker ions. We identified marker ions using two basic rules (1) the marker needed to be unique, or nearly unique, to the compound class of interest and (2) the marker ion needed to make up a non-trivial amount (ideally >5%) of the overall signal for the compound class.

While there are common marker ions routinely used in chromatography, they are not necessarily available for use in our analysis. For example, *m/z* 57 is a common marker ion for hydrocarbons, but it is a poor marker ion for our samples because *m/z* 57 appears in the mass spectrum for nearly every molecule with a large carbon chain. Therefore, it is not specific enough to use as a marker ion in this analysis. Instead, we used the NIST mass spectral library (U.S. Secretary of Commerce on behalf of the United States of America 2018) to determine marker ions for each of our nine compound classes. Marker ions and their percent contribution to their compound class are listed in Table 4.5 in the SI. Once marker ions for each class were selected their average contribution to that class of compounds' mass spectra was calculated.

During analysis, the GC-MS signal was therefore apportioned by both compound class and volatility. We extracted the signal for each marker ion and scaled it up by the corresponding volatility-dependent multiplier from Table 4.5 SI. Signal was subsequently converted to mass using calibrations from compound class and volatility bin specific representative compounds (Table 4.4 in SI). Volatility was then apportioned using the predefined volatility bins. The net result of this analysis is shown in Figure 4.1a, where the colors indicate apportionment of the

total signal to different compound classes. Any unapportioned signal (the white area in Figure 4.1a) was assumed to have the same volatility relationship and mass calibration as alkanes. Class apportioned chromatographs for headspace samples of each paint type can be found in Figure 4.5 in the SI.

A second major challenge is that our PTR-MS has unit mass resolution. It therefore is unable to separate isobaric ions, nor can it distinguish between compounds with the same elemental composition. We addressed this in several ways, as detailed below.

For most *m/z*, compound identification relied on the PTR-MS library (Pagonis, Sekimoto, and de Gouw 2019). One exception was for *m/z* 45. This ion is traditionally identified as acetaldehyde, but it has been suggested that for paint emissions ethylene glycol is a more appropriate compound (Stockwell et al. 2020). There are many other mass-to-charge ratios which may have contributions from multiple compounds. For those *m/z* a search on PubChem was conducted to identify the most likely of the suggested compounds to be found in paints.

In addition, head space samples were collected with a high resolution Thermo Exactive EMR mass spectrometer. The EMR technique used was atmospheric pressure chemical ionization (APCI). A full list of ions scanned, and their compound identification can be found in Table 4.6 in the SI. The EMR data allowed us to better constrain isobaric species that could not be separated by the PTR-MS.

Emission measurements from the PTR-MS were also classed into one of the nine compound groups (i.e. alcohols, aldehydes, alkanes, amines, amides, aromatics, esters, ethers, and ketones). Saturation concentrations (C*) were calculated using the SIMPOL method (Pankow and Asher 2008) in order to identify compounds as either IVOCs or VOCs. The outputs of the PTR-MS are raw responses for scanned mass-to-charge ratios. Raw responses were

converted to concentrations in ppb using laboratory calibrations and subsequently converted to mass emitted per mass of paint applied [μg/g]. Ultimately masses of I/VOCs measured by both the GC-MS and PTR-MS were added together to obtain total I/VOC emissions per mass of paint applied for all six of the test paint types.

4.3 Results and Discussion

4.3.1 Total Emissions

Figure 4.2 shows the results for the total mass emitted over 48 hours during the extended emissions tests on a per mass of paint applied (μg/g) basis for each of the six paint types tested. The upper panels show the total emissions split among VOCs and IVOCs, and the bottom panels show emissions by compound class.

24) Figure 4.2 Mass emitted per paint applied

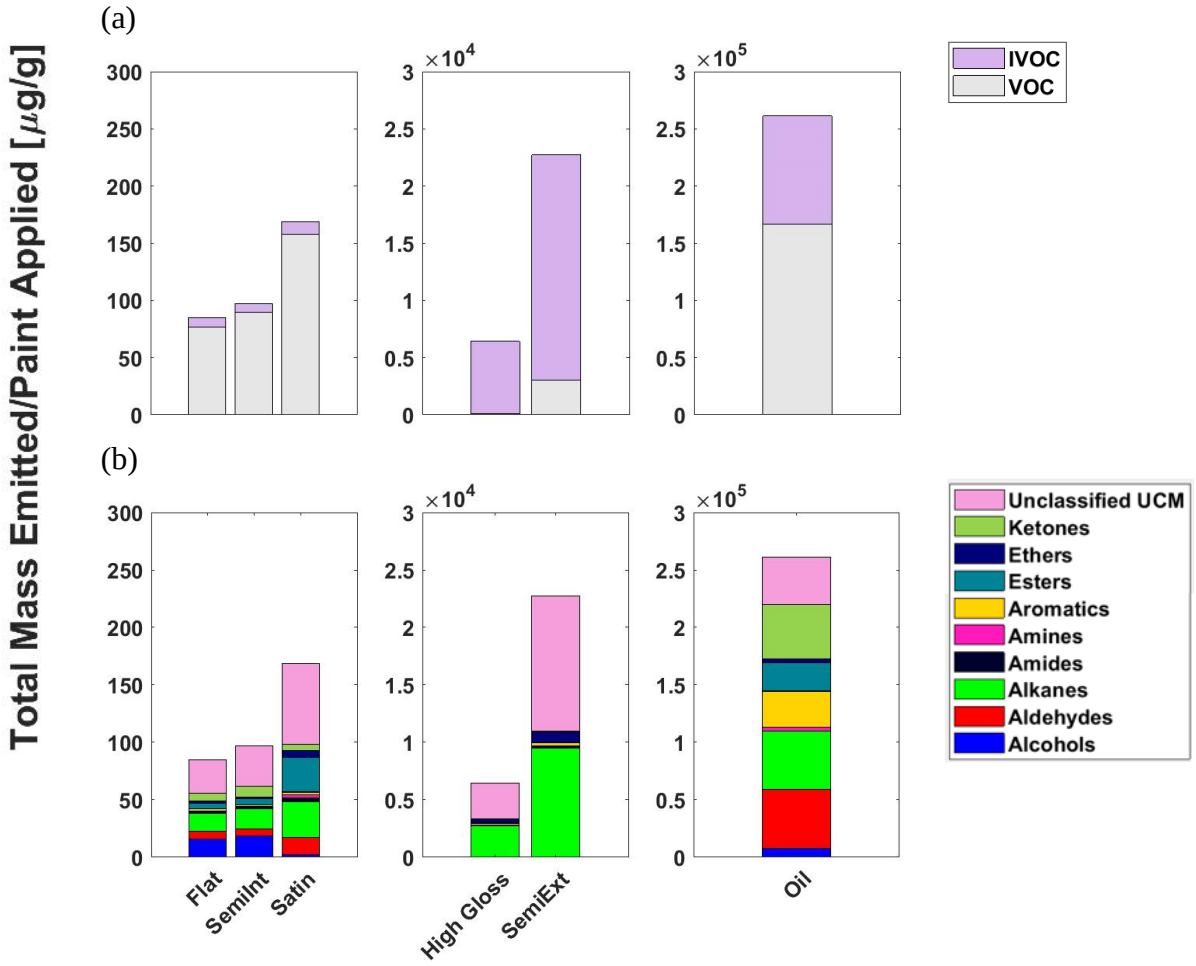

Total I/VOC emissions (μg/g-paint) over two-day extended emissions experiments. Panel (a) separates the emissions into IVOC and VOC and (b) separates by compound class. The magnitude and composition of emissions differ between the indoor, low-gloss paints (Flat, SemiInt, and Satin), the higher gloss paints (High Gloss and SemiExt), and the oil-based paint (Oil). The emissions span several orders of magnitude between the three different paint groupings. The lower gloss paints emit predominately alkanes, alcohols, and aldehydes while the oil-based paint emits aldehydes, alkanes, and aromatics.

Total I/VOC emissions varied by several orders of magnitude across the paint types. I/VOCs emitted from the low-gloss, indoor, water-based paints (Flat, SemInt, and Satin) are on the order of 10^2 μg/g of paint applied. The higher gloss, water-based paints emitted ~10^4 μg/g of I/VOC. Lastly the oil-based paints emitted the most I/VOCs with emissions > 10^5 μg/g of paint. This suggests that representing paint I/VOC emissions in chemical transport models (CTMs) will

require information on both the total mass of paint used and the types of paint used. From our findings we can make recommendations on the granularity of how many different types of paints should be tested for input into CTMs. We recommend incorporating information on three categories of paints: 1) low-gloss, water-based paints, 2) higher-gloss, water-based paints, and 3) oil-based paints.

The second major observation from these experiments is the difference in distribution of IVOC versus VOC emissions from the different types of paint. The emissions from the lower gloss, indoor paints are predominately VOCs. Furthermore, as we show in more detail below, the IVOC emissions from the lower gloss, indoor paints are small in magnitude and fall below our detection limits after the first hour following paint application. This implies that emissions from the lower-gloss, indoor paints have little impact on outdoor I/VOC concentrations and SOA formation.

By contrast, a significant fraction of the detected emissions from the High Gloss (98%) and SemiExt (87%) are IVOCs. These less volatile emissions have larger SOA formation potential. Presumably, since the SemiExt paints are exterior paints this means that 100% of their I/VOC emissions get released into the outdoor environment and therefore impact ambient I/VOC concentrations and SOA formation.

The Oil paints has a closer to even split between IVOC and VOC emissions (36% and 64% respectively). Total I/VOC emissions from oil paints are about a factor of 10 larger than emissions for SemiExt, and the Oil paint has the largest emissions of IVOCs among the paints tested here. Oil paints are used both indoors and outdoors but primarily outdoors due to their hard-wearing properties. Therefore the large amount of IVOC emissions from oil paints will also have a significant impact on SOA formation.

Figure 4.2b shows that the distribution of compound classes emitted by the different types of paints varies. Alkanes are a major component of the High Gloss and SemiExt emissions (42%). The low-gloss, indoor, water-based paints (Satin, SemiInt, and Flat) and oil-based paint emit a wider spectrum of compounds. A significant portion of emissions from the oil-based paints (12%) are aromatics. Aromatics are known to be good SOA precursors (Akherati et al. 2020) and are likely to significantly contribute to the SOA formation potential from paints. Other important compound classes that are emitted by the paints are alcohols, aldehydes, and ketones. With the exception of emissions of aldehydes our paint emissions' profiles (which are dominated by the Oil paint emissions) are in line with inventory based projected emission profiles from previous studies (McDonald et al. 2018). This indicates that inventory based projections may serve as an adequate estimator of I/VOC emissions from paints when laboratory tests are not feasible.

4.3.2 Time evolution of emissions

One potential characteristic of VCP emissions is that they can serve as long-term, low-level emissions sources (Drozd, Weber, and Goldstein 2021; Khare and Gentner 2018). The extended emissions experiments allowed us to examine how emissions evolved over time. Figure 4.3 shows how emissions evolved over the course of multiple days as measured by the Tenax tubes (mostly IVOCs) and the PTR-MS (mostly VOCs). We look at the fraction of the total measured emissions as a function of time. Overall our total I/VOCs measured are in good agreement with the literature as we project from our measurements a total 291 g total VOCs (TVOCs) emitted per kg of paint applied and McDonald et al., estimates a range of 200 – 600 g TVOCs per kg of paint emitted.

25) Figure 4.3 Cumulative emissions over time

a) b)

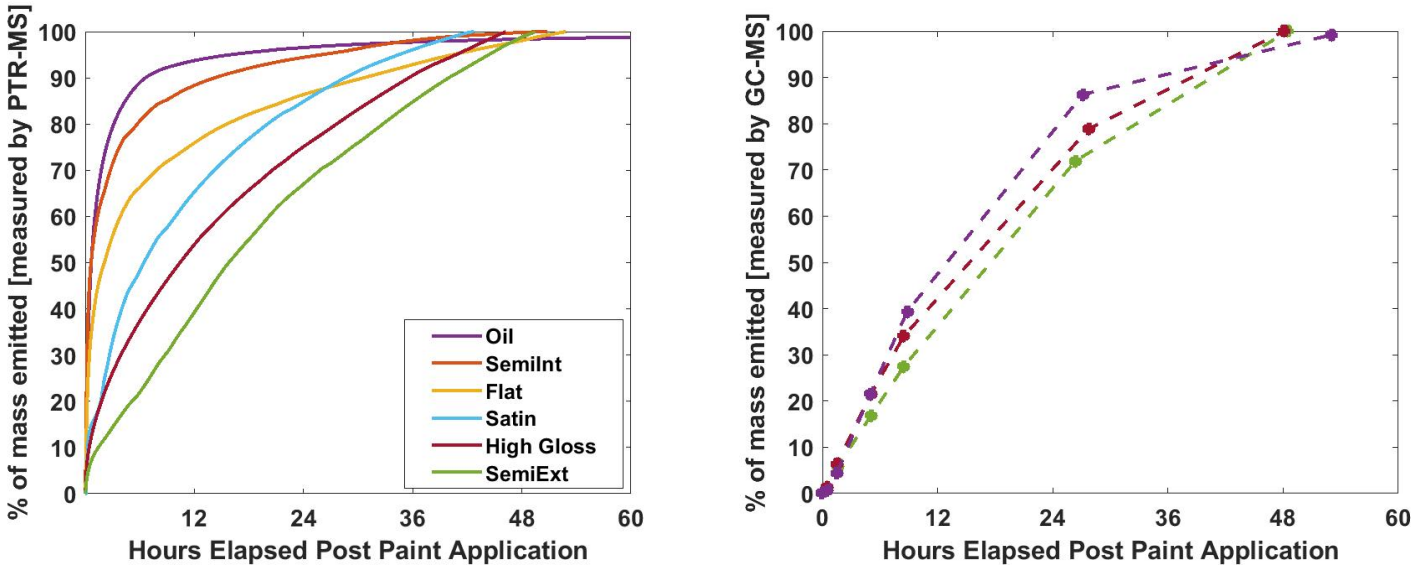

Cumulative emissions measured by the (a) PTR-MS and (b) Tenax tubes as function of time elapsed after paint application. For these experiments, the PTR-MS operated continuously with ~2-minute time resolution. Dashed lines in (b) are to guide the eye between the periodic Tenax samples.

The three lower-gloss, indoor paints were the fastest emitting of the six paints tested. For low-gloss, indoor paints there are no long term I/VOC emissions. Measurements of IVOCs using Tenax tubes were below detection limits after one hour following paint application. Additionally, all of the compounds measured with the PTR-MS reached background levels by the end of the two day experiment. Figure 4.2 shows that the emissions from the indoor paints (Flat, Satin, SemiInt) as well as the Oil paint were primarily VOCs. Figure 4.3 shows that the emissions from these paints fall off rapidly. All four of these paints emit more than 50% of their total emissions within 12 hours after application. The temporal profile is most extreme for the Oil and SemiInt paints, which emit >90% and >80% of their emissions within 12 hours, respectively.

For the oil based paints the extended emissions experiments were run for more than two days. During preliminary tests, the oil paint showed a significantly higher magnitude of I/VOC emissions compared to the water based paints. Therefore, a longer, one week (rather than two

day) extended emissions experiment was conducted for the oil based paint. Surprisingly IVOC emissions from the oil paints also reached below limits of quantitation by the second day indicating little effects of long term IVOC emissions from oil based paints as well. The majority of ions detected by the PTR-MS measurements also reached background concentrations within the two day drying period. A list of ions that were still at concentrations greater than 5ppb above background levels are included in Table 4.7 in the SI.

While the emissions from the Oil paint fall off rapidly, the emissions transition from being VOC-dominated to IVOC-dominated over time, this is consistent with previous research (Khare and Gentner 2018). In general, the IVOCs are emitted more slowly than the VOCs, as would be expected based on volatility. Figure 4.3b and Figure 4.4b show that IVOC emissions from the oil paint persist for approximately one day after application.

Emissions from the SemiExt and High Gloss paints are dominated by IVOCs. Overall these paints emit more slowly. Figure 4.3a shows that after 12 hours these paints emitted <50% of the total emissions detected by the PTR-MS. Most of these emissions are IVOCs (i.e. naphthalene and hydroxyphenol). For these paints all but two ions measured by the PTR-MS reached background levels by the end of the two day extended emissions experiment but there were still IVOC emissions measured by the GC-MS at the end of the two days. A list of ions still detected at the end of the two day drying period are shown in Table 4.7 the SI.

26) Figure 4.4 IVOC emissions

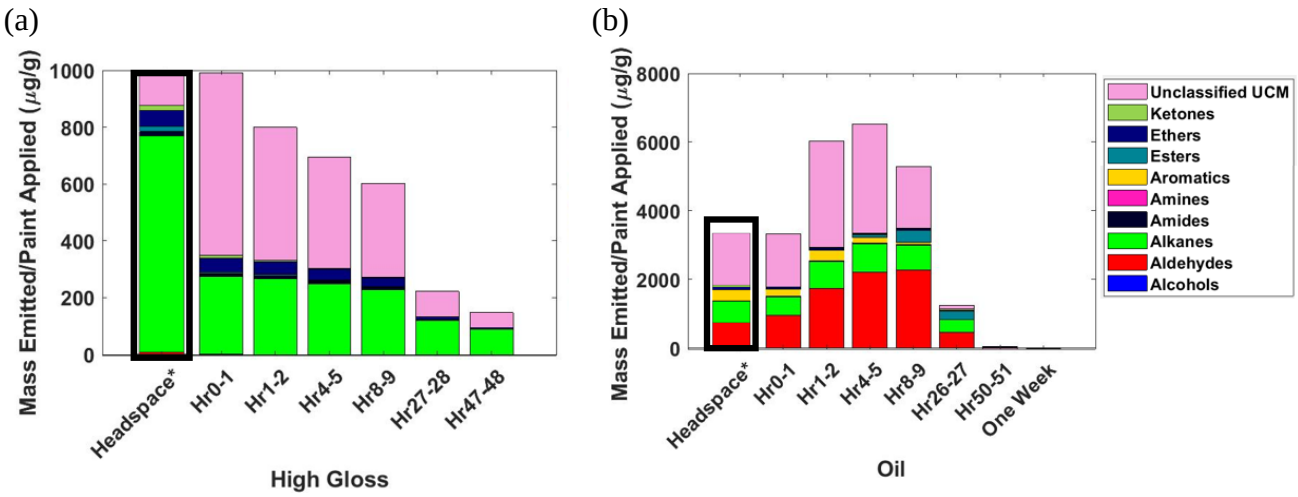

Headspace and extended emission samples of (a) High Gloss and (b) Oil based paints measured on Tenax tubes. The total height of the headspace samples is matched to the emission rate for the Hour 0-1 samples to aid comparison. The headspace sample mirrors the emission profile of the respective paints at select points throughout the emission timeframe but do not accurately represent emissions from their respective paint over the entire drying and emitting timescale. The Oil paint headspace mirrors the emissions from the Oil paint during the first hour following paint application, however the headspace does not represent a true fingerprint of the Oil IVOC emissions over the entire paint drying timescale. Less volatile emissions, for example the esters, that are emitted after four hours after paint application take longer to volatize and therefore would be neglected if the headspace was used as an emission profile for Oil paint. Similarly (4a) the High Gloss headspace does not accurately represent the ratio of emitted alkanes to other compounds being emitted over the course of the drying timeframe. The magnitude of the emissions from the Oil paint increases over the course of the first day post-paint application but reach levels indistinguishable from zero by the second day post-paint application while the High Gloss paints continue to emit IVOCs at low levels into the second day after paint application.

Figure 4.4 shows the temporal evolution of IVOC emissions for the Oil and High Gloss paints. IVOC emissions from the High Gloss gradually and continually decline over the course of two days. However, even after 48 hours, the High Gloss paint continued to emit IVOCs. The paints with low IVOC emissions (Flat, SemiInt, Satin) had a similar profile of declining IVOC emissions with time, with emissions falling below the detection limit within 1-2 hours after paint application. This suggests that some paints can act as extended sources of IVOC emissions.

The composition of High Gloss IVOC emissions changed over time. While alkanes were an important component of the emissions over the entire two days, they changed from being 28% during hour 0-1 to 60% at hour 47-48.

The evolution of IVOC emissions from the Oil paint was different. Emissions increased relative to the hour 0-1 sample for hours 1-2, 4-5, and 8-9, before falling rapidly and eventually reaching zero. As with the High Gloss, the composition of the IVOC emissions from the oil paint also changed over time, with increasing aldehyde and ester fractions contributing to the higher emissions around hours 1-2, 4-5, and 8-9.

One question our data can address is whether or not the headspace samples of different paints can serve as a fingerprint for the I/VOC emissions of paints over their entire emission lifetime. Figure 4.5 clearly shows that this is not possible for VOCs. Figure 4.5 shows the PTR-MS measurements of VOCs emitted from both a headspace sample and an extended emission sample of High Gloss paint. The headspace sample is dominated by acetone (*m/z* 59) and methanol (*m/z* 33). On the other hand, over the lifetime of the paint drying as measured by the extended emissions tests methanol and acetone make up less than 10% of the total VOC emissions.

Similarly the GC-MS measurements also demonstrate how a simple headspace sample cannot capture the total emissions profile of a paint over the course of its emission lifetime. Figure 4.4 shows the headspace composition of the Oil and High Gloss paints next to the emission composition over the drying period. The headspace composition is similar to the emissions within the first hour following the application of the oil paint. However, as the oil paint dries the composition of the emissions changes. Aldehydes become a more important part of the emissions for the 1-2, 4-5, and 8-9 hour samples. Less volatile esters that are in the paint

are also emitted, but only after 8 hours following paint application. If headspace samples were used as an emission fingerprint these less volatile emissions, which potentially have greater SOA formation implications, would be underestimated.

Overall, the majority of the I/VOC emissions from paints dissipate by the end of two days at varying rates, with the exception of continued IVOC emissions from the High Gloss and SemiExt paints at low levels by the end of the two days. Additionally composition of the I/VOC emissions changes over the course of the two day drying period thus making using headspace samples as fingerprints to represent total I/VOC emissions insufficient.

27) Figure 4.5 Headspace and extended emissions comparison

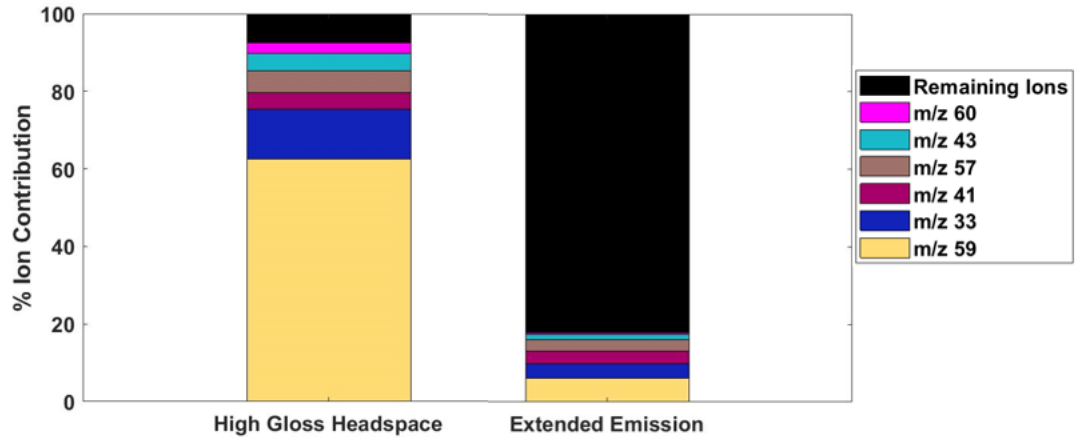

Composition of headspace vapors and 48-hr emissions measured by PTR-MS for the High Gloss paint. The headspace measurements are dominated by acetone (m/z 59) and methanol (m/z 33) as well as minor contributions from m/z 60, cyclopropane (m/z 43), hydrocarbons (m/z 57), and propyne (m/z 41). However, over the course of the extended emissions High Gloss experiment these six ions make up less than 20% of the mass emitted. Headspace samples do not create a sufficient fingerprint for paint emissions of the entire drying timescale.

4.3.3 Implications for SOA formation

Here we use our emissions data to estimate total I/VOC emissions from paints in the U.S. and potential impacts on SOA formation. We used the US Economic Census to scale up our measured I/VOC emission factors to a national scale (US Census Bureau 2012). The US Economic Census lists out 23 different subcategories of "Architectural Coatings" which were

each mapped to one of our six paint types tested. Since the census reported paint usage for 2010 the usage was scaled up by population growth to obtain estimated paint usage for 2021. The mass of paints used for each of the six classes of paints tested were multiplied by the normalized I/VOC emission factors calculated in order to estimate the total expected I/VOC emissions from paints in the US.

Figure 4.6a and Table 4.1 summarize the paint usage. Flat, SemiInt, SemiExt, and Oil paints each contribute ~20-30% (~600-900 Gg) of annual paint usage in the U.S. Satin and High Gloss each contribute less than 10% of total paint usage. We estimate total paint I/VOC emissions of ~169 Gg/year. The majority of these emissions (59%, Figure 4.6c) are VOCs, with the remainder being IVOCs. The NEI does not report VOC emissions on as fine of a grain as we are however they do estimate that 337,414 tons of VOCs are emitted from "non-industrial surface coatings" which is about three times the amount of I/VOCs we measure (186,192 tons of I/VOCs are emitted from paints) however this lines up as paints are only some fraction of the total “non-industrial surface coatings” sector the NEI reports (EPA 2017).

Total emissions I/VOCs from paints are high on a mass of product used basis; emissions are approximately 290.7 g I/VOC emissions per kg of paint used. This amounts to 0.51kg/person of I/VOCs emitted per year in the US. This is one to two orders of magnitude greater than the I/VOC emission rates of gasoline and diesel related emissions (on a gram of I/VOC per kg of fuel used basis) (McDonald et al. 2018). Our per-person and per mass of “fuel used” estimates of paint I/VOC emissions are similar to recent estimates by McDonald et al (~300g/kg of product) (McDonald et al. 2018) and Seltzer et al (0.67kg/person per year) (Seltzer et al. 2020).

28) Figure 4.6 SOA mass formed

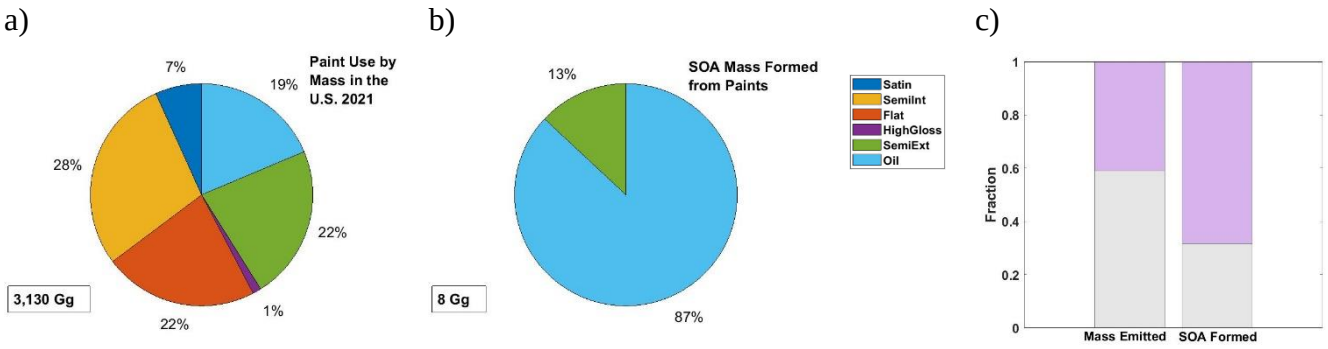

(a) Total paint usage in the U.S. reported by U.S. Census Bureau data (b) SOA mass formed, and (c) contributions of I/VOCs to paint emissions and SOA formation. The split between paint use by mass is fairly evenly divided between SemiInt, Flat, SemiExt, and Oil based paints. However, SOA mass formed is dominated by I/VOC emissions from Oil and SemiExt paints. Furthermore the IVOCs on the whole are more influential in the formation of SOA than the VOCs emitted by the paints.

7) Table 4.1 Paint usage and emissions

Paint Type	Paint Usage in US 2021 [Gg]	IVOC+VOC Emissions [Gg]	SOA Mass Formed [Mg]
Oil	584	152.6	6,947
Semi-Gloss Interior (SemiInt)	892	0.09	2.1
Flat	702	0.06	1.5
Satin	212	0.04	0.9
Semi-Gloss Exterior (SemiExt)	701	15.9	1,042
High Gloss	39	0.3	18.7

Total paint usage in the U.S. for each paint type, the total I/VOC yearly emissions in the U.S. for each paint type, and the SOA mass formed each year in the U.S. by paints.

While usage is somewhat evenly distributed across several paint types, I/VOC emissions are dominated by two classes: Oil and SemiExt. These two classes have the highest emission factors (µg/g) shown in Figure 4.2, and together they contribute 98% of total emissions. In particular, oil paints alone account for 90% of total paint I/VOC emissions.

We estimated the contribution of paint-emitted I/VOCs to ambient SOA production. We estimated SOA production by multiplying the total I/VOC emissions by SOA mass yields for

each compound classes. The SOA formation potentials (g/g) were calculated using the Statistical Oxidation Model (SOM) (Cappa and Wilson 2012) and are the same SOA yield estimates used in McDonald et al. (McDonald et al. 2018). A table showing the compounds used for general compound class SOA yield calculations can be found in Table 4.8 in the SI.

We estimate total SOA production of ~8 Gg from paint I/VOCs (Table 4.1). Figure 4.6 and Table 4.1 show that SOA production, much like I/VOC emissions, are dominated by Oil and SemiExt paints. The other four paint types contribute negligibly to predicted SOA formation. IVOCs account for 68% of predicted SOA formation, reflective of their lower volatility and higher SOA yield. To put the SOA production from paints in perspective the global SOA yearly formation is estimated to be between ~13 – 119 Tg/year (Hodzic et al. 2016; Tsigaridis et al. 2014). On a national scale the ~8 Gg of SOA formed from paints is about 1% of the SOA formed from combustion sources in the U.S. (700 Gg) (Jathar et al. 2014).

There are several potential sources of uncertainty in our estimates of paint I/VOC emissions and subsequent SOA formation. These include uncertainty in SOA yield estimates, especially for UCM and oxygenated VOCs that have not been directly measured in the laboratory. There may be significant variation in paint emissions rate and composition across manufacturers that we did not capture here. Since emissions and SOA formation is dominated by paints that are often used outdoors, the role of sunlight-driven changes in emissions (Khare et al. 2020) should be considered in the future.

However, we are able to largely reduce one potential source of uncertainty in the contribution of paint I/VOCs to ambient SOA. The four paint types that are often used indoors (Satin, SemiInt, Flat, and High Gloss) all had low emissions and negligible SOA contributions. One potential confounder for the ambient impact of these emissions is indoor-to-outdoor transit

(i.e., paint fumes need to leave the building without being lost to walls or other surfaces). Our data suggest that these indoor use paints are a minor contributor to I/VOC emissions from the paints and coatings sector, and that emissions are dominated by paints used outdoors.

4.4 Conclusions

Paints are an important segment of the VCP sector in terms of I/VOC emissions and SOA formation. I/VOC emissions from paints in the U.S. total to 168.9 Gg per year. These emissions occur on fast time scales (<2 days following paint applications). On a per person basis these emissions amount to 0.51kg/person of I/VOCs emitted per year in the US which is 290.7 g I/VOC emissions per kg of paint used. Furthermore the projected SOA yield of paints overall in this study is 4.7% [+/- 2%]. Paints are an important source of I/VOCs which should be further controlled in order to decrease the formation of SOA.

Particular attention should be directed to oil-based and semi-gloss exterior paints as they produce the largest amount of SOA of all paint types. Although over the past few decades the performance of water-based paints have improved leading toward the switch from oil-based to water-based paints for many paint jobs, oil-based paints are still sometimes chosen for their durability and ease of application, especially for exterior work. Further work is suggested to explore the effect of different ambient conditions (i.e. presence of light, temperature, humidity etc.) on I/VOC emissions and therefore SOA formation as well as experiments which directly measure SOA formation from paints.

4.5 Supplemental Information

4.5.1 Headspace Sampling Procedure

For the PTR-MS headspace samples each can of paint was opened inside a fume hood and a Teflon tube connected to the PTR-MS inlet drew air from ~ 5 cm above the headspace of

the opened can for ~15 minutes. A fume hood background was taken for approximately 10 minutes before each consecutive paint sample to ensure that the air was flushed out and in order to obtain a background measurement for subtraction from the headspace measurement. For the Tenax tubes a similar tactic was employed in which each can of paint was opened and a Tenax tube was held about 5 cm above the paint surface. The Tenax tube was connected to a vacuum and mass flow controller (Alicat Scientific) set to 0.2 L/min. The Tenax tube was allowed to sample for 1 hour.

4.5.2 PTR-MS Run Specifications

While conducting measurements with the PTR-MS (Ionicon Analytik) we set the instrument to run in scan mode, where the PTR-MS scans through integer mass to charge ratios (*m/z*) 21 through 155 and dwells at each *m/z* for 500ms. The drift tube is operated at 600 V, a constant pressure of 2.1 ±0.1 mbar, and the measured flowrate is 0.3695 L/min.

4.5.3 Tenax Tube and GC-MS Specifications

The GC-MS has a thermal desorption sample extraction and injection system manufactured by Gerstel Inc. USA. Within the GC-MS is a DB-5 capillary column (5% phenol and 95% dimethylpolysiloxane). This column was selected as it is a common column that is suitable for the high temperatures which are desired to clean the Tenax tubes. This column type has been previously utilized for identification and quantification of lower volatility species which are of interest in this study (Jaoui et al. 2004; Lambe et al. 2010; Zhao et al. 2013).

Prior to sampling the Tenax tubes are cleaned via thermal desorption. The tubes were cleaned by heating to 300°C for 2 hours with continuous He purge flow. Once the tubes are cleaned they are capped and placed in a freezer until use in order to prevent unwanted artifacts on the tubes.

Following sampling the Tenax tubes are returned to the freezer until analysis in the GC-MS. During analysis, the Thermal Desorption System (TDS) is set to an initial temperature of 30°C, ramped up to 275°C at a rate of 6°C/minute and then held at 275°C for 6 minutes. The desorbed vapors are collected on a Cooled Injection System (CIS) initially held at -70o C. At the end of the TDS temperature ramp, the CIS is quickly ramped up to 320°C at a rate of 12°C/second and held at 300°C allowing each of the trapped compounds to elute into the column. The GC oven temperature program starts at 45°C is ramped up to 320°C at a rate of 5°C/min and held for 5 minutes. This results in an analysis run time of 65.4 minutes, during which the MSD detector detects compounds as they elute through the column at their characteristic times.

Immediately prior to analysis the Tenax tubes are spiked with an internal standard (IS) in order to assure losses aren't occurring in the GC system. The IS is composed of deuterated alkane and aromatic compounds which have retention times within the window of retention times for the compounds we are measuring (≤ 27 minutes). The IS includes deuterated Naphthalene D8, deuterated Acenaphthene D10, and deuterated Hexadecane D34. Intra-batch percent deviation of response for each compound are ≤11%.

8) Table 4.2 Paints selected

Paint Type	Solvent/Water	Gloss Level	Indoor/Outdoor
Satin	Water	Low-gloss	Indoor
Flat	Water	Low-gloss	Indoor
Semi-Gloss Interior (SemiInt)	Water	Low-gloss	Indoor
Semi-Gloss Exterior	Water	Higher-gloss	Outdoor
High-Gloss	Water	Higher-gloss	Indoor
Oil	Solvent	Low-gloss	Indoor/Outdoor

Listed are the six paints chosen for experiments, whether they are solvent or water based, their gloss level, and their intended use environment (i.e. outdoor vs. indoor). These paints were selected as they represented a wide array of products in the paint phase space.

29) Figure 4.7 Schematic of headspace and extended emissions experiments

a) b)

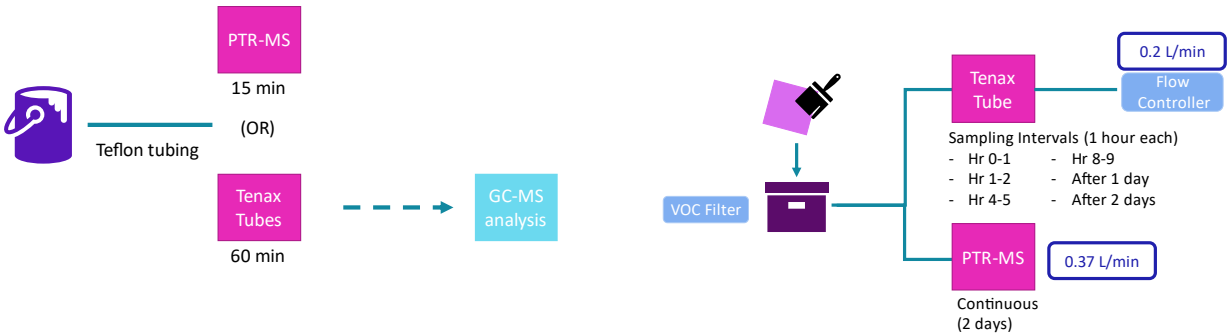

Schematics for the a) headspace sampling set-up and the b) extended emissions set up. In both cases the PTR-MS sampled continuously throughout the experiment and the Tenax tubes were analyzed offline with the thermal desorption GC-MS.

9) Table 4.3 Experiment specifications

Experiment Name, Instruments used, total time	Paint Applied [g]	Tenax Tube sampling times [recorded as hours elapsed since paint application at the midpoint of one hour samples]
Satin-1 · PTR-MS and GC-MS · [42.6 hours]	0.6633	0.5 1.7 4.9 8.3 21.9 42.1 [hours]
Satin-2 · PTR-MS and GC-MS · [45.9 hours]	0.7871	0.5 1.5 5.1 8.3 24.1 45.4 [hours]
Satin-3 · PTR-MS and GC-MS · [50 hours]	1.0196	0.5 1.6 4.9 8.3 49.5 [hours]
Flat-1 · PTR-MS and GC-MS · [52.8 hours]	1.6579	0.5 1.5 5.4 9.0 29.1

		52.3 [hours]
Flat-2 · PTR-MS and GC-MS · [36 hours]	1.5667	0.5 1.6 5.9 35.5 [hours]
SemiInt-1 · PTR-MS and GC-MS · [50.6 hours]	1.3307	0.5 1.4 4.7 8.4 50.1 [hours]
SemiInt-2 · PTR-MS and GC-MS · [47.8 hours]	2.0094	0.5 1.5 5.0 8.3 27.3 47.3 [hours]
SemiExt-1 · PTR-MS and GC-MS · [49 hours]	1.099	0.5 1.6 5.1 8.5 26.4 48.5 [hours]
SemiExt-2 · PTR-MS · [93.9 hours]	2.0377	n/a
High Gloss-1 · GC-MS · [48.6 hours]	1.5589	0.5 1.5 5.1 8.5 27.7 48.1 [hours]
High Gloss-2 · PTR-MS · [46.2 hours]	1.4264	n/a
Oil-1 · GC-MS · [341.6 hours]	1.1649	0.5 1.5 5.0 8.8 27.1 53.0 341.1 [hours]
Oil-2 · PTR-MS · [138.25]	1.6499	n/a
Shown in column 1: name of experiments performed, instruments used, and total run time, in column 2: mass of paint applied, and column 3 shows the Tenax tube sampling times. The		

sampling times show the midpoint of the sampling hour (i.e. 1.5 means a Tenax tube sample was taken from time t = 1 to time t = 2 hours following paint application). The mass of paint applied in each of the experiments is displayed in grams. For the paint types which had more than one experiment conducted the measurements from all duplicate experiments were averaged in order to get the total I/VOC emissions from that paint type.

10) Table 4.4 Volatility binning by compound class

Compound Class	Volatility Bin	Bin Limits [min]	Calibration Compound	Retention Time	Response Factor [GC response area/ng]
Alkanes	7	<15.777	undecane	14.254	83,675
	6	[15.777:24.05]	tridecane	20.2	96,648
	5	>24.05	pentadecane	25.30	84,109
Aromatics	7	<15.777	(1-Methylethyl)benzene	8.628	151,974
	7		Propylbenzene	9.449	246,118
	7		mean bin 7	-	199,046
	6	[15.777:24.05]	*interpolated*	-	229,907
	5	>24.05	*interpolated*	-	200,078
Esters	7	<12.5925	butyl butyrate	10.984	137,388
	6	>12.5925	Propyl hexanoate	14.201	250,796
	6		Pentyl valerate	17.111	299,236
	6		Nonyl acetate	20.594	105,683
	6		mean bin 6	-	218,572
Ketones	6	<15.777	acetophenone	14.059	241,848
	5	[15.777:24.05]	*interpolated*	-	279,345
	4	>24.05	*interpolated*	-	243,102
Alcohols	7	<14.945	butanol	12.105	109,669
	6	[14.945:17.784]	*interpolated*	-	90,360
	5	>17.784	nonanol	20.624	47,035

Volatility bins, bins limits, calibration compounds used for each compound bin, and resulting response factors. The response factors were calculated by creating a best fit line after plotting the GC-response area (y) versus the calibration mass (nonpolar calibration: [2.5, 5, 12.5, 25, 50]ng; polar calibration [2.5, 5, 25, 50]ng) (x). A formula for each calibration curve was generated [y = mx] and the response factor (m) was determined for each volatility bin for each compound class [units: GC area response/ng]. For some bins of some compound classes no compound was included in the calibration mixture and for those bins the response factor was interpolated based off of the present bins' relationship with the corresponding alkane bin's response factor. For amides, amines, aldehydes, and ethers there was not enough data to generate unique response factors, for these classes the binning and corresponding response factors for alkanes were used.

30) Figure 4.8 Calibration curves

(a)

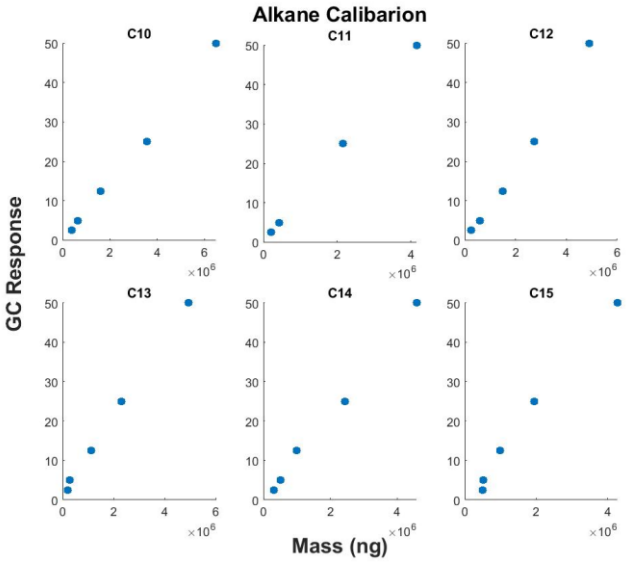

(b)

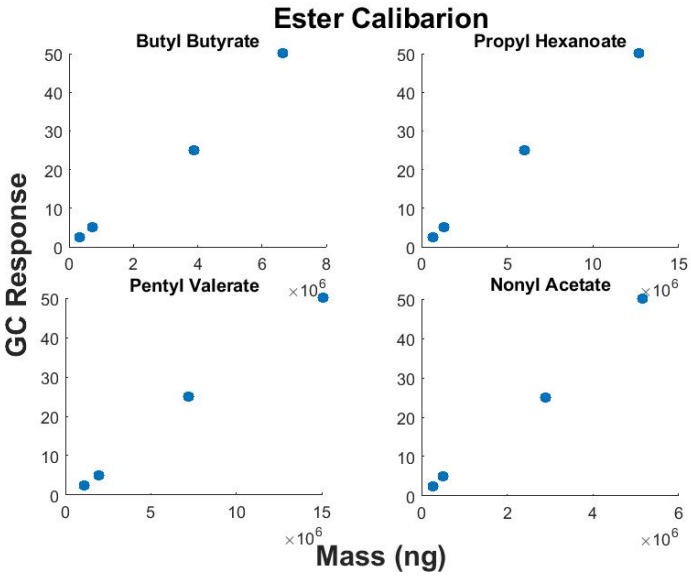

(c) (d)

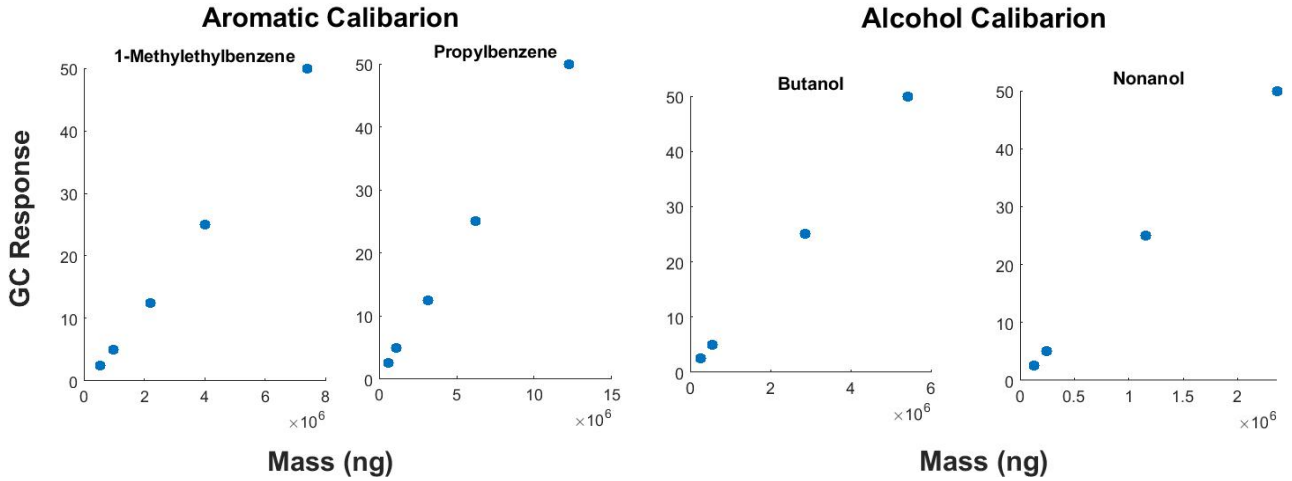

Calibration curves for (a) alkanes, (b) esters, (c) aromatics, and (d) alcohols. Response factors were determined for each compound class' volatility bins based off of calibration response factors. For compounds class bins which were not represented in calibration mixtures, alkane responses were used.

11) Table 4.5 Marker ions

Compound Class	Compound	Percent Contribution (%)	Marker Ion (*m/z*)	Mean Percent Contribution (%)
Aromatics			91	35%
	Toluene	38.85		
	Ethylbenzene	40.63		
	p-Xylene	33.18		
	o-Xylene	34.40		
	Benzene, propyl-	53.12		
	Benzene, n-butyl-	34.07		
	Benzene, hexyl-	30.15		
	Benzene, heptyl-	25.40		
	Benzene, octyl-	27.32		
Alcohols			31	6%
	Butan-1-ol	15.23		
	Pentan-1-ol	6.71		
	1-Hexanol	7.75		
	1-Heptanol	3.80		
	1-Octanol	3.31		
	1-Nonanol	2.67		
	1-Decanol	1.77		
Ketones			58	12%
	2-propanone	13.08		
	2-heptanone	19.10		

	5-Dodecanone	9.83		
	5-Tridecanone	12.30		
	9-Heptadecanone	6.63		
	5-Octadecanone	10.98		
	2-Nonadecanone	17.79		
Alkanes			71	11%
	decane	7.98		
	undecane	10.72		
	dodecane	11.72		
	tridecane	11.55		
	tetradecane	13.51		
	pentadecane	13.23		
	hexadecane	13.27		
	heptadecane	13.57		
	octadecane	9.43		
	nonadecane	10.58		
	icosane	12.69		
Aldehydes			82	5%
	Octanal	2.45		
	Nonanal	2.73		
	Decanal	3.36		
	Undecanal	4.46		
	Dodecanal	5.34		
	Tridecanal	6.32		
	Tetradecanal	6.75		
	Pentadecanal-	7.29		
	Hexadecanal	7.32		
	Octadecanal	5.69		
Esters			60	3%
	Ethyl butyrate	3.72		
	Ethyl pentanoate	6.71		
	Ethyl isovalerate	7.50		
	Ethyl hexanoate	5.14		
	Ethyl heptanoate	5.40		
	Propyl acetate	0.26		
	Propyl propanoate	0.05		
	Butyl formate	0.59		
	Butyl acetate	0.14		
	Butyl butyrate	2.42		
	Isobutyl acetate	0.10		
	Amyl acetate	0.08		
	Pentyl butyrate	1.58		
	Pentyl hexanoate	2.79		

Amines			30	58%
	1-Hexanamine	68.84		
	1-Heptanamine	64.29		
	1-Octanamine	64.72		
	1-Nonanamine	64.93		
	1-Decanamine	59.13		
	1-Undecanamine	55.04		
	1-Dodecanamine	50.22		
	1-Tridecanamine	55.43		
	1-Tetradecanamine	40.77		
Amides			59	38%
	Hexanamide	43.25		
	Octanamide	34.50		
	Nonanamide	45.58		
	Decanamide-	35.94		
	Dodecanamide	38.68		
	Tetradecanamide	29.50		
Ethers			45	28%
	Methyl propyl ether	57.52		
	Butane, 1-methoxy-	59.93		
	Pentane, 1-methoxy-	36.01		
	Hexane, 1-methoxy-	33.44		
	Octane, 1-methoxy-	22.28		
	Methyl nonyl ether	18.99		
	1-Methoxydecane	12.36		
	Methyl undecyl ether	14.70		
	Methyl tridecyl ether	10.96		
	methyl tetradecyl ether	11.03		

Compounds used to determine marker ion and percent contribution of the marker to the class mass. The marker ions for each compound group were selected based off of a group of compounds in the compound class groups with relevant saturation concentrations. An ion was selected to become a classes' marker if it (1) was (nearly) unique to that class of compounds and

(2) contributed a significant portion of the total ion response for that compound based off of the NIST mass spectral library.

31) Figure 4.9 Marker ion examples

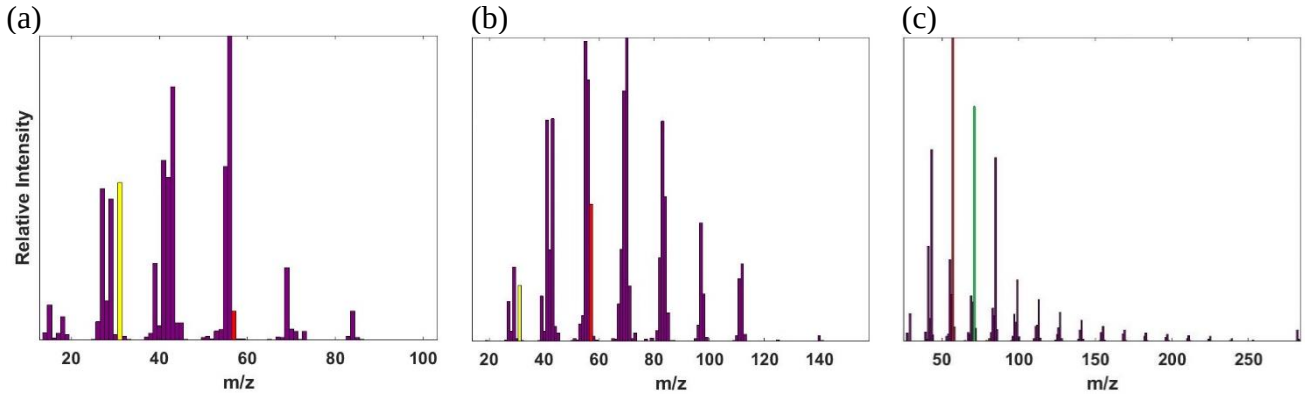

The mass spectrum for (a) hexanol, (b) decanol, and (c) eicosane. Although m/z 57 shown in red is a prominent contributor to the total mass spectrum for decanol (4.3%) it cannot be used as the marker ion for alcohols because it is also a significant contributor to alkanes as shown in (c) for eicosane (16%) and many other compounds with a long hydrocarbon chain. Instead m/z 31 is selected as the marker ion for alcohols (shown in yellow) as it is a significant contributor to many alcohols (hexanol and decanol shown as examples) and not found in other compound classes as often (not present in eicosane as shown). Similarly, although m/z 57 is a significant contributor to alkane mass spectra (as shown in c) it cannot be the marker ion for alkanes, instead m/z 71 was selected as the marker ion for alkanes (shown in green).

32) Figure 4.10 Headspace chromatographs

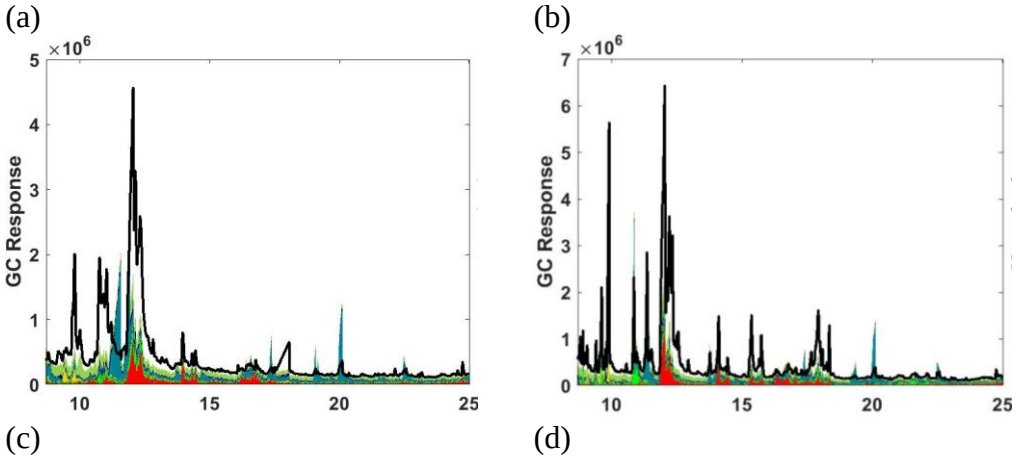

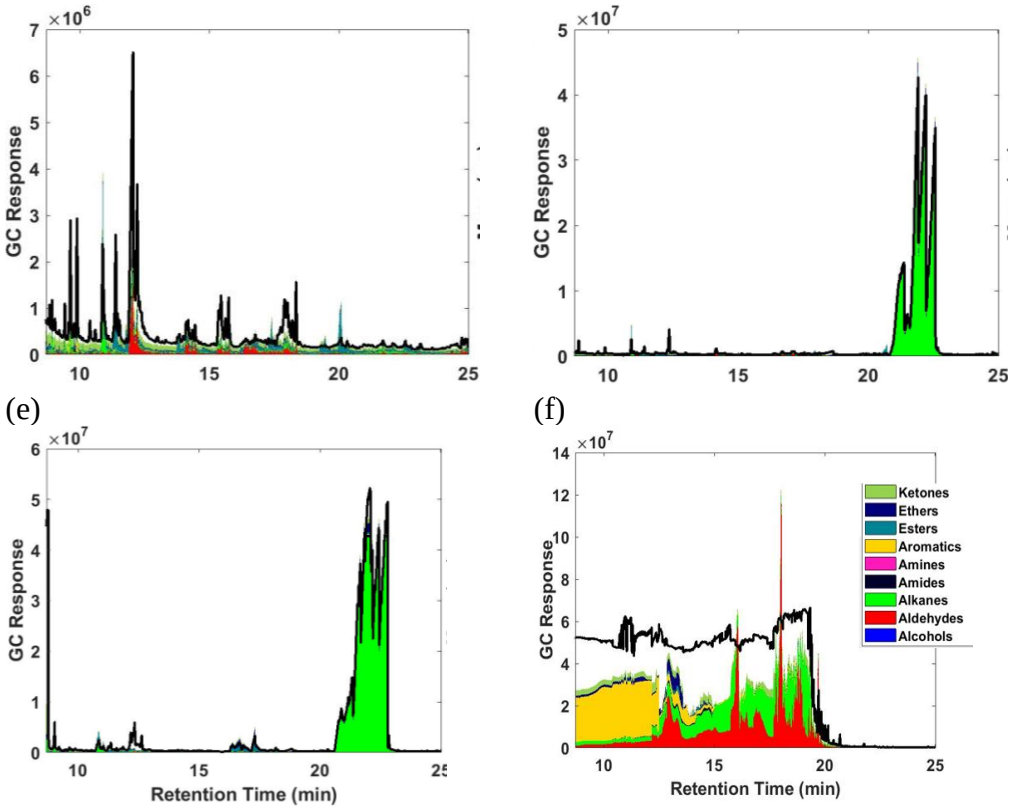

Headspace samples collected on Tenax tubes and analyzed with GC-MS of (a) Satin, (b) SemiInt, (c) Flat, (d) SemiExt, (e) High Gloss, and (f) Oil.

12) Table 4.6 List of PTR-MS ions

m/z	Compound ID	Source of ID	Class	[1:IVOC] [2:VOC]
27	ethyne	PTR library	3	2
28	ethene	PTR library	3	2
29	C2H4	-	3	2
31	formaldehyde	PTR library	2	2
33	methanol	PTR library	1	2
34	hydrogen sulfide	PTR library	3	0
40	C3H3	-	3	2
41	propyne	PTR library PubChem	3	2
42	acetonitrile	PTR library	3	0
43	cyclopropane	PTR library PubChem	3	2
44	ethenamine	PTR library PubChem	5	2
45	ethylene glycol	Stockwell et al. 2020	2	2

46	dimethylamine, ethylamine, dimethylamine	PTR library PubChem	5	2
47	ethanol	PTR library PubChem	1	2
48	nitrous acid	PTR library	4	2
49	methane thiol	PTR library PubChem	3	2
50	CH2Cl	-	3	2
51	methyl chloride	PTR library	3	2
52	C4H3	-	3	2
53	1-buten-3-yne	PTR library	3	2
54	acrylonitrile	PTR library	3	2
55	butadiene	PTR library PubChem	3	2
56	propane nitrile	PTR library	3	2
57	hydrocarbon mix	PTR library PubChem	3	0
58	propenamine	PTR library PubChem	5	2
59	acetone	PTR library PubChem	9	2
60	trimethylamine, 1-propylamine, isopropylamine, methylethylamine, trimethylamine	PTR library PubChem	5	1
61	acetic acid	PTR library PubChem EMR	7	2
62	nitromethane	PTR library	3	2
63	1,2-ethanediol	PTR library PubChem	1	1
64	C2H7O2	EMR	7	0
65	hydrocarbon	PTR library	3	2
66	hydrocarbon	PTR library	3	2
67	hydrocarbon	PTR library	3	2
68	C5H7	PTR library EMR	3	2
69	isoprene	PTR library PubChem	3	2
70	butane nitrile	PTR library PubChem	3	2

71	methyl vinyl ketone	PTR library PubChem	9	2
72	pyrrolidine	PTR library PubChem	5	2
73	butanal	PTR library PubChem	2	2
74	diethylamine	PTR library PubChem	5	2
75	methyl acetate	PTR library PubChem	7	2
76	nitroethane	PTR library PubChem	4	2
77	1,2-propanediol	PTR library PubChem	1	1
78	amine	PTR library PubChem	5	0
79	benzene	PTR library	6	2
80	pyridine	PTR library PubChem	6	2
81	C5H6N	PTR library EMR	3	2
82	C6H9	PTR library EMR	3	2
83	C4H3O2	PTR library EMR	7	2
84	C6H11	PTR library EMR	3	2
85	1-hexene, cyclohexane, methylcyclopentane	PTR library PubChem	3	2
86	2-pyrrolidinone	PTR library PubChem	9	2
87	n-hexane	PTR library PubChem EMR	3	2
88	C4H7O2	PTR library EMR	7	2
89	ethyl acetate	PTR library PubChem	7	2
90	1-nitropropane, 2-nitropropane	PTR library PubChem	4	1
91	lactic acid	PTR library PubChem	1	2
92	ethynylpyrrole	PTR library	6	0
93	toluene	PTR library	6	2

94	aromatic	PTR library	6	0
95	phenol	PTR library	1	1
96	aromatic	PTR library	6	0
97	2-furfural	PTR library PubChem	8	2
98	C6H9O	PTR library EMR	9	2
99	Cyclohexanone	PTR library PubChem EMR	9	2
100	aromatic	PTR library	6	0
101	methyl methacrylate	PTR library PubChem EMR	7	2
102	triethylamine	PTR library	5	2
103	acetic anhydride, isopropyl acetate, propyl acetate, ethyl propanoate	PTR library PubChem	7	2
104	aromatics	PTR library	6	0
105	styrene	PTR library PubChem	6	2
106	aromatics	PTR library	6	2
107	benzaldehyde, m-xylene, p-xylene, ethyl benzene, o-xylene	PTR library PubChem	6	2
108	aromatics	PTR library	6	2
109	aromatics	PTR library	6	2
110	C8H13	EMR	3	2
111	2-hydroxyphenol	PTR library PubChem	6	1
112	aromatics	PTR library	6	0
113	1-octene	PTR library PubChem	3	2
114	C6H9O2	PTR library EMR	7	1
115	n-octane	PTR library PubChem EMR	3	2
116	Hexanoate	EMR	7	2
117	ethyl butanoate, propyl propanoate, butyl acetate	PTR library PubChem	7	2

118	indole	PTR library PubChem	6	1
119	indane	PTR library PubChem	6	2
120	aromatics	PTR library	6	0
121	trimethylbenzene, acetophenone, n-propyl benzene	PTR library PubChem	6	2
122	C8H9O	EMR	6	1
123	2-phenylethanol, 4-ethylphenol	PTR library PubChem	6	1
124	aromatics	PTR library	6	1
125	guaiacol	PTR library PubChem	6	1
126	C8H13O	EMR	1	1
127	benzylchloride	PTR library PubChem	6	2
128	C8H15O	EMR	8	2
129	naphthalene	PTR library PubChem EMR	6	1
130	C7H13O2	EMR	7	1
131	butyl propanoate	PTR library PubChem EMR	7	2
132	Heptyl peroxy radical	PTR library EMR	8	2
133	1,2,3,4-tetrahydronaphthalene	PTR library PubChem	6	1
134	C6H13O3	EMR	8	1
135	aromatics	PTR library	6	1
136	bromoacetone	PTR library	9	2
137	a-pinene	PTR library	3	2
138	nitrotoluene	PTR library	6	1
139	2-methoxy-4-methylphenol	PTR library PubChem	6	1
140	C9H15O	EMR	2	1
141	1-decene	PTR library PubChem	3	2
142	C8H13O2	PTR library EMR	7	1
143	n-decane	PTR library PubChem	3	2

		EMR		
144	C8H15O2	EMR	7	1
145	butyl butyrate, isobutyl isobutyrate	PTR library PubChem	7	2
146	C8H17O2	EMR	1	1
147	C8H17O2	PTR library PubChem EMR	1	1
148	Cinnamate	EMR	6	1
149	C4[13]C3H13O3	EMR	7	0
150	Phenylglyoxylate	EMR	6	1
151	benzyl acetate	PTR library PubChem	6	1
152	aromatics	PTR library	6	1
153	vanillin, methyl salicylate, camphor	PTR library PubChem	6	1
154	C10H17O	EMR	9	1
155	biphenyl	PTR library PubChem	6	1

Mass-to-charge ratios scanned and recorded by the PTR-MS, compound identified at each m/z, method of identification, compound class and I/VOC identifications. In the column labelled "Compound ID" is the compound selected as the most likely compound at that m/z determined from a combination of one to three of the following methods. (1) PTR-MS library (Pagonis et al. 2019) was referenced (2) a search of compounds identified by the PTR-MS library were confirmed as likely products in paint with PubChem (NIH 2020) and (3) m/z that still could not be identified were IDed with analysis of open paint headspaces with a Thermo Exactive EMR mass spectrometer to generate a likely chemical formula. Based on the compound ID, compounds were sorted into one of nine class compound groups based on the best fit [1: alcohols, 2: aldehydes, 3: hydrocarbon chain/ring, 4: amides, 5: amines, 6: aromatics, 7: esters, 8: ethers, 9: ketones]. Each m/z was assigned as either [1: IVOC] or [2: VOC] based on calculation of the compound's saturation vapor pressure (C) using the SIMPOL method (Pankow and Asher 2008) [IVOCs have log(C*) ≤ 6; VOCs have log(C*) ≥ 7]. For a few ions where a specific chemical structure could not be determined the I/VOC designation was not labeled and it was left blank (0). Ultimately, when mass was split between IVOCs and VOCs the mass of compounds that were unidentified was split proportionally between the IVOC and VOC classes.*

13) Table 4.7 Ions still detected at the end of two-day extended emissions experiment

Paint Type	Ion m/z	Concentration above LOQ [ppb]
High Gloss	111	17
	129	6.5
SemExt	69	7.9

	111	12.3
Oil*	45	37.5
	61	5.1
	83	5.9
	98	34.5
	117	13.2
	145	5.3

*Ions still above background concentrations at the end of two day drying period. At the end of the two-day paint drying period (*one week for the Oil paint) although the majority of the ions were no longer detected by the PTR-MS at elevated concentrations there were a few ions that were still able to be detected at concentrations > 5ppb above the limit of quantitation (LOQ). These ions and their concentration above the LOQ are recorded here.*

14) Table 4.8 SOA yields

Compound Class	Compounds Used	SOA yield [g/g] (McDonald et al. 2018)	Uncertainty [g/g]	Mean VOC SOA yield [g/g]	Mean IVOC SOA yield [g/g]
Alkanes				0.018	0.069
VOCs	hexane	0.0028	0.0013		
	heptane	0.0066	0.0028		
	octane	0.013	0.004		
	nonane	0.021	0.006		
	decane	0.033	0.007		
	undecane	0.05	0.007		
	branched c8	0.003	0.0014		
	2-methylheptane	0.003	0.0014		
	branched c9	0.0083	0.0046		
	branched c10	0.02	0.011		
	branched c11	0.04	0.021		
IVOCs	branched c12	0.069	0.027		
	2,2,4,6,6-pentamethylheptane	0.069	0.027		
	dodecane	0.069	0.006		
Aromatics				0.067	0.217
VOCs	toluene	0.09	0.023		

	ethylbenzene	0.049	0.013		
	isomers of xylene	0.049	0.013		
	m-xylene	0.049	0.013		
	styrene	0.049	0.013		
	4-ethyltoluene	0.073	0.017		
	3-ethyltoluene	0.073	0.017		
	c9 disubstituted benzenes	0.073	0.017		
	1,2,4-trimethylbenzene	0.073	0.017		
	1,2,3-trimethylbenzene	0.073	0.017		
	1,3,5-trimethylbenzene	0.073	0.017		
	misc trimethylbenzenes	0.073	0.017		
	c9 trisubstituted benzenes	0.073	0.017		
IVOCs	indene	0.16	0.09		
	methyl indanes	0.21	0.09		
	c11 tetralins or indanes	0.28	0.08		
Alcohols				0.022	0.077
VOCs	cyclohexanol	0.022	0.018		
IVOCs	diacetone alcohol	0.067	0.061		
	hexylene glycol	0.16	0.15		
	2-butoxyethanol	0.052	0.046		
	butyl carbitol	0.16	0.15		
	texanol	0.0048	0		
	benzyl alcohol	0.09	0.023		
	phoxyethanol	0.023	0.008		
	1-phyoxy-2-propanol	0.036	0.014		
	c10 alkyl phenols	0.1	0.03		
Esters				0.013	0.302
VOCs	propyl acetate	0.0085	0.0084		
	i-propyl acetate	0.0085	0.0084		
	pentanedioic acid, dimethyl ester	0.029	0.028		
	n-butyl acetate	0.014	0.013		
	i-butyl acetate	0.014	0.013		
	dimethy succinate	0.038	0.037		
	ethyl-3-ethoxypropianate	0.038	0.037		
	i-butyl isobutyrate	0.029	0.028		

IVOCs	dimethyl adipate	0.11	0.11		
	2-ethylhexyl benzoate	0.067	0.033		
Ethers				0.016	0.106
VOCs	ethylene glycol propyl ether	0.039	0.036		
	methyl carbitol	0.066	0.062		
	propylene glocol n-propyl ether	0.052	0.046		
	propylene glycol methyl ether acetate	0.029	0.028		
IVOCs	propylene glycol butyl ether	0.068	0.06		
	di(propylene glycol) methyl ether	0.12	0.11		
	butyl carbitol	0.16	0.15		
Ketones				0.011	0.069
VOCs	methyl isobutyl ketone	0.013	0.013		
	methyl amyl ketone	0.014	0.013		
	c9 ketones	0.029	0.028		
	cyclohexanone	0.0019	0.0012		
Amides				0.018	0.069
Amines				0.018	0.069
Aldehydes				0.018	0.069

Lists of compounds used to develop general SOA yields for each compound class I/VOCs. The SOA yields for the IVOCs and VOCs for each compound class were determined through selecting compounds which were reported in McDonald et al. 2018 that had relevant saturation concentrations [3<log(C)<10] and averaging their SOA yields. For the unclassified UCM as well as compound classes where there was not enough information on SOA yields the SOA yields for alkane I/VOCs were used.*

Chapter 5

Conclusions

The first step to mitigating pollutant emissions is understanding them. $PM_{2.5}$ comes from many different sources; anthropogenic and biogenic, as well as from both primary and secondary emissions. Additionally, emissions travel over time and space to impact locations sometimes many miles away from their point source. It is important to understand these different emission sources in order to take steps toward reducing emissions.

Findings in chapter two show the utility of deploying a low-cost sensor network. The high spatial and temporal resolution of the network allows for discerning between emission sources (e.g. traffic and industry) and an understanding of which areas are at higher risk of persistent pollutant enhancements. NO_2 and SO_2 were used as tracers for traffic and industrial emissions, respectively. Areas with high traffic experienced elevated $PM_{2.5}$ and NO_2 concentrations that were dominated by traffic emissions. While sites downwind of industrial sources experienced elevated $PM_{2.5}$ concentrations influenced by industrial point sources, indicated by higher SO_2 levels. Additionally, our investigations allowed us to explore whether or not there were connections between elevated pollutant concentrations and socio-economic factors like poverty and presence of minority populations. Although there have been studies that indicate such relationships exist on a national scale, we did not find such relations within our study domain. This highlights how concepts such as environmental justice are complex and need to be examined in location specific contexts. Our analysis demonstrated the value of a dense sensor network and its ability to capture temporospatial pollutant patterns that cannot be resolved

by the sparse network of regulatory monitors. The approach we use here could easily be replicated in other cities and we suggest further deployment of dense sensor networks throughout sparsely monitored locations.

In chapter three we further expanded the use of our low-cost sensor network. In response to the COVID-19 pandemic and the ensuing business and school closures pollutant concentrations decreased around the globe. On a local level our sensor network was able to capture the impact of modifiable factors (e.g. traffic, industrial emissions, etc.) on pollutant concentrations, particularly $PM_{2.5}$. Over the course of the study we were able to discern a clear decrease in air pollution driven in large part by reductions in vehicle traffic. While the COVID-related shutdowns are unprecedented, they can offer insights into air pollution concentrations under future emissions scenarios. We found that a 50% reduction in vehicle emissions (which could result in a post-COVID world via tighter emissions standards or widescale adoption of electric vehicles) would drastically reduce the morning rush hour peak of $PM_{2.5}$, CO, and NO_2. This in turn would reduce acute exposures, especially in high traffic or near-road environments. We encourage further investigations to take place to better constrain the impact of transitioning the national fleet towards low or no-emitting vehicles.

In chapter four we turn our attention towards examining additional sources of ambient $PM_{2.5}$ and quantify volatile gas emissions from paints in order to predict their SOA mass yields. We found that I/VOC emissions from paints amount to 168.9 Gg per year in the U.S. and are projected to yield 8.0 Gg of SOA mass each year in the U.S. The paint emissions vary by paint type and use. Interestingly, findings suggest that the majority of the emissions from paints come from paints used outdoors and therefore can have a significant impact on SOA formation. It is important to continue to develop a thorough understanding of less traditional emission sources

like paints and other VCPs in order to better constrain where $PM_{2.5}$ mass is coming from and move towards reductions. Additionally, we would recommend there be steps taken to minimize the IVOC components of outdoor paints which are the highest contributor to ambient SOA mass formation from paints.

Overall this work took a multi-faceted approach to understanding pollutant concentrations. We utilized the novel technology of low-cost sensor networks to understand patterns of $PM_{2.5}$ dispersion and evolution over time as well as other gaseous pollutants. We saw that local point sources from industry as well as traffic related emissions play a large role in variations in local ambient pollutant concentrations. We then took a zoomed out approach to understand a non-traditional source of $PM_{2.5}$. We analyzed volatile organic emissions from paints (I/VOCs) and predicted SOA mass yields.

This work highlights many of the benefits of utilizing low-cost sensors in dense sensor networks. As research moves forward we would highly encourage the continued study of enhancing technologies of low-cost sensors to push them closer and closer to the data quality of regulatory monitors. As the accuracy and precision of low-cost air quality sensors increases the opportunities to further understand spatiotemporal variations in pollutant concentrations and their impact on people's daily lives will increase as well. Furthermore, we would urge that work be continued on the quantification of SOA mass formation from paints and other VCPs. Some next steps would be to conduct measurements of I/VOC emissions from paints and other VCPs under varying conditions as well as measuring actual SOA formed through use of an Oxidation Flow Reactor. Experimentation to measure SOA formed from paints to confirm the predictions made in this work which were based off of the theoretical SOA yields would be an important step toward further understanding sources of SOA. In all, in order to mitigate the unwanted

environmental and health effects of $PM_{2.5}$ and other pollutants it is imperative to fully understand not only real-time pollutant concentrations, but also emission sources as well as the evolution of those emissions over time and space.

Bibliography

Akherati, Ali, Yicong He, Matthew M. Coggon, Abigail R. Koss, Anna L. Hodshire, Kanako Sekimoto, Carsten Warneke, Joost De Gouw, Lindsay Yee, John H. Seinfeld, Timothy B. Onasch, Scott C. Herndon, Walter B. Knighton, Christopher D. Cappa, Michael J. Kleeman, Christopher Y. Lim, Jesse H. Kroll, Jeffrey R. Pierce, and Shantanu H. Jathar. 2020. "Oxygenated Aromatic Compounds Are Important Precursors of Secondary Organic Aerosol in Biomass-Burning Emissions." *Environmental Science and Technology* 54(14):8568–79.

Allegheny County Health Department. 2020. "Air Monitoring Network Plan for 2021." 1–94.

Anttila, Pia, Juha Pekka Tuovinen, and Jarkko V. Niemi. 2011. "Primary NO2 Emissions and Their Role in the Development of NO2 Concentrations in a Traffic Environment." *Atmospheric Environment* 45(4):986–92.

Bernstein, Jonathan A., Neil Alexis, Charles Barnes, I. Leonard Bernstein, Jonathan A. Bernstein, Andre Nel, David Peden, David Diaz-Sanchez, Susan M. Tarlo, and P. Brock Williams. 2004. "Health Effects of Air Pollution." *Journal of Allergy and Clinical Immunology* 114(5):1116–23.

Bishop, Gary A. and Donald H. Stedman. 2008. "A Decade of On-Road Emissions Measurements." *Environmental Science and Technology* 42(5):1651–56.

Boogaard, Hanna, Annemoon M. van Erp, Katherine D. Walker, and Rashid Shaikh. 2017. "Accountability Studies on Air Pollution and Health: The HEI Experience." *Current Environmental Health Reports* 4(4):514–22.

Bosco, Tom. 2020. "3 COVID-19 Cases Confirmed in Ohio, DeWine Declaring State of Emergency." March 9, 1–7.

Cappa, C. D. and K. R. Wilson. 2012. "Multi-Generation Gas-Phase Oxidation, Equilibrium Partitioning, and the Formation and Evolution of Secondary Organic Aerosol." *Atmospheric Chemistry and Physics* 12(20):9505–28.

Castell, Nuria, Franck R. Dauge, Philipp Schneider, Matthias Vogt, Uri Lerner, Barak Fishbain, David Broday, and Alena Bartonova. 2017. "Can Commercial Low-Cost Sensor Platforms Contribute to Air Quality Monitoring and Exposure Estimates?" *Environment International* 99.

Caubel, Julien J., Troy E. Cados, and Thomas W. Kirchstetter. 2018. "A New Black Carbon Sensor for Dense Air Quality Monitoring Networks." *Sensors (Switzerland)* 18(3):1–18.

Chan, A. W. H., K. E. Kautzman, P. S. Chhabra, J. D. Surratt, M. N. Chan, J. D. Crounse, A. Kürten, P. O. Wennberg, R. C. Flagan, and J. H. Seinfeld. 2009. "Secondary Organic Aerosol Formation from Photooxidation of Naphthalene and Alkylnaphthalenes: Implications for Oxidation of Intermediate Volatility Organic Compounds (IVOCs)." *Atmospheric Chemistry and Physics* 9(9):3049–60.

Chang, John C. S. 1999. "Evaluation of Low-VOC Latex Paints." *Indoor Air* 9(4):253–58.

Charan, Sophia M., Reina S. Buenconsejo, and John H. Seinfeld. 2020. "Secondary Organic Aerosol Yields from the Oxidation of Benzyl Alcohol." *Atmospheric Chemistry and Physics* 20(21):13167–90.

Chow, Judith C. and Judith C. Chow. 2012. "Measurement Methods to Determine Compliance with Ambient Air Quality Standards for Suspended Particles Measurement Methods to

Determine Compliance with Ambient Air Quality Standards for Suspended Particles.” 2247.
Clark, Lara P., Dylan B. Millet, and Julian D. Marshall. 2014. “Changes in Transportation-Related Air Pollution Exposures by Race-Ethnicity and Socioeconomic Status : Outdoor Nitrogen Dioxide in the United States in 2000 and 2010.” (2005):1–10.
Clark, Lara P., Dylan B. Millet, and Julian D. Marshall. 2017. “Changes in Transportation-Related Air Pollution Exposures by Race-Ethnicity and Socioeconomic Status.” *Environmental Health Perspectives* 125(9):1–10.
Clausen, Per A., Peder Wolkoff, Erik Hoist, and Peter A. Nielsen. 1991. “Long-term Emission of Volatile Organic Compounds from Waterborne Paints – Methods of Comparison.” *Indoor Air* 1(4):562–76.
Cross, Eben S., Leah R. Williams, David K. Lewis, Gregory R. Magoon, Timothy B. Onasch, Michael L. Kaminsky, Douglas R. Worsnop, and John T. Jayne. 2017. “Use of Electrochemical Sensors for Measurement of Air Pollution: Correcting Interference Response and Validating Measurements.” *Atmospheric Measurement Techniques* 10(9):3575–88.
Current Results. 2020. “Average Temperatures for Large US Cities.” 1–5. Retrieved (https://www.currentresults.com/Weather/US/average-city-temperatures-in-february.php).
Di, Qian, Yan Wang, Antonella Zanobetti, Yun Wang, Petros Koutrakis, Christine Choirat, Francesca Dominici, and Joel D. Schwartz. 2017. “Air Pollution and Mortality in the Medicare Population.” *New England Journal of Medicine* 376(26):2513–22.
Dockery, Douglas W., C. Arden Pope III, Xiping Xu, John D. Spengler, James H. Ware, Martha E. Fay, Benjamin G. Jr Ferris, and Frank E. Speizer. 1993. “The New England Journal of Medicine as Published by New England Journal of Medicine. Downloaded from Www.Nejm.Org on August 16, 2010. For Personal Use Only. No Other Uses without Permission. Copyright © 1993 Massachusetts Medical Society. All Rights Reser.” *N Engl J Med* 329(24):1753–59.
Dominici, F., RD Peng, ML Bell, L. Pham, A. McDermott, SL Zeger, and JM. Samet. 2006. “Fine Particulate Air Pollution and Hospital Admission for Cardiovascular and Respiratory Diseases.” *JAMA (Journal of the American Medical Association)* 295(10):1127–34.
Downey, Liam. 2011. “Assessing Environmental Inequality: How the Conclusions We Draw Vary According to the Definitions We Employ.” *NIH Public Access Sociol Spectr* 25(3):349–69.
Drozd, Greg T., Robert Jay Weber, and Allen H. Goldstein. 2021. “Highly Resolved Composition during Diesel Evaporation with Modeled Ozone and Secondary Aerosol Formation: Insights into Pollutant Formation from Evaporative Intermediate Volatility Organic Compound Sources.” *Environmental Science & Technology*.
Eeftens, Marloes, Ming Yi Tsai, Christophe Ampe, Bernhard Anwander, Rob Beelen, Tom Bellander, Giulia Cesaroni, Marta Cirach, Josef Cyrys, Kees de Hoogh, Audrey De Nazelle, Frank de Vocht, Christophe Declercq, Audrius Dedele, Kirsten Eriksen, Claudia Galassi, Regina Gražulevičiene, Georgios Grivas, Joachim Heinrich, Barbara Hoffmann, Minas Iakovides, Alex Ineichen, Klea Katsouyanni, Michal Korek, Ursula Krämer, Thomas Kuhlbusch, Timo Lanki, Christian Madsen, Kees Meliefste, Anna Mölter, Gioia Mosler, Mark Nieuwenhuijsen, Marieke Oldenwening, Arto Pennanen, Nicole Probst-Hensch, Ulrich Quass, Ole Raaschou-Nielsen, Andrea Ranzi, Euripides Stephanou, Dorothee Sugiri, Orsolya Udvardy, Éva Vaskövi, Gudrun Weinmayr, Bert Brunekreef, and Gerard Hoek. 2012. “Spatial Variation of PM2.5, PM10,PM2.5absorbance and PMcoarseconcentrations

between and within 20 European Study Areas and the Relationship with NO2- Results of the ESCAPE Project." *Atmospheric Environment* 62:303–17.
Eilenberg, Rose, R. Subramanian, Carl Malings, Aliaksei Hauryliuk, Albert A. Presto, and Allen L. Robinson. 2020. "Using a Network of Lower-Cost Monitors to Identify the Influence of Modifiable Factors Driving Spatial Patterns in Fine Particulate Matter Concentrations in an Urban Environment . 1 Abstract 2 Introduction." *Journal of Exposure Science & Environmental Epidemiology* 30:949–961.
Environmental Justice Work Group. 2001. "Environmental Justice Work Group." (June).
EPA. 2014. "Environmental Justice Related Terms As Defined Across the PSC Agencies." (1):1–16.
EPA. 2017. "National Emissions by NEI Year 2017." Retrieved (https://gispub.epa.gov/neireport/2017/).
Esposito, E., S. De Vito, M. Salvato, V. Bright, R. L. Jones, and O. Popoola. 2016. "Sensors and Actuators B : Chemical Dynamic Neural Network Architectures for on Field Stochastic Calibration of Indicative Low Cost Air Quality Sensing Systems." *Sensors & Actuators: B. Chemical* 231:701–13.
Fortmann, Roy, Nancy Roache, John C. S. Chang, and Zhishi Guo. 1998. "Characterization of Emissions of Volatile Organic Compounds from Interior Alkyd Paint." *Journal of the Air and Waste Management Association* 48(10):931–40.
Friedman, Michael S., Kenneth E. Powell, Lori Hutwagner, Le Roy M. Graham, and W. Gerald Teague. 2001. "Impact of Changes in Transportation and Commuting Behaviors during the 1996 Summer Olympic Games in Atlanta on Air Quality and Childhood Asthma." *Journal of the American Medical Association* 285(7):897–905.
Gakidou, Emmanuela, Ashkan Afshin, Amanuel Alemu Abajobir, Kalkidan Hassen Abate, Cristiana Abbafati, Kaja M. Abbas, Foad Abd-Allah, Abdishakur M. Abdulle, Semaw Ferede Abera, Victor Aboyans, Laith J. Abu-Raddad, Niveen M. E. Abu-Rmeileh, Gebre Yitayih Abyu, Isaac Akinkunmi Adedeji, Olatunji Adetokunboh, Mohsen Afarideh, Anurag Agrawal, Sutapa Agrawal, Aliasghar Ahmad Kiadaliri, Hamid Ahmadieh, Muktar Beshir Ahmed, Amani Nidhal Aichour, Ibtihel Aichour, Miloud Taki Eddine Aichour, Rufus Olusola Akinyemi, Nadia Akseer, Fares Alahdab, Ziyad Al-Aly, Khurshid Alam, Noore Alam, Tahiya Alam, Deena Alasfoor, Kefyalew Addis Alene, Komal Ali, Reza Alizadeh-Navaei, Ala'a Alkerwi, François Alla, Peter Allebeck, Rajaa Al-Raddadi, Ubai Alsharif, Khalid A. Altirkawi, Nelson Alvis-Guzman, Azmeraw T. Amare, Erfan Amini, Walid Ammar, Yaw Ampem Amoako, Hossein Ansari, Josep M. Antó, Carl Abelardo T. Antonio, Palwasha Anwari, Nicholas Arian, Johan Ärnlöv, Al Artaman, Krishna Kumar Aryal, Hamid Asayesh, Solomon Weldegebreal Asgedom, Tesfay Mehari Atey, Leticia Avila-Burgos, Euripide Frinel G. Arthu. Avokpaho, Ashish Awasthi, Peter Azzopardi, Umar Bacha, Alaa Badawi, Kalpana Balakrishnan, Shoshana H. Ballew, Aleksandra Barac, Ryan M. Barber, Suzanne L. Barker-Collo, Till Bärnighausen, Simon Barquera, Lars Barregard, Lope H. Barrero, Carolina Batis, Katherine E. Battle, Bernhard T. Baune, Justin Beardsley, Neeraj Bedi, Ettore Beghi, Michelle L. Bell, Derrick A. Bennett, James R. Bennett, Isabela M. Bensenor, Adugnaw Berhane, Derbew Fikadu Berhe, Eduardo Bernabé, Balem Demtsu Betsu, Mircea Beuran, Addisu Shunu Beyene, Anil Bhansali, Zulfqar A. Bhutta, Boris Bikbov, Charles Birungi, Stan Biryukov, Christopher D. Blosser, Dube Jara Boneya, Ibrahim R. Bou-Orm, Michael Brauer, Nicholas J. K. Breitborde, Hermann Brenner, Traolach S. Brugha, Lemma Negesa Bulto Bulto, Blair R. Baumgarner, Zahid A. Butt,

Lucero Cahuana-Hurtado, Rosario Cárdenas, Juan Jesus Carrero, Carlos A. Castañeda-Orjuela, Ferrán Catalá-López, Kelly Cercy, Hsing Yi Chang, Fiona J. Charlson, Odgerel Chimed-Ochir, Vesper Hichilombwe Chisumpa, Abdulaal A. Chitheer, Hanne Christensen, Devasahayam Jesudas Christopher, Massimo Cirillo, Aaron J. Cohen, Haley Comfort, Cyrus Cooper, Josef Coresh, Leslie Cornaby, Paolo Angelo Cortesi, Michael H. Criqui, John A. Crump, Lalit Dandona, Rakhi Dandona, José Das Neves, Gail Davey, Dragos V. Davitoiu, Kairat Davletov, Barbora De Courten, Louisa Degenhardt, Selina Deiparine, Robert P. Dellavalle, Kebede Deribe, Aniruddha Deshpande, Samath D. Dharmaratne, Eric L. Ding, Shirin Djalalinia, Huyen Phuc Do, Klara Dokova, David Teye Doku, E. Ray Dorsey, Tim R. Driscoll, Manisha Dubey, Bruce Bartholow Duncan, Sarah Duncan, Natalie Ebert, Hedyeh Ebrahimi, Ziad Ziad El-Khatib, Ahmadali Enayati, Aman Yesuf Endries, Sergey Petrovich Ermakov, Holly E. Erskine, Babak Eshrati, Sharareh Eskandarieh, Alireza Esteghamati, Kara Estep, Emerito Jose Aquino Faraon, Carla Sofia E. S. Farinha, André Faro, Farshad Farzadfar, Kairsten Fay, Valery L. Feigin, Seyed Mohammad Fereshtehnejad, João C. Fernandes, Alize J. Ferrari, Tesfaye Regassa Feyissa, Irina Filip, Florian Fischer, Christina Fitzmaurice, Abraham D. Flaxman, Nataliya Foigt, Kyle J. Foreman, Joseph J. Frostad, Nancy Fullman, Thomas Fürst, Joao M. Furtado, Morsaleh Ganji, Alberto L. Garcia-Basteiro, Tsegaye Tewelde Gebrehiwot, Johanna M. Geleijnse, Ayele Geleto, Bikila Lencha Gemechu, Hailay Abrha Gesesew, Peter W. Gething, Alireza Ghajar, Katherine B. Gibney, Paramjit Singh Gill, Richard F. Gillum, Ababi Zergaw Giref, Melkamu Dedefo Gishu, Giorgia Giussani, William W. Godwin, Philimon N. Gona, Amador Goodridge, Sameer Vali Gopalani, Yevgeniy Goryakin, Alessandra Carvalho Goulart, Nicholas Graetz, Harish Chander Gugnani, Jingwen Guo, Rajeev Gupta, Tanush Gupta, Vipin Gupta, Reyna A. Gutiérrez, Vladimir Hachinski, Nima Hafezi-Nejad, Gessessew Bugssa Hailu, Randah Ribhi Hamadeh, Samer Hamidi, Mouhanad Hammami, Alexis J. Handal, Graeme J. Hankey, Hilda L. Harb, Habtamu Abera Hareri, Mohammad Sadegh Hassanvand, Rasmus Havmoeller, Caitlin Hawley, Simon I. Hay, Mohammad T. Hedayati, Delia Hendrie, Ileana Beatriz Heredia-Pi, Hans W. Hoek, Nobuyuki Horita, H. Dean Hosgood, Sorin Hostiuc, Damian G. Hoy, Mohamed Hsairi, Guoqing Hu, Hsiang Huang, John J. Huang, Kim Moesgaard Iburg, Chad Ikeda, Manami Inoue, Caleb Mackay Salpeter Irvine, Maria Delores Jackson, Kathryn H. Jacobsen, Nader Jahanmehr, Mihajlo B. Jakovljevic, Alejandra Jauregui, Mehdi Javanbakht, Panniyammakal Jeemon, Lars R. K. Johansson, Catherine O. Johnson, Jost B. Jonas, Mikk Jürisson, Zubair Kabir, Rajendra Kadel, Amaha Kahsay, Ritul Kamal, André Karch, Corine Kakizi Karema, Amir Kasaeian, Nicholas J. Kassebaum, Anshul Kastor, Srinivasa Vittal Katikireddi, Norito Kawakami, Peter Njenga Keiyoro, Sefonias Getachew Kelbore, Laura Kemmer, Andre Pascal Kengne, Chandrasekharan Nair Kesavachandran, Yousef Saleh Khader, Ibrahim A. Khalil, Ejaz Ahmad Khan, Young Ho Khang, Ardeshir Khosravi, Jagdish Khubchandani, Christian Kieling, Daniel Kim, Jun Y. Kim, Yun Jin Kim, Ruth W. Kimokoti, Yohannes Kinfu, Adnan Kisa, Katarzyna A. Kissimova-Skarbek, Mika Kivimaki, Luke D. Knibbs, Ann Kristin Knudsen, Jacek A. Kopec, Soewarta Kosen, Parvaiz A. Koul, Ai Koyanagi, Michael Kravchenko, Kristopher J. Krohn, Hans Kromhout, Barthelemy Kuate Defo, Burcu Kucuk Bicer, G. Anil Kumar, Michael Kutz, Hmwe H. Kyu, Dharmesh Kumar Lal, Ratilal Lalloo, Tea Lallukka, Qing Lan, Van C. Lansingh, Anders Larsson, Alexander Lee, Paul H. Lee, James Leigh, Janni Leung, Miriam Levi, Yichong Li, Yongmei Li, Xiaofeng Liang, Misgan Legesse Liben, Shai Linn, Patrick Liu, Rakesh Lodha, Giancarlo Logroscino, Katherine J. Looker, Alan D.

Lopez, Stefan Lorkowski, Paulo A. Lotufo, Rafael Lozano, Raimundas Lunevicius, Erlyn Rachelle King Macarayan, Hassan Magdy Abd El Razek, Mohammed Magdy Abd El Razek, Marek Majdan, Reza Majdzadeh, Azeem Majeed, Reza Malekzadeh, Rajesh Malhotra, Deborah Carvalho Malta, Abdullah A. Mamun, Helena Manguerra, Lorenzo G. Mantovani, Chabila C. Mapoma, Randall V. Martin, Jose Martinez-Raga, Francisco Rogerlândio Martins-Melo, Manu Raj Mathur, Kunihiro Matsushita, Richard Matzopoulos, Mohsen Mazidi, Colm McAlinden, John J. McGrath, Suresh Mehata, Man Mohan Mehndiratta, Toni Meier, Yohannes Adama Melaku, Peter Memiah, Ziad A. Memish, Walter Mendoza, Melkamu Merid Mengesha, George A. Mensah, Gert B. M. Mensink, Seid Tiku Mereta, Atte Meretoja, Tuomo J. Meretoja, Haftay Berhane Mezgebe, Renata Micha, Anoushka Millear, Ted R. Miller, Shawn Minnig, Mojde Mirarefin, Erkin M. Mirrakhimov, Awoke Misganaw, Shiva Raj Mishra, Karzan Abdulmuhsin Mohammad, Kedir Endris Mohammed, Shafiu Mohammed, Norlinah Mohamed Ibrahim, Murali B. V. Mohan, Ali H. Mokdad, Lorenzo Monasta, Julio Cesar Montañez Hernandez, Marcella Montico, Maziar Moradi-Lakeh, Paula Moraga, Lidia Morawska, Shane D. Morrison, Cliff Mountjoy-Venning, Ulrich O. Mueller, Erin C. Mullany, Kate Muller, Gudlavalleti Venkata Satyanarayana Murthy, Kamarul Imran Musa, Mohsen Naghavi, Aliya Naheed, Vinay Nangia, Gopalakrishnan Natarajan, Ionut Negoi, Ruxandra Irina Negoi, Cuong Tat Nguyen, Grant Nguyen, Minh Nguyen, Quyen Le Nguyen, Trang Huyen Nguyen, Emma Nichols, Dina Nur Anggraini Ningrum, Marika Nomura, Vuong Minh Nong, Ole F. Norheim, Bo Norrving, Jean Jacques N. Noubiap, Carla Makhlouf Obermeyer, Felix Akpojene Ogbo, In Hwan Oh, Olanrewaju Oladimeji, Andrew Toyin Olagunju, Tinuke Oluwasefunmi Olagunju, Pedro R. Olivares, Helen E. Olsen, Bolajoko Olubukunola Olusanya, Jacob Olusegun Olusanya, John Nelson Opio, Eyal Oren, Alberto Ortiz, Erika Ota, Mayowa O. Owolabi, Mahesh Pa, Rosana E. Pacella, Adrian Pana, Basant Kumar Panda, Songhomitra Panda-Jonas, Jeyaraj D. Pandian, Christina Papachristou, Eun Kee Park, Charles D. Parry, Scott B. Patten, George C. Patton, David M. Pereira, Norberto Perico, Konrad Pesudovs, Max Petzold, Michael Robert Phillips, Julian David Pillay, Michael A. Piradov, Farhad Pishgar, Dietrich Plass, Martin A. Pletcher, Suzanne Polinder, Svetlana Popova, Richie G. Poulton, Farshad Pourmalek, Narayan Prasad, Carrie Purcell, Mostafa Qorbani, Amir Radfar, Anwar Rafay, Afarin Rahimi-Movaghar, Vafa Rahimi-Movaghar, Mahfuzar Rahman, Mohammad Hifz Ur Rahman, Muhammad Aziz Rahman, Rajesh Kumar Rai, Sasa Rajsic, Usha Ram, Salman Rawaf, Colin D. Rehm, Jürgen Rehm, Robert C. Reiner, Marissa B. Reitsma, Luz Myriam Reynales-Shigematsu, Giuseppe Remuzzi, Andre M. N. Renzaho, Serge Resnikoff, Satar Rezaei, Antonio L. Ribeiro, Juan A. Rivera, Kedir Teji Roba, David Rojas-Rueda, Yesenia Roman, Robin Room, Gholamreza Roshandel, Gregory A. Roth, Dietrich Rothenbacher, Enrico Rubagotti, Lesley Rushton, Nafis Sadat, Mahdi Safdarian, Sare Safi, Saeid Safiri, Ramesh Sahathevan, Joseph Salama, Joshua A. Salomon, Abdallah M. Samy, Juan Ramon Sanabria, Maria Dolores Sanchez-Niño, Tania G. Sánchez-Pimienta, Damian Santomauro, Itamar S. Santos, Milena M. Santric Milicevic, Benn Sartorius, Maheswar Satpathy, Monika Sawhney, Sonia Saxena, Elke Schaeffner, Maria Inês Schmidt, Ione J. C. Schneider, Aletta E. Schutte, David C. Schwebel, Falk Schwendicke, Soraya Seedat, Sadaf G. Sepanlou, Berrin Serdar, Edson E. Servan-Mori, Gavin Shaddick, Amira Shaheen, Saeid Shahraz, Masood Ali Shaikh, Teresa Shamah Levy, Mansour Shamsipour, Morteza Shamsizadeh, Sheikh Mohammed Shariful Islam, Jayendra Sharma, Rajesh Sharma, Jun She, Jiabin Shen, Peilin Shi, Kenji Shibuya, Chloe Shields, Mekonnen Sisay

Shiferaw, Mika Shigematsu, Min Jeong Shin, Rahman Shiri, Reza Shirkoohi, Kawkab Shishani, Haitham Shoman, Mark G. Shrime, Inga Dora Sigfusdottir, Diego Augusto Santos Silva, João Pedro Silva, Dayane Gabriele Alves Silveira, Jasvinder A. Singh, Virendra Singh, Dhirendra Narain Sinha, Eirini Skiadaresi, Erica Leigh Slepak, David L. Smith, Mari Smith, Badr H. A. Sobaih, Eugene Sobngwi, Samir Soneji, Reed J. D. Sorensen, Luciano A. Sposato, Chandrashekhar T. Sreeramareddy, Vinay Srinivasan, Nicholas Steel, Dan J. Stein, Caitlyn Steiner, Sabine Steinke, Mark Andrew Stokes, Bryan Strub, Michelle Subart, Muawiyyah Babale Sufiyan, Rizwan Abdulkader Suliankatchi, Patrick J. Sur, Soumya Swaminathan, Bryan L. Sykes, Cassandra E. I. Szoeke, Rafael Tabarés-Seisdedos, Santosh Kumar Tadakamadla, Ken Takahashi, Jukka S. Takala, Nikhil Tandon, Marcel Tanner, Yihunie L. Tarekegn, Mohammad Tavakkoli, Teketo Kassaw Tegegne, Arash Tehrani-Banihashemi, Abdullah Sulieman Terkawi, Belay Tesssema, J. S. Thakur, Ornwipa Thamsuwan, Kavumpurathu Raman Thankappan, Andrew M. Theis, Matthew Lloyd Thomas, Alan J. Thomson, Amanda G. Thrift, Taavi Tillmann, Ruoyan Tobe-Gai, Myriam Tobollik, Mette C. Tollanes, Marcello Tonelli, Roman Topor-Madry, Anna Torre, Miguel Tortajada, Mathilde Touvier, Bach Xuan Tran, Thomas Truelsen, Kald Beshir Tuem, Emin Murat Tuzcu, Stefanos Tyrovolas, Kingsley Nnanna Ukwaja, Chigozie Jesse Uneke, Rachel Updike, Olalekan A. Uthman, Job F. M. Van Boven, Aaron Van Donkelaar, Santosh Varughese, Tommi Vasankari, Lennert J. Veerman, Vidhya Venkateswaran, Narayanaswamy Venketasubramanian, Francesco S. Violante, Sergey K. Vladimirov, Vasiliy Victorovich Vlassov, Stein Emil Vollset, Theo Vos, Fiseha Wadilo, Tolassa Wakayo, Mitchell T. Wallin, Yuan Pang Wang, Scott Weichenthal, Elisabete Weiderpass, Robert G. Weintraub, Daniel J. Weiss, Andrea Werdecker, Ronny Westerman, Harvey A. Whiteford, Charles Shey Wiysonge, Belete Getahun Woldeyes, Charles D. A. Wolfe, Rachel Woodbrook, Abdulhalik Workicho, Sarah Wulf Hanson, Denis Xavier, Gelin Xu, Simon Yadgir, Bereket Yakob, Lijing L. Yan, Mehdi Yaseri, Hassen Hamid Yimam, Paul Yip, Naohiro Yonemoto, Seok Jun Yoon, Marcel Yotebieng, Mustafa Z. Younis, Zoubida Zaidi, Maysaa El Sayed Zaki, Luis Zavala-Arciniega, Xueying Zhang, Stephanie Raman M. Zimsen, Ben Zipkin, Sanjay Zodpey, Stephen S. Lim, and Christopher J. L. Murray. 2017. "Global, Regional, and National Comparative Risk Assessment of 84 Behavioural, Environmental and Occupational, and Metabolic Risks or Clusters of Risks, 1990-2016: A Systematic Analysis for the Global Burden of Disease Study 2016." *The Lancet* 390(10100):1345–1422.

Gandolfo, Adrien, Sylvain Marque, Brice Temime-Roussel, Rachel Gemayel, Henri Wortham, Delphine Truffier-Boutry, Vincent Bartolomei, and Sasho Gligorovski. 2018. "Unexpectedly High Levels of Organic Compounds Released by Indoor Photocatalytic Paints." *Environmental Science & Technology* 52(19):11328–37.

Gkatzelis, Georgios I., Matthew M. Coggon, Brian C. McDonald, Jeff Peischl, Kenneth C. Aikin, Jessica B. Gilman, Michael Trainer, and Carsten Warneke. 2021. "Identifying Volatile Chemical Product Tracer Compounds in U.S. Cities." *Environmental Science & Technology* 55(1):188–99.

Goliff, Wendy S., Dennis R. Fitz, Kathy Cocker, Kurt Bumiller, Charles Bufalino, and Dylan Switzer. 2012. "Ambient Measurements of 2,2,4-Trimethyl, 1,3-Pentanediol Monoisobutyrate in Southern California." *Journal of the Air and Waste Management Association* 62(6):680–85.

Google LLC. 2020. *Pennsylvania April 11, 2020 Mobility Changes*. Mountain View, CA.

De Gouw, Joost and Carsten Warneke. 2007. “Measurements of Volatile Organic Compounds in the Earth’s Atmosphere Using Proton-Transfer-Reaction Mass Spectrometry.” *Mass Spectrometry Reviews* 26(2):223–57.

De Gouw, Joost, Carsten Warneke, Thomas Karl, Gunter Eerdekens, Carina Van der Veen, and Ray Fall. 2003. “Sensitivity and Specificity of Atmospheric Trace Gas Detection by Proton-Transfer-Reaction Mass Spectrometry.” *International Journal of Mass Spectrometry* 223–224:365–82.

Gu, Peishi, Hugh Z Li, Qing Ye, Ellis S. Robinson, Joshua S. Apte, Allen L. Robinson, and Albert A. Presto. 2018. “Intracity Variability of Particulate Matter Exposure Is Driven by Carbonaceous Sources and Correlated with Land-Use Variables.” *Environmental Science & Technology* 52(September):11545–54.

Gu, Peishi, Hugh Z. Li, Qing Ye, Ellis S. Robinson, Joshua S. Apte, Allen L. Robinson, and Albert A. Presto. 2018. “Intracity Variability of Particulate Matter Exposure Is Driven by Carbonaceous Sources and Correlated with Land-Use Variables.” *Environmental Science and Technology* 52(20):11545–54.

Guo, Zhishi, John C. S. Chang, Leslie E. Sparks, and Roy C. Fortmann. 1999. “Estimation of the Rate of VOC Emissions from Solvent-Based Indoor Coating Materials Based on Product Formulation.” *Atmospheric Environment* 33(8):1205–15.

Hagan, David H., Gabriel Isaacman-vanwertz, Jonathan P. Franklin, Lisa M. M. Wallace, Benjamin D. Kocar, Colette L. Heald, and Jesse H. Kroll. 2018. “Calibration and Assessment of Electrochemical Air Quality Sensors by Co-Location with Regulatory-Grade Instruments.” *Atmospheric Measurement Techniques* 315–28.

Heinrich, Joachim, Bernd Hoelscher, Christian Frye, Ines Meyer, Mike Pitz, and H. Erich. 2002. “Improved Air Quality in Reunified Germany and Decreases in Respiratory Symptoms Cyrys , Matthias Wjst , Lucas Neas and H . -Erich Wichmann Published by : Lippincott Williams & Wilkins Stable URL : Http://Www.Jstor.Org/Stable/3703762 . Your Use of the JSTO.” *Epidemiology* 13(4):394–401.

Helmig, Detlev and Lee Vierling. 1995. “Water Adsorption Capacity of the Solid Adsorbents Tenax TA, Tenax GR, Carbotrap, Carbotrap C, Carbosieve SIII, and Carboxen 569 and Water Management Techniques for the Atmospheric Sampling of Volatile Organic Trace Gases.” *Analytical Chemistry* 67(23):4380–86.

Hodzic, A., J. L. Jimenez, S. Madronich, M. R. Canagaratna, P. F. Decarlo, L. Kleinman, and J. Fast. 2010. “Modeling Organic Aerosols in a Megacity: Potential Contribution of Semi-Volatile and Intermediate Volatility Primary Organic Compounds to Secondary Organic Aerosol Formation.” *Atmospheric Chemistry and Physics* 10(12):5491–5514.

Hodzic, Alma, Prasad S. Kasibhatla, Duseong S. Jo, Christopher D. Cappa, Jose L. Jimenez, Sasha Madronich, and Rokjin J. Park. 2016. “Rethinking the Global Secondary Organic Aerosol (SOA) Budget: Stronger Production, Faster Removal, Shorter Lifetime.” *Atmospheric Chemistry and Physics* 16(12):7917–41.

Janechek, Nathan J., Rachel F. Marek, Nathan Bryngelson, Ashish Singh, Robert L. Bullard, William H. Brune, and Charles O. Stanier. 2019. “Physical Properties of Secondary Photochemical Aerosol from OH Oxidation of a Cyclic Siloxane.” *Atmos. Chem. Phys* 19:1649–64.

Jaoui, M., T. E. Kleindienst, M. Lewandowski, and E. O. Edney. 2004. “Identification and Quantification of Aerosol Polar Oxygenated Compounds Bearing Carboxylic or Hydroxyl Groups. 1. Method Development.” *Analytical Chemistry* 76(16):4765–78.

Jathar, Shantanu H., Timothy D. Gordona, Christopher J. Hennigan, Havala O. T. Pye, George Pouliot, Peter J. Adams, Neil M. Donahue, and Allen L. Robinson. 2014. "Unspeciated Organic Emissions from Combustion Sources and Their Influence on the Secondary Organic Aerosol Budget in the United States." *Proceedings of the National Academy of Sciences of the United States of America* 111(29):10473–78.

Jathar, Shantanu H., Matthew Woody, Havala O. T. Pye, Kirk R. Baker, and Allen L. Robinson. 2017. "Chemical Transport Model Simulations of Organic Aerosol in Southern California: Model Evaluation and Gasoline and Diesel Source Contributions." *Atmos. Chem. Phys* 17:4305–18.

Jayaratne, Rohan, Xiaoting Liu, Phong Thai, Matthew Dunbabin, and Lidia Morawska. 2018. "The Influence of Humidity on the Performance of a Low-Cost Air Particle Mass Sensor and the Effect of Atmospheric Fog." 4883–90.

Jimenez, J. L., M. R. Canagaratna, N. M. Donahue, A. S. H. Prevot, Q. Zhang, J. H. Kroll, P. F. Decarlo, J. D. Allan, H. Coe, N. L. Ng, A. C. Aiken, I. M. Ulbrich, A. P. Grieshop, J. Duplissy, K. R. Wilson, V. A. Lanz, C. Hueglin, Y. L. Sun, J. Tian, A. Laaksonen, T. Raatikainen, J. Rautiainen, P. Vaattovaara, M. Ehn, M. Kulmala, J. M. Tomlinson, M. J. Cubison, E. J. Dunlea, M. R. Alfarra, P. I. Williams, K. Bower, Y. Kondo, J. Schneider, F. Drewnick, S. Borrmann, S. Weimer, K. Demerjian, D. Salcedo, L. Cottrell, A. Takami, T. Miyoshi, A. Shimono, J. Y. Sun, Y. M. Zhang, K. Dzepina, D. Sueper, J. T. Jayne, S. C. Herndon, L. R. Williams, E. C. Wood, A. M. Middlebrook, C. E. Kolb, U. Baltensperger, and D. R. Worsnop. 2009. "Evolution of Organic Aerosols in the Atmosphere." *Science* (December):1525–30.

Kelly, K. E., J. Whitaker, A. Petty, C. Widmer, A. Dybwad, D. Sleeth, R. Martin, and A. Butter. 2017. "Ambient and Laboratory Evaluation of a Low-Cost Particulate Matter." 221:491–500.

Khare, Peeyush and Drew R. Gentner. 2018. "Considering the Future of Anthropogenic Gas-Phase Organic Compound Emissions and the Increasing Influence of Non-Combustion Sources on Urban Air Quality." 5391–5413.

Khare, Peeyush, Jo Machesky, Ricardo Soto, Megan He, Albert A. Presto, and Drew R. Gentner. 2020. "Asphalt-Related Emissions Are a Major Missing Nontraditional Source of Secondary Organic Aerosol Precursors." *Science Advances* 6(36):eabb9785.

Khare, Puja and B. P. Baruah. 2011. "Estimation of Emissions of SO2, PM2.5, and Metals Released from Coke Ovens Using High Sulfur Coals." *Environmental Progress & Sustainable Energy* 30(1):123–29.

Kiil, Søren. 2006. "Drying of Latex Films and Coatings: Reconsidering the Fundamental Mechanisms." *Progress in Organic Coatings* 57(3):236–50.

Kiser, Jennifer. 2020. "Coronavirus in Ohio : Governor Orders Schools to Take Extended Spring Breaks Starting Monday." 1–11. Retrieved April 22, 2020 (https://www.nbc4i.com/news/local-news/coronavirus-in-ohio-governor-orders-schools-to-take-extended-spring-breaks-starting-monday/).

Koehler, Kirsten A. and Thomas M. Peters. 2015. "New Methods for Personal Exposure Monitoring for Airborne Particles." 399–411.

Krudysz, M., K. Moore, M. Geller, C. Sioutas, and J. Froines. 2009. "Intra-Community Spatial Variability of Particulate Matter Size Distributions in Southern California/Los Angeles." *Atmospheric Chemistry and Physics* 9(3):1061–75.

Kumar, Prashant, Lidia Morawska, Claudio Martani, George Biskos, Marina Neophytou, Silvana

Di Sabatino, Margaret Bell, Leslie Norford, and Rex Britter. 2015. “The Rise of Low-Cost Sensing for Managing Air Pollution in Cities.” *Environment International* 75.
Laden, Francine, Joel Schwartz, Frank E. Speizer, and Douglas W. Dockery. 1998. “Reduction in Fine Particulate Air Pollution and Mortality Extended Follow-up of the Harvard Six Cities Study.” (7).
Lambe, Andrew T., Heber J. Chacon-madrid, Ngoc T. Nguyen, A. Emily, Nathan M. Kreisberg, Susanne V Hering, Allen H. Goldstein, Neil M. Donahue, Allen L. Robinson, Andrew T. Lambe, Heber J. Chacon-madrid, Ngoc T. Nguyen, A. Emily, Nathan M. Kreisberg, Susanne V Hering, Allen H. Goldstein, Neil M. Donahue, Allen L. Robinson, Organic Aerosol, Speciation Intercomparison, Andrew T. Lambe, Heber J. Chacon-madrid, Ngoc T. Nguyen, Emily A. Weitkamp, Nathan M. Kreisberg, Susanne V Hering, Allen H. Goldstein, Neil M. Donahue, and Allen L. Robinson. 2010. “Organic Aerosol Speciation : Intercomparison of Thermal Desorption Aerosol GC / MS (TAG) and Filter-Based Techniques Organic Aerosol Speciation : Intercomparison of Thermal Desorption Aerosol GC / MS (TAG) and Filter-Based Techniques.” 6826.
Li, Hugh Z., Timothy R. Dallmann, Peishi Gu, and Albert A. Presto. 2016. “Application of Mobile Sampling to Investigate Spatial Variation in Fine Particle Composition.” *Atmospheric Environment* 142:71–82.
Li, Hugh Z., Peishi Gu, Qing Ye, Naomi Zimmerman, Ellis S. Robinson, and R. Subramanian. 2019. “Spatially Dense Air Pollutant Sampling : Implications of Spatial Variability on the Representativeness of Stationary Air Pollutant Monitors Atmospheric Environment : X Spatially Dense Air Pollutant Sampling : Implications of Spatial Variability on the Rep.” *Atmospheric Environment: X* 2(January):100012.
Li, Lijie and David R. Cocker. 2018. “Molecular Structure Impacts on Secondary Organic Aerosol Formation from Glycol Ethers.” *Atmospheric Environment* 180:206–15.
Lin, C. C. and R. L. Corsi. 2007. “Texanol® Ester Alcohol Emissions from Latex Paints: Temporal Variations and Multi-Component Recoveries.” *Atmospheric Environment* 41(15):3225–34.
Lindinger, W., A. Hansel, and A. Jordan. 1998. “On-Line Monitoring of Volatile Organic Compounds at Pptv Levels by Means of Proton-Transfer-Reaction Mass Spectrometry (PTR-MS) Medical Applications, Food Control and Environmental Research.” *International Journal of Mass Spectrometry and Ion Processes* 173(3):191–241.
Ma, Jiesi, Xiang Li, Peishi Gu, Timothy R. Dallmann, Albert A. Presto, and Neil M. Donahue. 2016. “Estimating Ambient Particulate Organic Carbon Concentrations and Partitioning Using Thermal Optical Measurements and the Volatility Basis Set.” *Aerosol Science and Technology* 50(6):638–51.
Maier, I. and M. Fieber. 1988. “Retention Characteristics of Volatile Compounds on Tenax TA.” *Journal of High Resolution Chromatography* 11(8):566–76.
Malings, Carl, Rebecca Tanzer, Aliaksei Hauryliuk, Sriniwasa P. N. Kumar, Naomi Zimmerman, Levent B. Kara, Albert A. Presto, and R. Subramanian. 2019. “Development of a General Calibration Model and Long-Term Performance Evaluation of Low-Cost Sensors for Air Pollutant Gas Monitoring.” *Atmospheric Measurement Techniques* 12:903–20.
Malings, Carl, Rebecca Tanzer, Aliaksei Hauryliuk, Provat K. Saha, L. Allen, Albert A. Presto, R. Subramanian, Carl Malings, Rebecca Tanzer, Aliaksei Hauryliuk, Provat K. Saha, L. Allen, Carl Malings Ã, Rebecca Tanzer, Aliaksei Hauryliuk, Provat K. Saha, Allen L. Robinson, Albert A. Presto, and R. Subramanian. 2019. “Fine Particle Mass Monitoring

with Low-Cost Sensors : Corrections and Long-Term Performance Evaluation Term Performance Evaluation." *Aerosol Science and Technology* 54(2):160–74.
McDonald, Brian C., Drew R. Gentner, Allen H. Goldstein, and Robert A. Harley. 2013. "Long-Term Trends in Motor Vehicle Emissions in U.S. Urban Areas." *Environmental Science and Technology* 47(17):10022–31.
McDonald, Brian C., Joost A. De Gouw, Jessica B. Gilman, Shantanu H. Jathar, Ali Akherati, Christopher D. Cappa, Jose L. Jimenez, Julia Lee-Taylor, Patrick L. Hayes, Stuart A. McKeen, Yu Yan Cui, Si Wan Kim, Drew R. Gentner, Gabriel Isaacman-VanWertz, Allen H. Goldstein, Robert A. Harley, Gregory J. Frost, James M. Roberts, Thomas B. Ryerson, and Michael Trainer. 2018. "Volatile Chemical Products Emerging as Largest Petrochemical Source of Urban Organic Emissions." *Science* 359(6377):760–64.
Mead, M. I., O. A. M. Popoola, G. B. Stewart, P. Landshoff, M. Calleja, M. Hayes, J. J. Baldovi, M. W. Mcleod, T. F. Hodgson, J. Dicks, A. Lewis, J. Cohen, R. Baron, J. R. Saffell, and R. L. Jones. 2013. "The Use of Electrochemical Sensors for Monitoring Urban Air Quality in Low-Cost , High-Density Networks." *Atmospheric Environment* 70:186–203.
Miracolo, Marissa A., Albert A. Presto, Andrew T. Lambe, Christopher J. Hennigan, Neil M. Donahue, Jesse H. Kroll, Douglas R. Worsnop, and Allen L. Robinson. 2010. "Photo-Oxidation of Low-Volatility Organics Found in Motor Vehicle Emissions: Production and Chemical Evolution of Organic Aerosol Mass." *Environmental Science and Technology* 44(5):1638–43.
Möllmann-Coers, Michael, Dieter Klemp, Katja Mannschreck, and Franz Slemr. 2002. "Determination of Anthropogenic Emissions in the Augsburg Area by the Source-Tracer-Ratio Method." *Atmospheric Environment* 36(SUPPL. 1):95–107.
Moltchanov, Sharon, Ilan Levy, Yael Etzion, Uri Lerner, David M. Broday, and Barak Fishbain. 2015. "On the Feasibility of Measuring Urban Air Pollution by Wireless Distributed Sensor Networks." *Science of the Total Environment* 502:537–47.
Morris, Ralph E., Jaegun Jung, Bonyoung Koo, and Jason Maranche. 2013. "Application of an Integrated Plume to Regional Photochemical Model for the Allegheny County Liberty-Clairton PM2.5 Attainment Demonstration Modeling." *Air and Waste Management Association - Guideline on Air Quality Models 2013: The Path Forward* 2:874–901.
Murphy, Benjamin N., Matthew C. Woody, Jose L. Jimenez, Ann Marie G. Carlton, Patrick L. Hayes, Shang Liu, Nga L. Ng, Lynn M. Russell, Ari Setyan, Lu Xu, Jeff Young, Rahul A. Zaveri, Qi Zhang, and Havala O. T. Pye. 2017. "Semivolatile POA and Parameterized Total Combustion SOA in CMAQv5.2: Impacts on Source Strength and Partitioning." *Atmospheric Chemistry and Physics* 17(18):11107–33.
National Centers for Environmental Information. 2020. "NOAA: Local Climatological Data." *NOAA*. Retrieved (https://www.ncdc.noaa.gov/data-access/quick-links).
NIH. 2020. "PubChem Database." *Pubchem Database* 1–2.
Oolman, Larry. 2020. "Atmospheric Sounding Data." 2020. Retrieved (http://weather.uwyo.edu/upperair/sounding.html).
Pagonis, Demetrios, Kanako Sekimoto, and Joost de Gouw. 2019. "A Library of Proton-Transfer Reactions of H3O+ Ions Used for Trace Gas Detection." *Journal of the American Society for Mass Spectrometry* 30(7):1330–35.
Pankow, J. F. and W. E. Asher. 2008. "SIMPOL.1: A Simple Group Contribution Method for Predicting Vapor Pressures and Enthalpies of Vaporization of Multifunctional Organic Compounds." *Atmospheric Chemistry and Physics* 8(10):2773–96.

Parsons, Jim. 2020. “Gov . Wolf Orders Restaurants, Bars to Close Dine-in Service in Several Counties, Including Allegheny.” 1–8.
Pennsylvania Department of Environemental Protection. n.d. “Attainment Status by Principal Pollutants.” Retrieved May 26, 2020 (https://www.dep.pa.gov/Business/Air/BAQ/Regulations/Pages/Attainment-Status.aspx).
Pollack, Ilana B., Thomas B. Ryerson, Michael Trainer, J. A. Neuman, James M. Roberts, and David D. Parrish. 2013. “Trends in Ozone, Its Precursors, and Related Secondary Oxidation Products in Los Angeles, California: A Synthesis of Measurements from 1960 to 2010.” *Journal of Geophysical Research Atmospheres* 118(11):5893–5911.
Presto, Albert A., Christopher J. Hennigan, Ngoc T. Nguyen, and Allen L. Robinson. 2012. “Determination of Volatility Distributions of Primary Organic Aerosol Emissions from Internal Combustion Engines Using Thermal Desorption Gas Chromatography Mass Spectrometry.” *Aerosol Science and Technology* 46(10):1129–39.
Presto, Albert A., Marissa A. Miracolo, Neil M. Donahue, and Allen L. Robinson. 2010. “Secondary Organic Aerosol Formation from High-NOx Photo-Oxidation of Low Volatility Precursors: N-Alkanes.” *Environmental Science and Technology* 44(6):2029–34.
Presto, Albert a, Timothy R. Dallmann, Peishi Gu, and Unnati Rao. 2016. “BTEX Exposures in an Area Impacted by Industrial and Mobile Sources: Source Attribution and Impact of Averaging Time.” *Journal of the Air & Waste Management Association (1995)* 66(4):387–401.
Rai, Aakash C., Prashant Kumar, Francesco Pilla, Andreas N. Skouloudis, Silvana Di, Carlo Ratti, Ansar Yasar, and David Rickerby. 2017. “Science of the Total Environment End-User Perspective of Low-Cost Sensors for Outdoor Air Pollution Monitoring.” *Science of the Total Environment* 607–608:691–705.
Ransom, Michael R. and C. Arden Pope III. 1995. “External Health Costs of a Steel Mill.” *Contemporary Economic Policy* 13(2):86–97.
Rich, David Q., Kaibo Liu, Jinliang Zhang, Sally W. Thurston, Timothy P. Stevens, Ying Pan, Cathleen Kane, Barry Weinberger, Pamela Ohman-Strickland, Tracey J. Woodruff, Xiaoli Duan, Vanessa Assibey-Mensah, and Junfeng Zhang. 2015. “Differences in Birth Weight Associated with the 2008 Beijing Olympics Air Pollution Reduction: Results from a Natural Experiment.” *Environmental Health Perspectives* 123(9):880–87.
Robinson, Allen L., Neil M. Donahue, Manish K. Shrivastava, Emily A. Weitkamp, Amy M. Sage, Andrew P. Grieshop, Timothy E. Lane, Jeffrey R. Pierce, and Spyros N. Pandis. 2007. “Rethinking Organic Aerosols : Semivolatile Emissions And.” *Science* 1259(2007):1259–63.
Rothweiler, Heinz, Patrick A. Wäger, and Christian Schlatter. 1991. “Comparison of Tenax Ta and Carbotrap for Sampling and Analysis of Volatile Organic Compounds in Air.” *Atmospheric Environment. Part B, Urban Atmosphere* 25(2):231–35.
Seltzer, Karl, Elyse Pennington, Venkatesh Rao, Benjamin Murphy, Madeleine Strum, Kristin Isaacs, and Havala Pye. 2020. “Reactive Organic Carbon Emissions from Volatile Chemical Products.” *Atmospheric Chemistry and Physics* 1–33.
Sergent, Jim, George Petras, and Veronica Bravo. 2020. “5 Maps Show How States Differ on Protecting Americans against Coronavirus.” 1–25. Retrieved April 22, 2020 (https://www.usatoday.com/in-depth/news/2020/03/24/coronavirus-state-measures-contain-disease-vary-widely/2897975001/).
Shah, Rishabh U., Matthew M. Coggon, Georgios I. Gkatzelis, Brian C. McDonald, Antonios

Tasoglou, Heinz Huber, Jessica Gilman, Carsten Warneke, Allen L. Robinson, and Albert A. Presto. 2020. “Urban Oxidation Flow Reactor Measurements Reveal Significant Secondary Organic Aerosol Contributions from Volatile Emissions of Emerging Importance.” *Environmental Science and Technology* 54(2):714–25.

Silva, Gabriela V., M. Teresa S. D. Vasconcelos, Armando M. Santos, and Eduardo O. Fernandes. 2003. “Comparison of the Substrate Effect on VOC Emissions from Water Based Varnish and Latex Paint.” *Environmental Science and Pollution Research* 10(4):209–16.

Snyder, Emily G., Timothy H. Watkins, Paul A. Solomon, Eben D. Thoma, Ronald W. Williams, Gayle S. W. Hagler, David Shelow, David A. Hindin, Vasu J. Kilaru, and Peter W. Preuss. 2013. “The Changing Paradigm of Air Pollution Monitoring.” *Environmental Science & Technology* 47(20):11369–77.

Spinelle, Laurent, Michel Gerboles, Maria Gabriella Villani, Manuel Aleixandre, and Fausto Bonavitacola. 2015. “Field Calibration of a Cluster of Low-Cost Available Sensors for Air Quality Monitoring. Part A: Ozone and Nitrogen Dioxide.” *Sensors & Actuators: B. Chemical* 215:249–57.

Stetter, Joseph R. 2008. “Amperometric Gas Sensors s A Review.” *Chem. Rev.* 108(2):352–66.

Stockwell, Chelsea, Matthew Coggon, Georgios Gkatzelis, John Ortega, Brian McDonald, Jeff Peischl, Kenneth Aikin, Jessica Gilman, Michael Trainer, and Carsten Warneke. 2020. “Volatile Organic Compound Emissions from Solvent- and Water-Borne Coatings: Compositional Differences and Tracer Compound Identifications.” *Atmospheric Chemistry and Physics Discussions* (October):1–29.

Subramanian, R., Aja Ellis, Elvis Torres-delgado, Rebecca Tanzer, Carl Malings, Felipe Rivera, Maite Morales, Darrel Baumgardner, Albert Presto, and Olga L. Mayol-bracero. 2018. “Air Quality in Puerto Rico in the Aftermath of Hurricane Maria: A Case Study on the Use of Lower Cost Air Quality Monitors.” *ACS Earth and Space Chemistry* 1179–86.

Tang, Wei, Timothy Raymond, Beth Wittig, Cliff Davidson, Spyros Pandis, Allen Robinson, and Kevin Crist. 2004. “Spatial Variations of PM2.5 during the Pittsburgh Air Quality Study.” *Aerosol Science and Technology* 38(SUPPL. 2):80–90.

Tanzer, Rebecca, Carl Malings, Aliaksei Hauryliuk, and R. Subramanian. 2019. “Demonstration of a Low-Cost Multi-Pollutant Network to Quantify Intra-Urban Spatial Variations in Air Pollutant Source Impacts and to Evaluate Environmental Justice.” *International Journal of Environmental Research and Public Health* (2).

Tsigaridis, K., N. Daskalakis, M. Kanakidou, P. J. Adams, P. Artaxo, R. Bahadur, Y. Balkanski, S. E. Bauer, N. Bellouin, A. Benedetti, T. Bergman, T. K. Berntsen, J. P. Beukes, H. Bian, K. S. Carslaw, M. Chin, G. Curci, T. Diehl, R. C. Easter, S. J. Ghan, S. L. Gong, A. Hodzic, C. R. Hoyle, T. Iversen, S. Jathar, J. L. Jimenez, J. W. Kaiser, A. Kirkeväg, D. Koch, H. Kokkola, Y. H Lee, G. Lin, X. Liu, G. Luo, X. Ma, G. W. Mann, N. Mihalopoulos, J. J. Morcrette, J. F. Müller, G. Myhre, S. Myriokefalitakis, N. L. Ng, D. O’donnell, J. E. Penner, L. Pozzoli, K. J. Pringle, L. M. Russell, M. Schulz, J. Sciare, Seland, D. T. Shindell, S. Sillman, R. B. Skeie, D. Spracklen, T. Stavrakou, S. D. Steenrod, T. Takemura, P. Tiitta, S. Tilmes, H. Tost, T. Van Noije, P. G. Van Zyl, K. Von Salzen, F. Yu, Z. Wang, Z. Wang, R. A. Zaveri, H. Zhang, K. Zhang, Q. Zhang, and X. Zhang. 2014. “The AeroCom Evaluation and Intercomparison of Organic Aerosol in Global Models.” *Atmospheric Chemistry and Physics* 14(19):10845–95.

U.S. Secretary of Commerce on behalf of the United States of America. 2018. “NIST Chemistry

WebBook, SRD 69." Retrieved May 3, 2021 (https://webbook.nist.gov/).
US Census Bureau. 2012. *2012 Economic Census Survey, Manufacturing Industry Series: Materials Consumed by Kind for the U.S.*
US EPA. 2019. *Policy Assessment for the Review of the Particulate Matter National Ambient Air Quality Standards*. Vol. EPA 452/R-. Research Triangle Park, NC.
Volkamer, Rainer, Jose L. Jimenez, Federico San Martini, Katja Dzepina, Qi Zhang, Dara Salcedo, Luisa T. Molina, Douglas R. Worsnop, and Mario J. Molina. 2006. "Secondary Organic Aerosol Formation from Anthropogenic Air Pollution: Rapid and Higher than Expected." *Geophysical Research Letters* 33(17):7–10.
Wang, Yang, Jiayu Li, He Jing, Qiang Zhang, Jingkun Jiang, Pratim Biswas, Yang Wang, Jiayu Li, He Jing, Qiang Zhang, Jingkun Jiang, and Pratim Biswas. 2015. "Laboratory Evaluation and Calibration of Three Low-Cost Particle Sensors for Particulate Matter Measurement Laboratory Evaluation and Calibration of Three Low-Cost Particle Sensors for Particulate Matter Measurement." 6826.
Weitkamp, Emily A., Eric M. Lipsky, Patrick J. Pancras, John M. Ondov, Andrea Polidori, Barbara J. Turpin, and Allen L. Robinson. 2005. "Fine Particle Emission Profile for a Large Coke Production Facility Based on Highly Time-Resolved Fence Line Measurements." *Atmospheric Environment* 39(36):6719–33.
Williams, Anzio. 2020. "Pennsylvania, Delaware Close All Schools Due to Outbreak." 1–8.
Williams, B. J., A. H. Goldstein, N. M. Kreisberg, S. V. Hering, D. R. Worsnop, I. M. Ulbrich, K. S. Docherty, and J. L. Jimenez. 2010. "Major Components of Atmospheric Organic Aerosol in Southern California as Determined by Hourly Measurements of Source Marker Compounds." *Atmospheric Chemistry and Physics* 10(23):11577–603.
Wolf, Tom. 2020a. "All Non-Life-Sustaining Businesses in Pennsylvania to Close Physical Locations as of 8 PM Today to Slow Spread of COVID-19." 1–2. Retrieved April 22, 2020 (https://www.governor.pa.gov/newsroom/all-non-life-sustaining-businesses-in-pennsylvania-to-close-physical-locations-as-of-8-pm-today-to-slow-spread-of-covid-19/).
Wolf, Tom. 2020b. *Industry Operation Guidance*. USA.
Wu, Yue and Murray V Johnston. 2017. "Aerosol Formation from OH Oxidation of the Volatile Cyclic Methyl Siloxane (CVMS) Decamethylcyclopentasiloxane." *Environmental Science & Technology* 51(8):4445–51.
Xu, L., S. Suresh, H. Guo, R. J. Weber, and N. L. Ng. 2015. "Aerosol Characterization over the Southeastern United States Using High-Resolution Aerosol Mass Spectrometry: Spatial and Seasonal Variation of Aerosol Composition and Sources with a Focus on Organic Nitrates." *Atmospheric Chemistry and Physics* 15(13):7307–36.
Xu, Ruixin, Mohammed S. Alam, Christopher Stark, and Roy M. Harrison. 2020. "Behaviour of Traffic Emitted Semi-Volatile and Intermediate Volatility Organic Compounds within the Urban Atmosphere." *Science of the Total Environment* 720:137470.
Zhang, Q., Jose L. Jimenez, M. R. Canagaratna, J. D. Allan, H. Coe, I. Ulbrich, M. R. Alfarra, A. Takami, A. M. Middlebrook, Y. L. Sun, K. Dzepina, E. Dunlea, K. Docherty, P. F. DeCarlo, D. Salcedo, T. Onasch, J. T. Jayne, T. Miyoshi, A. Shimono, S. Hatakeyama, N. Takegawa, Y. Kondo, J. Schneider, F. Drewnick, S. Borrmann, S. Weimer, K. Demerjian, P. Williams, K. Bower, R. Bahreini, L. Cottrell, R. J. Griffin, J. Rautiainen, J. Y. Sun, Y. M. Zhang, and D. R. Worsnop. 2007. "Ubiquity and Dominance of Oxygenated Species in Organic Aerosols in Anthropogenically-Influenced Northern Hemisphere Midlatitudes." *Geophysical Research Letters* 34(13):1–6.

Zhao, Jing, Laura Gladson, and Kevin Cromar. 2018. “A Novel Environmental Justice Indicator for Managing Local Air Pollution.” *International Journal of Environmental Research and Public Health* 15(6).

Zhao, Ping, Yu-Hsiang Cheng, Chi-Chi Lin, and Yu-Lin Cheng. 2016. “Effect of Resin Content and Substrate on the Emission of BTEX and Carbonyls from Low-VOC Water-Based Wall Paint.” *Environ. Sci. Pollut. Res.* 12:3799–3808.

Zhao, Yunliang, Christopher J. Hennigan, Andrew A. May, Daniel S. Tkacik, Joost A. De Gouw, Jessica B. Gilman, William C. Kuster, Agnes Borbon, and Allen L. Robinson. 2014. “Intermediate-Volatility Organic Compounds: A Large Source of Secondary Organic Aerosol.” *Environmental Science and Technology* 48(23):13743–50.

Zhao, Yunliang, Nathan M. Kreisberg, David R. Worton, Alexander P. Teng, Susanne V Hering, Allen H. Goldstein, Yunliang Zhao, Nathan M. Kreisberg, David R. Worton, Alexander P. Teng, Susanne V Hering, Allen H. Goldstein, Situ Thermal, Yunliang Zhao, Nathan M. Kreisberg, David R. Worton, Alexander P. Teng, Susanne V Hering, and Allen H. Goldstein. 2013. “Development of an In Situ Thermal Desorption Gas Chromatography Instrument for Quantifying Atmospheric Semi-Volatile Organic Compounds Development of an In Situ Thermal Desorption Gas Chromatography Instrument for Quantifying Atmospheric Semi-Volatile Org.” 6826.

Zheng, Tongshu, Michael H. Bergin, Karoline K. Johnson, Sachchida N. Tripathi, Shilpa Shirodkar, Matthew S. Landis, Ronak Sutaria, and David E. Carlson. 2018. “Field Evaluation of Low-Cost Particulate Matter Sensors in High- and Low-Concentration Environments.” 4823–46.

Zimmerman, Naomi, Hugh Z. Li, Aja Ellis, Aliaksei Hauryliuk, Ellis S. Robinson, Peishi Gu, Rishabh U. Shah, Qing Ye, Luke Snell, R. Subramanian, Allen L. Robinson, Joshua S. Apte, and Albert A. Presto. 2020. “Improving Correlations between Land Use and Air Pollutant Concentrations Using Wavelet Analysis: Insights from a Low-Cost Sensor Network.” *Aerosol and Air Quality Research* 20(2):314–28.

Zimmerman, Naomi, Albert A. Presto, Sriniwasa P. N. Kumar, Jason Gu, Aliaksei Hauryliuk, Ellis S. Robinson, Allen L. Robinson, and R. Subramanian. 2018. “A Machine Learning Calibration Model Using Random Forests to Improve Sensor Performance for Lower-Cost Air Quality Monitoring.” *Atmospheric Measurement Techniques* 291–313.